Doctoral Dissertation

A Numerical Study on Second-Order Hydro dynamic Force and Response of an Elastic Body by Using Higher-Order Boundary Element Method

Kyeonguk Heo

August 2019

Department of Naval Architecture and Ocean Engineering
Division of Global Architecture
Graduate School of Engineering
Osaka University

Abstract

As one of the classical academic topics, hydroelasticity has been researched by many scholars in the field of naval architecture and ocean engineering. From the 2000s, the industrial importance has been increased due to enlargement in size of commercial ships. Accordingly, much investigation has been implemented by various organizations. Springing and whipping are well recognized as hydroelastic responses. In particular, the springing is known as a resonance phenomenon induced by harmonic incoming waves, which could occur not only by linear waves but also non-linear waves. The higher-order springing has been confirmed in various types of ships at several model experiments. On the other hands, most of the numerical studies has been conducted based on linear formulation with non-linear correction incorporated from integration on the instantaneous wetted surface of ship-hull surface until now.

In this thesis, a computer code is developed for numerical calculation of the non-linear springing of an elastic body with forward speed. Due to mathematical and numerical difficulties, the study is focused on the second-order springing problem by using higher-order boundary element method (HOBEM) in the perturbation scheme under the assumption of small wave slope.

Chapter 1 describes the background, review of the related past work, objective and outline of the present study, and then in Chapter 2, general mathematical formulations are described for the first-order and second-order boundary-value problems of a rigid/elastic body. To obtain the force and response of an elastic body, the generalized eigen-function expansion method is adopted, and several equations such as variation of the normal vector, mode-shape functions, and so on are derived by using continuum mechanics and directional derivative formulation. These variables up to second-order are applied to obtain first- and second-order body boundary conditions with body's elastic deformation and several kinds of generalized forces on an elastic body.

In Chapter 3, to solve the boundary-value problems obtained, the time-domain Rankine panel method is introduced and discretization method for the boundary integral equation using HOBEM is presented. Various numerical schemes to calculate the derivatives of the velocity potential are given, and some schemes for implementing the time-domain Rankine panel method are explained, such as time-marching scheme, grid generation on the free-surface, numerical damping beach, and numerical filter for removing numerical instability.

In Chapter 4, the developed computer code has been validated step by step for each of different conditions. In monochromatic waves, the direct time-domain simulation based on Rankine panel method has been implemented for both rigid & elastic bodies with/without forward speed. Validity

of obtained results for the second-order forces and responses are discussed mainly through comparison with corresponding results obtained by other researchers. Furthermore, in Chapter 5, frequency-domain analysis in bichromatic waves without forward speed is conducted by using free-surface Green function HOBEM. Indirect method to calculate second-order velocity potential on an elastic body is introduced. Using semi-analytic solutions in published papers, the results of suggested equation are validated by showing good agreement.

In the final, obtained results in the present thesis are summarized together with future work.

Contents

Nomenclature

In this dissertation, both Greek and English alphabets are used as a notation of physical variables. Some of them are repeated at different chapter and if there is no additional explanation, each alphabet has following meaning.

- *Overdot* means time derivative.

t : time

ζ : wave elevation

λ : wave lamda

k : wave number

β : incident wave heading angle

υ : deep water wave number

$\phi_{I,S,R}$: incident wave & diffraction & radiation velocity potential

$\phi_{D,B}$: disturbed (radiation + diffraction) velocity potential

ξ_j : modal amplitude in the *j*-th mode.

$\vec{h}^j$: modal vector in the *j*-th mode.

H : second-order component of Euler angle tensor

$\vec{X}(X,Y,Z)$: position vector at inertial coordinates / field point vector in HOBEM

$\vec{X}'(X',Y',Z')$: source point vector in HOBEM

$\vec{x}(x,y,z)$: position vector at body-fixed coordinates

$\vec{x}_g(x_g,y_g,z_g)$: centre of mass vector

z^N : center of neutral axis

A : wave amplitude

EI : flexural rigidity

GA : Shear rigidity

w_j : vertical displacement

ψ_j : angular displacement

G : Green's function

H : water depth

U : forward speed of ship

g : gravitational acceleration

L : length of body

(i, j, k) : basis vector in Cartesian coordinates

m : body mass (kg)

m_s : sectional mass (kg/m)

M : body mass tensor (kg)

a : Added mass tensor (kg)

b : damping coefficient tensor

C : hydrostatic restoring stiffness tensor

K : structural stiffness tensor

I : inertia tensor of body mass

p : hydro- static and dynamic pressure

ω : encounter wave frequency

ω_n : natural frequency of body

T_e : wave period

S_B : instantaneous wetted body surface

S_F : instantaneous free-surface

S_{B_0} : mean wetted body surface

S_{F_0} : mean free-surface

S_D : instantaneous bottom surface

S_C : instantaneous radiation surface

i : imaginary unit

δ : Kronecker delta function

H_n : Hankel function of the second kind

K_n : Modified Bessel function of the second kind

J_n : Bessel function of the first kind

$\bar{\nabla}$: two dimensional gradient operator $\left(\frac{\partial}{\partial X}, \frac{\partial}{\partial Y}\right)$

∇ : three dimensional gradient operator $\left(\frac{\partial}{\partial X}, \frac{\partial}{\partial Y}, \frac{\partial}{\partial Z}\right)$

Abbreviation

If there is no additional explanation, capital letter is abbreviation of following words.

HOBEM : Higher-Order Boundary Element Method

CPM : Constant Panel Method

VLFS : Very Large Floating Structure

NWT : Numerical Wave Tank

MEL : Mixed Eulerian Lagrangian

FEM : Finite Element Method

QTF : Quadratic Transfer Function

RAO : Response Amplitude Operator

TLPs : Tension Leg Platforms

$\mathbf{F_n}$: Froude number

EUT : Enhanced Unified Theory

RPM : Rankine Panel Method

NSM : New Strip Method

NK : Neumann-Kelvin

WL : Water Line

List of table

List of figure

CHAPTER 1

Introduction

1.1 Research background

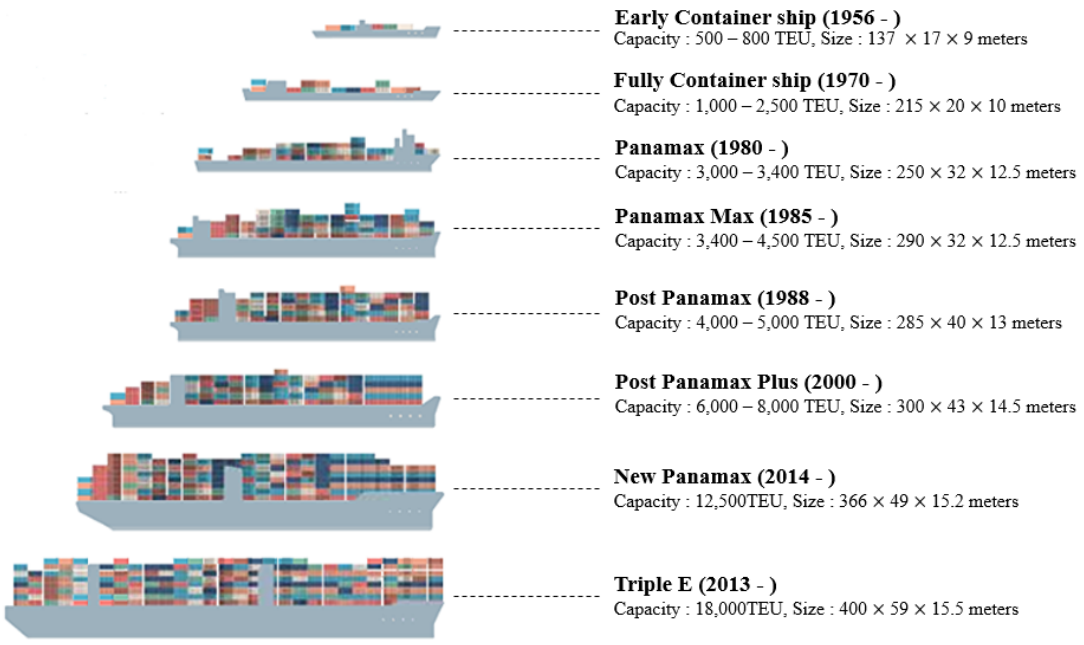

Fig. 1 Trend on the size of commercial vessels for 50 years (1960s ~ 2010s)

[source: jurnalmaritim.com]

One of continuous trends of the commercial vessel is enlargement of the size. Due to increase of the container traffic and economic feasibility, the ship's size has been increased continuously from several decades ago. If the ship size becomes large, the length overall necessarily increases and 400m lengthy ships appear in the 2010s as shown in Figure 1. It makes the structural strength be reduced and the ratio between stiffness and weight of hull girder decreases. As a result, a ship's

hull girder has relatively low natural frequency of wave induced vibration and the effect of wave induced vibration has been increased.

The effect by wave induced vibration which is also called hydroelastic response or high-frequency vibration on hull girder has been confirmed by continuous investigation over the past decades. From the systematic investigation on several ships conducted by various ways, many researchers reported that the high-frequency vibration has about 30~60% of total fatigue damage on large vessels (ISSC, 2015; 2018) and its effect should not be ignored. Accordingly, hydroelastic response has been considered in earnest at the stage of ship design and the rule on the dynamic response has been also changed.

Among global hydroelastic response, slamming induced whipping and springing are well recognized. Whipping is a transiently large response which happens by impact loads like slamming and decays after few seconds. On the other hands, springing is a resonance phenomenon by harmonic incoming waves. It could happen not only linear waves but also non-linear waves where it is so called super-harmonic resonance.

These wave induced vibrations have been studied by mainly three ways; *i.e.* real ship measurement, the model test, numerical analysis. The detail investigations on the hydroelastic responses have been conducted at each method to clarify various uncertainties.

In real ship measurement, several variables on hydroelastic response of a real sea-state have been considered. Since a real ship has complex geometry, the uncertainty which could not be predicted in the ship model has appeared. As one of them, structure damping has been measured to predict the effect of ship's high frequency vibrations. Since hydroelastic response generally happens at high-frequency region and the radiation damping is very small, the amplitude is relatively very sensitive to structural damping. From several reports, it has been confirmed that the hull's steel has small structural damping than other materials on a ship. It also has different value depending on the each vibration mode and generally torsional bending has larger damping than vertical bending modes due to cargos loaded on a ship (ISSC, 2018).

In model experiments, many kinds of non-linear factors have been confirmed. One of them non-linear springing has been shown in the model test clearly. It has appeared in various types of ships at several experiments (*e.g.* Storhaug, 2009) and its effect was considerable. For instance, some of non-linear springing have had up to fifth-order in bending modes (Miyake *et al*., 2008) and in moderate sea states, second-order springing could become predominant than linear springing (Hong and Kim, 2014). It is also expected that if the ship has forward speed, non-linear

springing could appear easily because it happens near 1/n of natural frequency of a ship. It also means the response spectrum could increase considerably.

In numerical analysis, the hydroelastic response has been calculated on a 3-dimensional ship model with development of several panel methods. Not only global response but also local quantities located on main points such as hot spot region have been considered in detail. However, most solution is based on *linear* variable with non-linear correction incorporated from integration on the instantaneous wetted surface of ship-hull surface to analyse springing phenomenon.

The detail analysis on contribution of non-linear hydrodynamic force has been remain work. In the real sea state, there are many kinds of wave non-linear components. Especially the sum-frequency wave loads could also be made by numerous combinations of wave frequencies and its non-linearity comes from body and free-surface non-linearity, respectively. Thus, it might be better for analysis of non-linear contribution to use numerical analysis.

1.2 Objective and scope of study

In this research background, our final goal is to develop the numerical analysis for the calculation of the non-linear springing of an elastic ship with forward speed. In numerical study, the second-order is almost the highest-order what could be considered due to limitation of mathematical and numerical difficulty. Thus, we are focusing on second-order springing of an elastic body in this dissertation.

However, it is also quite complex problem which includes several difficulty such as second-order wave-body interaction, elasticity, forward speed effect, structural modelling, etc. Thus, we conducted development procedure step by step from the initial stage. At each different condition, the developed code is first validated and it goes to the next step.

In hydroelastic problem, there are several important issues from both hydrodynamic and structural points of view. In this study, we are also focusing on mainly hydrodynamic aspect rather than structural aspect. Using relatively simple structural model, several fluid solvers based on the potential flow are used in both time- and frequency- domains. To consider hydroelastic response, some kinds of generalized forces and boundary conditions are re-derived and applied to the linear and second-order hydrodynamic problems of an elastic body. In the validation process, simple geometric body is mainly used to compare numerical result and non-linear hydroelastic response is discussed in these models.

1.3 Previous researches (state of the arts)

In this section, we introduce several previous researches in terms of both hydroelastic response and non-linear wave-body interaction because second-order springing includes all these issues. These topics are classical problems in naval architectures, thus huge amount of studies have been conducted by various research groups. Many more references could be confirmed other review papers (*e.g.* reports of ISSC or ITTC). We introduced only numerical study and also selected a few of them. The key issue of both hydroelastic response and non-linear wave body interaction is briefly described and at the last, numerical research on the non-linear hydroelastic response is introduced.

1.3.1 Numerical study on hydroelastic problem

Two-dimensional approach (strip theory)

Two-dimensional strip theory has been used widely due to its practicality and effective way as a seakeeping code. It is coupled with several structure solvers in both time- and frequency-domain to analyse hydroelastic response. Few published papers on two-dimensional approach are introduced briefly as follows:

Bishop and Price (1979) combined two-dimensional strip theory with FEM based on Timoshenko beam theory and calculated several kinds of linear hydroelastic responses using the mode superposition method.

Jensen and Pedersen (1978) developed second-order strip theory (SOST) which is based on linear strip theory of Gerristma and Beukelman (1972). In SOST, non-linear hydrodynamic coefficients and restoring force are obtained by using Taylor expansion based on hull's slope on the waterline. The strip theory is also coupled with Timoshenko beam to obtain vertical bending moment at each linear and second-order. Vidic-Perunovic and Jensen (2005) extended SOST for the bichromatic wave condition. They calculated both sum – and difference – frequency wave loads and discussed the second-order effect on the bending moment at multidirectional waves.

Using the time-domain analysis, various types of non-linear forces such as slamming, green water impact, and etc. can be considered. Thus nonlinear effects on the ship response have been investigated by using the time-domain strip theory in both rigid and flexible ships.

For instance, Fonseca and Guedes (1999) used time-memory effect function and considered non-linear effect in the time-domain. Xia and Wang (1997) used time-domain strip theory and calculated wave loads on the ship. Wu and Moan (1996) considered several non-linear forces such as slamming and non-linear restoring & Froude-Krylov forces on instantaneous wetted surface and Wu and Hermundstad (2005) suggested the semi-static solution for the high-mode which is difficult to be converged well.

Three-dimensional approach (Panel method)

From the 1990s, many three-dimensional seakeeping codes with forward speed have been developed; these are based on the linear potential flow using several types of Green functions and have been coupled with Finite Element Method (FEM) or beam theory for the hydroelastic response. As a result, the discussion is moved to consider both global & local quantities and more exact consideration of complex geometry of ships.

Newman (1994) calculated linear hydrodynamic force and response of an elastic body by using CPM and generalized mode expansion method. He showed that several mathematical formulations could be used instead of eigenvalue solution for modal vector and also derived generalized hydrostatic restoring stiffness on an elastic body. Huang and Rigg (2000) derived more improved hydrostatic restoring stiffness by using concept of continuum mechanics. Later, it is found that one term (pressure variation) is missing in Huang and Rigg (2000) and exact linear generalized hydrostatic restoring stiffness is confirmed by Malenica *et al*. (2009), and so on.

Malenica *et al.* (2003) developed hydroelastic code based on FEM and wave Green-function in the frequency-domain and their method is applied to the time-domain simulation by using retardation function. The validation process is also conducted by comparing with result of the experiment. Using segmented flexible barge, vertical motion of several points in regular waves are measured. The RAO result shows that vertical bending effect is well predicted in numerical simulation.

Senjanovic *et al*. (2007) also calculated not only vertical bending mode but also horizontal and torsional bending modes. The developed code is also compared with the experiment on flexible barge at different wave angles in both regular/irregular waves (Remy *et al*., 2006).

Although VLFS is not of interest in this study, hydroelastic response of VLFS has been conducted continuously by many researchers especially in Japan as reviewed by Kashiwagi (2000)

and Watanabe *et al*. (2004). Both linear and second-order forces have been considered by using several numerical methods such as zero-draft assumption, generalized modes method and so forth.

Ijima *et al*. (2008) used three-dimensional potential flow solver and FEM. They calculated both global and local quantities of symmetric & anti-symmetric vibration modes and also included non-linear effect from quadratic product of linear quantities and instantaneous wetted surface.

Kim *et al*. (2009, 2013, 2014) developed springing analysis code based on their three-dimensional Rankine panel code named WISH. They have developed different approaches such as direct coupling between potential solver and several structure solvers in the Cartesian and generalized coordinates, respectively.

Although many kinds of three-dimensional codes have been developed, most codes are adopting linear solution and as used in two-dimensional hydrodynamic codes, weakly non-linear variables are corrected by considering non-linear Froude-Krylov and restoring forces. (*e.g.* Kashiwagi *et al*., 2015; Kim and Kim, 2014).

1.3.2 Numerical study on second-order wave-body interaction problem

Second-order wave-body interaction has been researched mainly on the stationary structures. The non-linear wave force is generally smaller than linear wave force in moderate sea state. However, it dramatically increases as wave amplitude increases thus it could become more important in harsh environments. The non-linear force could also coincide with resonance at high-frequency or low-frequency; *e.g.* vertical loads on TLPs, horizontal response of moored vessels. Not only wave exciting force but also local quantities such as pressure, wave run-up in second-order have been also studied for better design of offshore-structure at operating and survival conditions.

The numerical study on second-order hydrodynamic force has been conducted by using mainly two ways. First is to use perturbation approximation in the frequency-domain with the weakly non-linear assumption. In this method, it is particularly important and difficult to calculate second-order velocity potential force thus many researches have been conducted to obtain exact second-order velocity potential by solving second-order boundary-value problem (Ogilvie, 1983). Another way is to solve initial-value problem on instantaneous boundary condition by using time-domain simulation. Numerical wave tank (NWT) based on semi-Lagrangian or MEL approaches on fixed and floating bodies has been developed by many researchers on both 2D/3D bodies (*e.g.*

Ferrant, 1998; Cointe *et al*., 1990; Tanizawa, 1995; Wu and Taylor, 2003; Kashiwagi *et al*., 1998; Koo and Kim, 2004). However, it generally needs re-meshing and evaluation of influence matrix at each time step to consider non-linearity of body & free-surfaces. Thus it should need a lot of time and stable treatment to keep the code.

As a combined method, the perturbation method is applied to time-domain analysis. In this method, linear and second-order velocity potentials are calculated by solving each boundary condition at each time step. Although it could not consider fully-nonlinear effects, it has advantage that it can consider linear & second-order wave forces and needs only once evaluation of influence matrix without re-meshing scheme.

Some of published papers on second-order wave body interaction by frequency/time-domain simulations based on perturbation method are introduced as follows:

Frequency-domain analysis on a rigid model

Molin (1979) showed that second-order velocity potential could be solved by separating the locked and free wave components. He also showed that second-order radiation condition is satisfied and suggested indirect method to obtain second-order velocity potential force by using only linear quantities.

Kim and Yue (1989, 1990) calculated second-order velocity potential by using ring source Green function on an axis-symmetric body. Their solution is known as a first complete solution of second-order velocity potential and QTF is also calculated by using indirect method in bichromatic waves. They discussed the effect of body and free-surface non-linearity, respectively. It is confirmed that the free-surface effect is important especially on sum-frequency wave forces.

Using bottom-mounted vertical cylinder, Newman (1990) derived asymptotic solution of second-order velocity potential. He regarded non-homogeneous component as an added oscillating pressure on free-surface and showed that far-field value of free-surface non-homogeneous term makes several properties of second-order unsteady wave & pressure. It is also shown that second-order free-surface effect is stronger at the double frequency summated by same frequency than summation of different frequency components.

Chau and Taylor (1992) derived special Green function which satisfies second-order boundary condition of bottom-mounted vertical cylinder and derived semi-analytic solution of second-order velocity potential based on eigen function expansion method. Their method is extended to third-order diffraction problem by Malenica and Molin (1995) and similar ways are also applied to

various conditions such as truncated vertical cylinder, multiple-column, porus cylinder, etc. (*e.g.* Huang and Taylor, 1996; Malenica *et al*., 1996; William and Li, 1994).

Kim (1991), Lee (1995) developed the numerical calculation of QTF for general floating body by using constant panel method (CPM) based on wave Green function and Choi *et al*. (2001) calculated second-order velocity potential force by using indirect method based on HOBEM in the frequency-domain.

Time-domain analysis on a rigid model

Isaacson and Cheung (1991, 1992) solved second-order diffraction problem in 2D & 3D bodies using perturbation time-domain simulation. Issacson and Ng (1993, 1995), Teng *et al.* (2002), Bai *et al*. (2003) also solved second-order wave force in forced oscillating 2D & 3D bodies. Duan *et al*. (2015a, 2015b) developed different BEM, so called second-order Taylor expansion BEM, to solve second-order diffraction/radiation problems. They also showed that their method is effective for higher-order potential flow problem.

Skourup *et al*. (2000) solved second-order wave force with/without a current and Buchmann *et al*. (1998) discussed the second-order wave run-up of vertical cylinder with result of fully-nonlinear waves in a current.

Shao and Faltinsen (2010, 2012, 2014) bring up the physical problem on the higher-order derivative of velocity potential with sharp corner. They also showed that the slow convergence of velocity potential's derivatives and developed so called body-fixed coordinate method in perturbation time-domain simulation based on HOBEM. Instead of using Taylor expansion on the body boundary condition, they obtained the force and boundary condition in the frame of body-fixed coordinate system without derivative of velocity potential. They presented that their method could be applied to second-order boundary value problem of general body with/without forward speed and ship motion & added resistance with forward speed where there are several higher-order derivative of velocity potential.

Wu and Taylor (1994), Hong and Nam (2011) used FEM instead of BEM to analyse non-linear wave-body interaction in the time-domain.

Frequency/time-domain analysis on an elastic model

We introduced numerical investigation on second-order wave force with rigid body assumption. However, there are relatively few researches which consider both non-linear hydrodynamic and

elasticity. As a last section, some of study on the non-linear hydroelasticity problem are introduced as follows:

Wu *et al*. (1997) and Chen *et al*. (2003) calculated generalized quadratic product of linear quantities on an elastic body in regular and irregular waves. They considered elasticity by adding the effect of elastic response to the normal and position vectors, respectively. Park *et al*. (2018) revised Wu's method and calculated added resistance of an elastic ship with forward speed.

The mean drift force on VLFS was also conducted by using near – and far-field approaches by Kashiwagi (1998) and Utsunomiya *et al*. (2001) based on zero draft assumption, respectively.

Choi (2004) derived the generalized second-order hydrodynamic force and calculated mean drift force & moment of an elastic barge by using HOBEM based on wave Green function and his approach is applied to analysis of the floating fish cage which is composed of multiple elastic torus (Choi and Yeo, 2009).

Recently, the second-order hydrodynamic force including second-order velocity potential is considered on an elastic body. Choi (2013) calculated second-order hydrodynamic force and response of bottom-mounted elastic vertical cylinder in semi-analytic way based on eigen function expansion. Malenica *et al*. (2018) calculated numerically second-order velocity potential force of an elastic body based on commercial software HydroSTAR.

However, it is difficult to find the numerical study on the second-order springing of an elastic body with forward speed with the full consideration of elasticity & hydrodynamics until now.

1.4 Outline of dissertation

Outline of dissertation is as follows:

In chapter 2, general mathematical formulations to solve boundary-value problem of a rigid/elastic body are described. Several boundary conditions and generalized forces on an elastic body are derived with consideration of body deformation based on perturbation scheme.

In chapter 3, numerical implementations used in fluid-domain solver are introduced. The basis of HOBEM is described and the discretization method of the boundary integral equation is presented. The Green function adopted in BEM is defined and various numerical schemes to

calculate derivative of velocity potential are also given. Several necessary schemes to implement time-domain Rankine panel method are introduced in the last section.

In chapter 4, the direct time-domain simulation is used to study on the rigid/elastic models in monochromatic waves with/without forward speed. The developed time-domain computer code is validated at several different conditions (with/without forward speed and rigid/elastic body) and applied to the second-order springing in limited condition. From the obtained result, discussion on perturbation time-domain simulation is conducted.

In chapter 5, the frequency-domain analysis is implemented to study on a simple elastic body model in bichromatic waves without forward speed. Several additional formulations are introduced for consideration of bichromatic waves. The detail formulation to calculate second-order velocity potential force is described and a few results are compared with semi-analytic solution as a validation process.

In the final chapter, the conclusion of this study and future works are summarized.

CHAPTER 2

Mathematical formulation

2.1 Introduction

In this chapter, the general mathematical formulation for the calculation of linear & second-order forces and responses are described on an elastic body. The fluid is assumed to be inviscid and incompressible with irrotational motion. Then with the potential flow theory, the Laplace equation becomes governing equation.

$$\Delta\phi = 0 \tag{2.1}$$

With assumption of weakly-nonlinear several quantities such as velocity potential, wave elevation, motion, force, and so forth are perturbated based on *wave slope*. The maximum order of physical quantities is second-order. They are expressed in this form.

$$\phi \cong \varepsilon\phi^{(1)} + \varepsilon^2\phi^{(2)} + O\left(\varepsilon^3\right) \tag{2.2}$$

$$\zeta \cong \varepsilon\zeta^{(1)} + \varepsilon^2\zeta^{(2)} + O\left(\varepsilon^3\right) \tag{2.3}$$

$$\vec{F} \cong \varepsilon\vec{F}^{(1)} + \varepsilon^2\vec{F}^{(2)} + O\left(\varepsilon^3\right) \tag{2.4}$$

2.2 Generalized mode expansion method

In the analysis of fluid-structure interaction, generalized eigen-mode expansion method is one of classic ways to consider the hydroelastic response on an elastic body (Newman, 1994). Both rigid and elastic body motions are calculated simply by extending the total number of modes. The mode-shape function can be obtained by solving eigenvalue problems of structure solvers such as the beam theory or Finite Element Method (FEM) with satisfied boundary conditions. The total

response is calculated by summation of the modal vector multiplied by its amplitude. It is as follows:

$$\vec{\tau} = \sum_{j=1}^{N} \xi_j \vec{h}^j \tag{2.5}$$

It is known that any function which satisfies geometric boundary condition could be adopted for the modal vector. This approach could also be applied to multi-body analysis in the generalized modes.

2.3 Coordinate systems

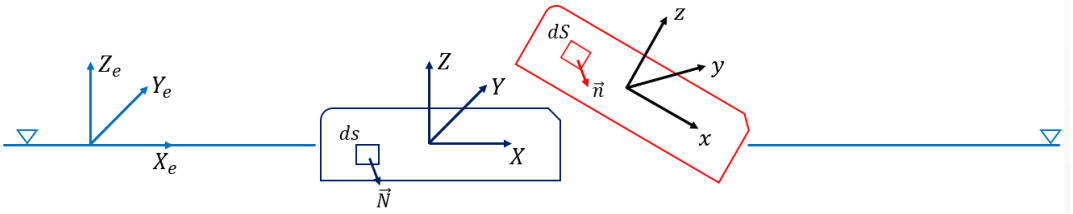

Fig. 2 Earth-fixed, inertial, body-fixed coordinate systems

In the analysis to follow, as shown in Fig. 2, we use both body-fixed coordinate system and inertial coordinate system with steady translation at velocity U along the X axis. Following classical ways, several approximations for boundary conditions, forces, and so forth are conducted on the inertial coordinates.

2.4 Deformed surface of an elastic body

In this study, we are considering elastic body dynamics and several physical variables are re-defined in the generalized mode to include the effect of an elastic motion. As a first procedure, linear and second-order normal vector variations which consider both rigid and elastic body motions are expressed by using the concept of continuum mechanics.

The normal vector of deformed surface could be approximated by using normal vector at initial state with displacement (Huang and Rigg, 2000). It is expressed in this form.

$$\vec{N}ds = J(\mathbf{F}^{-1})^T \vec{n}dS \tag{2.6}$$

Here, J: Jacobian, $\mathbf{F}$: Deformation gradient, $\vec{n}$: Deformed normal vector, $\vec{N}$: Initial normal vector, ds: Deformed surface, dS: Undeformed surface

If the position vector at each mode is expressed by

$$\vec{X} = \vec{x} + \vec{\tau} \tag{2.7}$$

$$\vec{\tau} \cong \varepsilon\vec{\tau}^{(1)} + \varepsilon^2\left(\vec{\tau}^{(2)} + \vec{\gamma}^{(2)}\right) + O(\varepsilon^3) \tag{2.8}$$

Here, $\vec{\gamma}^{(2)}$ is displacement obtained by quadratic product of linear displacements

Deformation gradient tensor could be written by substituting above equations.

$$\mathbf{F} = \begin{bmatrix} \frac{\partial X_1}{\partial x_1} & \frac{\partial X_1}{\partial x_2} & \frac{\partial X_1}{\partial x_3} \\ \frac{\partial X_2}{\partial x_1} & \frac{\partial X_2}{\partial x_2} & \frac{\partial X_2}{\partial x_3} \\ \frac{\partial X_3}{\partial x_1} & \frac{\partial X_3}{\partial x_2} & \frac{\partial X_3}{\partial x_3} \end{bmatrix} \tag{2.9}$$

$$= \begin{bmatrix} 1+\varepsilon\tau_{1,1}^{(1)} + \varepsilon^2\left(\tau_{1,1}^{(2)} + \gamma_{1,1}^{(2)}\right) & \varepsilon\tau_{1,2}^{(1)} + \varepsilon^2\left(\tau_{1,2}^{(2)} + \gamma_{1,2}^{(2)}\right) & \varepsilon\tau_{1,3}^{(1)} + \varepsilon^2\left(\tau_{1,3}^{(2)} + \gamma_{1,3}^{(2)}\right) \\ \varepsilon\tau_{2,1}^{(1)} + \varepsilon^2\left(\tau_{2,1}^{(2)} + \gamma_{2,1}^{(2)}\right) & 1+\varepsilon\tau_{2,2}^{(1)} + \varepsilon^2\left(\tau_{2,2}^{(2)} + \gamma_{2,2}^{(2)}\right) & \varepsilon\tau_{2,3}^{(1)} + \varepsilon^2\left(\tau_{2,3}^{(2)} + \gamma_{2,3}^{(2)}\right) \\ \varepsilon\tau_{3,1}^{(1)} + \varepsilon^2\left(\tau_{3,1}^{(2)} + \gamma_{3,1}^{(2)}\right) & \varepsilon\tau_{3,2}^{(1)} + \varepsilon^2\left(\tau_{3,2}^{(2)} + \gamma_{3,2}^{(2)}\right) & 1+\varepsilon\tau_{3,3}^{(1)} + \varepsilon^2\left(\tau_{3,3}^{(2)} + \gamma_{3,3}^{(2)}\right) \end{bmatrix}$$

After inversing and transposing the deformation gradient tensor, it multiplies with Jacobian. So then, it is rewritten by matrix form.

$$J(\mathbf{F}^{-1})^T = \begin{bmatrix} 1+\varepsilon\left(\tau_{2,2}^{(1)} + \tau_{3,3}^{(1)}\right) & -\varepsilon\tau_{2,1}^{(1)} & -\varepsilon\tau_{3,1}^{(1)} \\ -\varepsilon\tau_{1,2}^{(1)} & 1+\varepsilon\left(\tau_{1,1}^{(1)} + \tau_{3,3}^{(1)}\right) & -\varepsilon\tau_{3,2}^{(1)} \\ -\varepsilon\tau_{1,3}^{(1)} & -\varepsilon\tau_{2,3}^{(1)} & 1+\varepsilon\left(\tau_{1,1}^{(1)} + \tau_{2,2}^{(1)}\right) \end{bmatrix}$$

$$+\varepsilon^2\begin{bmatrix} \left\{\left(\tau_{2,2}^{(2)} + \tau_{3,3}^{(2)}\right) + \left(\gamma_{2,2}^{(2)} + \gamma_{3,3}^{(2)}\right)\right\} & -\tau_{2,1}^{(2)} - \gamma_{2,1}^{(2)} & -\tau_{3,1}^{(2)} - \gamma_{3,1}^{(2)} \\ -\tau_{1,2}^{(2)} - \gamma_{1,2}^{(2)} & \left\{\left(\tau_{1,1}^{(2)} + \tau_{3,3}^{(2)}\right) + \left(\gamma_{1,1}^{(2)} + \gamma_{3,3}^{(2)}\right)\right\} & -\tau_{3,2}^{(2)} - \gamma_{3,2}^{(2)} \\ -\tau_{1,3}^{(2)} - \gamma_{1,3}^{(2)} & -\tau_{2,3}^{(2)} - \gamma_{2,3}^{(2)} & \left\{\left(\tau_{1,1}^{(2)} + \tau_{2,2}^{(2)}\right) + \left(\gamma_{1,1}^{(2)} + \gamma_{2,2}^{(2)}\right)\right\} \end{bmatrix}$$

$$+\varepsilon^2\begin{bmatrix} \tau_{2,2}^{(1)}\tau_{3,3}^{(1)} - \tau_{2,3}^{(1)}\tau_{3,2}^{(1)} & \tau_{2,3}^{(1)}\tau_{3,1}^{(1)} - \tau_{2,1}^{(1)}\tau_{3,3}^{(1)} & \tau_{2,1}^{(1)}\tau_{3,2}^{(1)} - \tau_{2,2}^{(1)}\tau_{3,1}^{(1)} \\ \tau_{1,3}^{(1)}\tau_{3,2}^{(1)} - \tau_{1,2}^{(1)}\tau_{3,3}^{(1)} & \tau_{1,1}^{(1)}\tau_{3,3}^{(1)} - \tau_{1,3}^{(1)}\tau_{3,1}^{(1)} & \tau_{1,2}^{(1)}\tau_{3,1}^{(1)} - \tau_{1,1}^{(1)}\tau_{3,2}^{(1)} \\ \tau_{1,2}^{(1)}\tau_{2,3}^{(1)} - \tau_{1,3}^{(1)}\tau_{2,2}^{(1)} & \tau_{1,3}^{(1)}\tau_{2,1}^{(1)} - \tau_{1,1}^{(1)}\tau_{2,3}^{(1)} & \tau_{1,1}^{(1)}\tau_{2,2}^{(1)} - \tau_{1,2}^{(1)}\tau_{2,1}^{(1)} \end{bmatrix} + O\left(\varepsilon^3\right) \tag{2.10}$$

This could also be expressed by using following vector form (Choi, 2004).

$$\vec{N}ds\Big|_{S_B} \cong O(1)_{S_{B_0}} + O(\varepsilon)_{S_{B_0}} + O(\varepsilon^2)_{S_{B_0}} + \cdots \tag{2.11}$$

$$O(1) = \vec{n}dS \tag{2.12}$$

$$O(\varepsilon) = \left\{ \left(\nabla \cdot \vec{\tau}^{(1)} \right) \vec{n} - \left[\nabla \vec{\tau}^{(1)} \right]^T \cdot \vec{n} \right\} dS \tag{2.13}$$

$$O(\varepsilon^2) = \left\{ \begin{array}{l} \nabla \cdot \left(\vec{\tau}^{(2)} + \vec{\gamma}^{(2)} \right) \vec{n} - \left[\nabla \vec{\tau}^{(2)} + \nabla \vec{\gamma}^{(2)} \right]^T \cdot \vec{n} \\ + \left(\dfrac{\partial \vec{\tau}^{(1)}}{\partial y} \times \dfrac{\partial \vec{\tau}^{(1)}}{\partial z}, \dfrac{\partial \vec{\tau}^{(1)}}{\partial z} \times \dfrac{\partial \vec{\tau}^{(1)}}{\partial x}, \dfrac{\partial \vec{\tau}^{(1)}}{\partial x} \times \dfrac{\partial \vec{\tau}^{(1)}}{\partial y} \right) \cdot \vec{n} \end{array} \right\} dS \tag{2.14}$$

The defined normal vector variation is applied to the derivation of several generalized formulation which will be explained later. These expressions for the normal vector derived in the generalized mode correspond with classical equations for the rigid-body motion. The vector identity between generalized mode equation and classical expression is described in Appendix A.

2.5 Boundary-value problem in monochromatic waves

Boundary-value problem is considered to obtain velocity potentials. In the forward speed problem, velocity potential and wave elevation are decomposed into several components. They are as follows:

$$\phi = \Phi_B + \phi_I + \phi_S, \quad \zeta = \zeta_I + \zeta_S \tag{2.15}$$

where suffix *B* means the basis flow

The basis flow is taken as the double-body flow, which is expressed by a sum of uniform flow and steady disturbance flow as follows:

$$\Phi_B = -UX + \Phi \tag{2.16}$$

where Φ denotes the double-body velocity potential.

To solve the boundary-value problem, the boundary conditions should be described. The kinematic and dynamic free-surface and the body boundary condition on the instantaneous surface are written as follows:

2.5.1 Free-surface boundary condition

The kinematic & dynamic free-surface boundary conditions on instantaneous surface are expressed in this form.

$$\left[\frac{\partial}{\partial t}+\nabla\phi\cdot\nabla\right]\left(Z-\zeta\right)=0 \qquad \text{on } Z=\zeta(x,y,t) \tag{2.17}$$

$$\left[\frac{\partial}{\partial t}+\nabla\phi\cdot\nabla\right]\phi=-g\zeta+\frac{1}{2}\left(\nabla\phi\cdot\nabla\phi+U^2\right) \qquad \text{on } Z=\zeta(x,y,t) \tag{2.18}$$

Both kinematic and dynamic free-surface boundary conditions are approximated on the still water surface ($Z=0$) by taking Taylor expansion. They are as follows:

$$\frac{\partial\zeta_s^{(m)}}{\partial t}+\vec{V}\cdot\nabla\zeta_s^{(m)}=\frac{\partial\phi_s^{(m)}}{\partial Z}-\left(\frac{\partial\zeta_I^{(m)}}{\partial t}-\frac{\partial\phi_I^{(m)}}{\partial Z}\right)-\vec{V}\cdot\nabla\zeta_I^{(m)}+f_m \tag{2.19}$$

$$\frac{\partial\phi_s^{(m)}}{\partial t}+\vec{V}\cdot\nabla\phi_s^{(m)}=-g\zeta_s^{(m)}-\left(\frac{\partial\phi_I^{(m)}}{\partial t}+g\zeta_I^{(m)}\right)-\vec{V}\cdot\nabla\phi_I^{(m)}+h_m \tag{2.20}$$

where $f_1=\zeta^{(1)}\frac{\partial^2\Phi}{\partial Z^2}$, $f_2=-\frac{\partial\phi^{(1)}}{\partial X}\frac{\partial\zeta^{(1)}}{\partial X}-\frac{\partial\phi^{(1)}}{\partial Y}\frac{\partial\zeta^{(1)}}{\partial Y}+\zeta^{(1)}\frac{\partial^2\phi^{(1)}}{\partial Z^2}+\zeta^{(2)}\frac{\partial^2\Phi}{\partial Z^2}$

$$h_1=0,\quad h_2=-\frac{1}{2}\nabla\phi^{(1)}\cdot\nabla\phi^{(1)}-\zeta^{(1)}\frac{\partial}{\partial Z}\left\{\frac{\partial\phi^{(1)}}{\partial t}+\vec{V}\cdot\nabla\phi^{(1)}\right\}$$

and $\quad\vec{V}\equiv-U\vec{i}+\nabla\Phi$

2.5.2 Body-surface boundary condition

The kinematic body boundary condition on the instantaneous surface is expressed in this form.

$$\frac{\partial\phi}{\partial N}ds=\vec{N}\cdot\dot{\vec{\tau}}ds \qquad \text{on } S_B \tag{2.21}$$

Substituting the deformed normal vector defined in Eqs. (2.12~14) into kinematic body boundary condition Eq. (2.21), linear and second-order generalized body boundary conditions with forward speed are derived as follows:

$$\frac{\partial\phi_s^{(1)}}{\partial n}=\dot{\vec{\tau}}^{(1)}\cdot\vec{n}+\left(\vec{V}\cdot\left[\nabla\vec{\tau}^{(1)}\right]^T-\vec{\tau}^{(1)}\cdot\nabla\vec{V}\right)\cdot\vec{n}-\left(\nabla\cdot\vec{\tau}^{(1)}\right)\left(\vec{V}\cdot\vec{n}\right)-\frac{\partial\phi_I^{(1)}}{\partial n} \tag{2.22}$$

$$\frac{\partial \phi_s^{(2)}}{\partial n} = \left\{ \dot{\vec{\tau}}^{(2)} + \dot{\vec{\gamma}}^{(2)} - \vec{\tau}^{(1)} \cdot \nabla\nabla\phi^{(1)} - (\vec{\tau}^{(2)} + \vec{\gamma}^{(2)}) \cdot \nabla\vec{V} - \frac{1}{2}\sum_{l}^{3}\sum_{k}^{3} \tau_k^{(1)} \tau_l^{(1)} \frac{\partial}{\partial x_k}\frac{\partial}{\partial x_l}\vec{V} \right\} \cdot \vec{n}$$
$$+ \left\{ \dot{\vec{\tau}}^{(1)} - \nabla\phi^{(1)} - \vec{\tau}^{(1)} \cdot \nabla\vec{V} \right\} \cdot \left\{ \left(\nabla \cdot \vec{\tau}^{(1)}\right)\vec{n} - \left[\nabla \vec{\tau}^{(1)}\right]^T \cdot \vec{n} \right\} - \frac{\partial \phi_I^{(2)}}{\partial n} \tag{2.23}$$
$$- \vec{V} \cdot \left\{ \begin{array}{l} \nabla \cdot \left(\vec{\tau}^{(2)} + \vec{\gamma}^{(2)}\right)\vec{n} - \left[\nabla \vec{\tau}^{(2)} + \nabla \vec{\gamma}^{(2)}\right]^T \cdot \vec{n} \\ + \left(\frac{\partial \vec{\tau}^{(1)}}{\partial y} \times \frac{\partial \vec{\tau}^{(1)}}{\partial z}, \frac{\partial \vec{\tau}^{(1)}}{\partial z} \times \frac{\partial \vec{\tau}^{(1)}}{\partial x}, \frac{\partial \vec{\tau}^{(1)}}{\partial x} \times \frac{\partial \vec{\tau}^{(1)}}{\partial y} \right) \cdot \vec{n} \end{array} \right\}$$

Calculating the rotational motion by both rigid and elastic bodies, as shown in Appendix A, $\vec{\gamma}^{(2)}$ could be obtained and becomes equal to $\mathbf{H}\vec{x}$ in terms of the second-order expansion of Euler-angle matrix in case where only the rigid-body motion exists. It is also noteworthy that both linear and second-order boundary conditions have several terms which exist only for an elastic body; *e.g.* the divergence of displacement $\nabla \cdot \vec{\tau}^{(1)}$ in the linear boundary condition. In the first-order body-boundary condition, we can also find that the second term on the right-hand side of Eq. (2.22) corresponds to m_j-terms in the seakeeping problem.

2.6 Generalized hydrodynamic force

The hydrodynamic force acting on a body is defined with generalized mode in the following form (Newman, 1994):

$$F_j = \iint_{S_B} p\left(\vec{h}^j \cdot \vec{N}\right) ds \tag{2.24}$$

To calculate the generalized hydrodynamic force, the inner product of mode shape and normal vector on the body surface should be obtained. Huang and Rigg (2000) calculated the inner product and multiplied it by the hydrostatic pressure to calculate the linear hydrostatic stiffness of an elastic body. It can also be expanded up to second-order on the mean surface. Choi (2004) derived second-order inner product by taking Taylor expansion on mode-shape function and generalized normal vector defined in Eqs. (2.12-14). In this thesis, the variation of modal function is defined by directional derivative and it is coupled with generalized normal vector. The derived inner product could be expressed as follows:

$$\vec{h}^j \cdot \vec{N} ds\Big|_{S_B} = O(1)_{S_{B_0}} + O(\varepsilon)_{S_{B_0}} + O(\varepsilon^2)_{S_{B_0}} + \cdots \tag{2.25}$$

$$O(1)=\left\{\delta\vec{h}^{\,j}\cdot\delta\vec{n}\right\}^{(0)}dS=\vec{h}^{\,j}\cdot\vec{n}dS \tag{2.26}$$

$$O(\varepsilon)=\left\{\delta\vec{h}^{\,j}\cdot\delta\vec{n}\right\}^{(1)}dS=\left\{\nabla\vec{h}^{\,j}\cdot\vec{\tau}^{(1)}+\left(\nabla\cdot\vec{\tau}^{(1)}\right)\vec{h}^{\,j}-\nabla\vec{\tau}^{(1)}\cdot\vec{h}^{\,j}\right\}\cdot\vec{n}dS \tag{2.27}$$

$$O(\varepsilon^2)=\left\{\delta\vec{h}^{\,j}\cdot\delta\vec{n}\right\}^{(2)}dS=\left\{\begin{array}{c}\nabla\vec{h}^{\,j}\cdot\left(\vec{\gamma}^{(2)}+\vec{\tau}^{(2)}\right)-\nabla\left(\vec{\gamma}^{(2)}+\vec{\tau}^{(2)}\right)\cdot\vec{h}^{\,j}\\+\nabla\cdot\left(\vec{\gamma}^{(2)}+\vec{\tau}^{(2)}\right)\vec{h}^{\,j}+\left(\nabla\vec{h}^{\,j}\cdot\vec{\tau}^{(1)}\right)\cdot\nabla\vec{\tau}^{(1)}\\\left(\frac{\partial\vec{\tau}^{(1)}}{\partial y}\times\frac{\partial\vec{\tau}^{(1)}}{\partial z},\frac{\partial\vec{\tau}^{(1)}}{\partial z}\times\frac{\partial\vec{\tau}^{(1)}}{\partial x},\frac{\partial\vec{\tau}^{(1)}}{\partial x}\times\frac{\partial\vec{\tau}^{(1)}}{\partial y}\right)\vec{h}^{\,j}\end{array}\right\}\cdot\vec{n}dS \tag{2.28}$$

In the present study, the generalized hydrodynamic force for the forward speed problem is derived by considering the change in the pressure on the body surface. The linear external force is expressed as follows:

$$\begin{aligned}F_j^{(1)}=&-\rho\iint_{S_{B_0}}\left\{\frac{\partial\phi^{(1)}}{\partial t}+g\tau_3^{(1)}+\frac{1}{2}\vec{\tau}^{(1)}\cdot\nabla\left(\vec{V}\cdot\vec{V}\right)+\vec{V}\cdot\nabla\phi^{(1)}\right\}\left(\vec{h}^{\,j}\cdot\vec{n}\right)dS\\&-\rho\iint_{S_{B_0}}\left\{\left(\vec{V}-\frac{1}{2}\nabla\Phi\right)\cdot\nabla\Phi+gz\right\}\left\{\nabla\vec{h}^{\,j}\cdot\vec{\tau}^{(1)}+\left(\nabla\cdot\vec{\tau}^{(1)}\right)\vec{h}^{\,j}-\nabla\vec{\tau}^{(1)}\cdot\vec{h}^{\,j}\right\}\cdot\vec{n}dS\end{aligned} \tag{2.29}$$

Here, we can calculate the hydrostatic coefficient by evaluating the directional derivative for the displacement. The definition of derivative is written by

$$-\frac{d}{d\varepsilon}\left[F\left(\varepsilon\vec{\tau}\right)\right]_{\varepsilon=0} \tag{2.30}$$

After adding the linear gravity restoring force, the hydrostatic coefficient on an elastic body is obtained as follows:

$$\mathrm{C}_{ij}=\rho g\iint_{S_{B_0}}h_3{}^{j}\cdot\vec{h}^{\,i}\vec{n}dS+\rho_s g\iiint_{V_b}\left(\vec{h}^{\,i}\cdot\nabla\right)h_3{}^{j}dV+\rho g\iint_{S_{B_0}}z\left\{\left(\nabla\cdot\vec{h}^{\,i}\right)\vec{h}^{\,j}+\vec{h}^{\,j}\cdot\nabla\vec{h}^{\,i}-\left(\vec{h}^{\,i}\cdot\nabla\right)\vec{h}^{\,j}\right\}\cdot\vec{n}dS \tag{2.31}$$

This hydrostatic coefficient can be shown to be the same as other hydrostatic formulations for an elastic body (Malenica *et al*., 2009). In the second-order, the hydrodynamic force could be decomposed into several components by a typical way. They are as follows:

$$F_j^{(2)}=F_{p_j}^{(2)}+F_{res_j}^{(2)}+F_{q_j}^{(2)} \tag{2.32}$$

$$F_{p_j}^{(2)} = -\rho \iint_{S_{B_0}} \left(\frac{\partial \phi_{S+I}^{(2)}}{\partial t} + \vec{V} \cdot \nabla \phi_{S+I}^{(2)} \right) \left(\vec{h}^{\,j} \cdot \vec{n} \right) dS \tag{2.33}$$

$$F_{res_j}^{(2)} = \mathrm{C}_{ij} \xi_i^{(2)} \tag{2.34}$$

$$\begin{aligned} F_{q_j}^{(2)} = {} & \frac{\rho g}{2} \int_{WL} \left(\zeta^{(1)} - \tau_3^{(1)} \right)^2 \frac{\left\{ \delta \vec{h}^{\,j} \cdot \delta \vec{n} \right\}^{(0)}}{\sin \beta} \, dl - \rho \int_{WL} \left\{ \left(\vec{V} - \frac{1}{2} \nabla \Phi \right) \cdot \nabla \Phi \right\} \left(\zeta^{(1)} - \tau_3^{(1)} \right) \frac{\left\{ \delta \vec{h}^{\,j} \cdot \delta \vec{n} \right\}^{(1)}}{\sin \beta} \, dl \\ & - \rho \iint_{S_{B_0}} \left\{ \frac{1}{2} \nabla \phi^{(1)} \cdot \nabla \phi^{(1)} + \vec{\tau}^{(1)} \cdot \nabla \left(\frac{\partial \phi^{(1)}}{\partial t} + \vec{V} \cdot \nabla \phi^{(1)} \right) + g \gamma_3^{(2)} + \frac{1}{2} \vec{\gamma}^{(2)} \cdot \nabla \left(\vec{V} \cdot \vec{V} \right) \right\} \left\{ \delta \vec{h}^{\,j} \cdot \delta \vec{n} \right\}^{(0)} dS \\ & - \rho \iint_{S_{B_0}} \left\{ \frac{\partial \phi^{(1)}}{\partial t} + g \tau_3^{(1)} + \frac{1}{2} \vec{\tau}^{(1)} \cdot \nabla \left(\vec{V} \cdot \vec{V} \right) + \vec{V} \cdot \nabla \phi^{(1)} \right\} \left\{ \delta \vec{h}^{\,j} \cdot \delta \vec{n} \right\}^{(1)} dS \\ & - \rho \iint_{S_{B_0}} \left\{ \left(\vec{V} - \frac{1}{2} \nabla \Phi \right) \cdot \nabla \Phi + gz \right\} \left\{ \delta \vec{h}^{\,j} \cdot \delta \vec{n} \right\}^{(2)} dS \end{aligned} \tag{2.35}$$

2.7 Equation of motion in generalized mode

2.7.1 Generalized inertial force

Several generalized forces should be included to derive the equation of motion for the hydroelastic response. As the generalized force on the body, the inertial force shows the relation between inertia of the body mass and external force. Using the conservation of momentum, the inertial force of the body mass for the translational and rotational motion is expressed as follows (Newman, 1977):

$$\vec{F}' = \iiint_{V_b} \rho_s \left(\ddot{\vec{\alpha}}_T + \ddot{\vec{\alpha}}_R \times \vec{x} \right) dV \tag{2.36}$$

$$\vec{M}' = \iiint_{V_b} \rho_s \vec{X} \times \left(\ddot{\vec{\alpha}}_T + \ddot{\vec{\alpha}}_R \times \vec{x} \right) dV \tag{2.37}$$

where $\ddot{\vec{\alpha}}_T$: translational acceleration, $\ddot{\vec{\alpha}}_R$: rotational acceleration

In the generalized mode, these inertial forces can be redefined as follows:

$$F_j = \iiint_{V_b} \rho_s \left(\vec{h}_t^{\,j} \cdot \ddot{\vec{\tau}} \right) dV \tag{2.38}$$

$\vec{h}_t^{\,j}$ is the transformed modal vector where each position is described at inertial coordinates.

The non-linear inertial force could also be approximated by taking perturbation series in the following form.

$$F_j = \iiint_{V_b} \rho_s \left\{ \vec{h}_t^{\,j(0)} + \vec{h}_t^{\,j(1)} \right\} \cdot \left\{ \ddot{\vec{\tau}}^{(1)} + \ddot{\vec{\tau}}^{(2)} + \ddot{\vec{\gamma}}^{(2)} \right\} dV \tag{2.39}$$

After collecting the terms of each order, the first- and second-order inertial forces are expressed as follows:

$$F_j^{(1)} = \iiint_{V_b} \rho_s \left\{ \vec{h}_t^{\,j(0)} \cdot \ddot{\vec{\tau}}^{(1)} \right\} dV \tag{2.40}$$

$$F_j^{(2)} = \iiint_{V_b} \rho_s \left\{ \vec{h}_t^{\,j(0)} \cdot \left(\ddot{\vec{\gamma}}^{(2)} + \ddot{\vec{\tau}}^{(2)} \right) + \vec{h}_t^{\,j(1)} \cdot \ddot{\vec{\tau}}^{(1)} \right\} dV \tag{2.41}$$

Here, $\vec{h}_t^{\,j(0)} \cdot \ddot{\vec{\gamma}}^{(2)}$ becomes the time derivative of a dyadic product between the body-mass inertia and the angular velocity which include quadratic inertial force when the mode shape is rotational motion (Ogilvie, 1983). The vector identity between Eqs. (2.37), (2.41) on a rigid body and the quadratic inertial force for rotational motion is described in Appendix B. The linear inertial force can also be expressed by using the mass matrix which is defined by the inner product of each mode-shape function (Newman, 1977).

$$\mathrm{M}_{ij} \ddot{\xi}_j^{(1)} = F_i^{(1)} \tag{2.42}$$

$$\mathrm{M}_{ij} = \iiint_{V_b} \rho_s \left(\vec{h}^{\,i} \cdot \vec{h}^{\,j} \right) dV \tag{2.43}$$

By substituting the mode shape (1~6 modes; translation and rotation) into Eq. (2.43), we can confirm the classic mass matrix.

$$\left(h^1, h^2, h^3 \right) = (i, j, k), \ \left(h^4, h^5, h^6 \right) = (i, j, k) \times \vec{x} \tag{2.44}$$

$$\mathrm{M}_{ij} = \begin{bmatrix} m & 0 & 0 & 0 & mz_g & -my_g \\ 0 & m & 0 & -mz_g & 0 & mx_g \\ 0 & 0 & m & my_g & -mx_g & 0 \\ 0 & -mz_g & my_g & I_{11} & I_{12} & I_{13} \\ mz_g & 0 & -mx_g & I_{21} & I_{22} & I_{23} \\ -my_g & mx_g & 0 & I_{31} & I_{32} & I_{33} \end{bmatrix} \tag{2.45}$$

$$\text{where } I_{ij} = \iiint_V \rho_s \left(x_{ii}\delta_{ij} - x_i x_j \right) dV$$

2.7.2 Generalized gravity restoring force

The body could have the gravity restoring force due to rotation in case that the mode shape has variation. This force could be written in the generalized mode as follows (Malenica *et al*., 2003):

$$F_{m_j} = -g \iiint_{V_b} \rho_s \left(\delta\vec{h}_j \cdot \vec{k} \right) dV \tag{2.46}$$

This can also be approximated up to second-order by using perturbation series, and the results can be written as

$$F_{m_j} \approx F_{m_j}^{(1)} + F_{m_j}^{(2)} = -g \iiint_{V_b} \rho_s \left(\delta\vec{h}_j^{(1)} + \delta\vec{h}_j^{(2)} \right) \cdot \vec{k} dV \tag{2.47}$$

$$F_{m_j}^{(1)} = -g \iiint_{V_b} \rho_s \left(\nabla\vec{h}^{\,j} \cdot \vec{\tau}^{(1)} \right) \cdot \vec{k} dV \tag{2.48}$$

$$F_{m_j}^{(2)} = -g \iiint_{V_b} \rho_s \left(\nabla\vec{h}^{\,j} \cdot \vec{\tau}^{(2)} + \nabla\vec{h}^{\,j} \cdot \vec{\gamma}^{(2)} \right) \cdot \vec{k} dV \tag{2.49}$$

In the linear wave-body problem, the force is proportional to the displacement and therefore it is usually included in the restoring stiffness of both rigid and elastic bodies (Senyanovic *et al.*, 2007). In the second-order force, the first term means the force by pure second-order displacement and it is usually included in the second-order restoring coefficient.

2.7.3 Linear & second-order equations of motion

From Newton's equations, both first- and second-order equations of motion in the generalized mode can be derived by considering several generalized forces already described together with structural stiffness. The motion equations in the *i*-th direction are written as follows:

$$\sum_{j=1}^{N}\left[-\omega^2\left(\mathrm{M}_{ij}+a_{ij}^{(1)}\right)+i\omega b_{ij}^{(1)}+\mathrm{K}_{ij}+\mathrm{C}_{ij}\right]\xi_j^{(1)}=\left|F_{ex_i}^{(1)}\right|e^{i\theta_{ex}} \tag{2.50}$$

$$\begin{aligned}&\sum_{j=1}^{N}\left[-4\omega^2\left(\mathrm{M}_{ij}+a_{ij}^{(2)}\right)+2i\omega b_{ij}^{(2)}+\mathrm{K}_{ij}+\mathrm{C}_{ij}\right]\xi_j^{(2)}\\&=\left|F_{p_i}^{(2)}\right|e^{i\theta_p}+\left|F_{q_i}^{(2)}\right|e^{i\theta_q}+\iiint_{V_b}\rho_s\left\{\omega^2\left(\vec{h}^i\cdot\vec{\gamma}^{(2)}+\vec{h}_t^{i(1)}\cdot\vec{\tau}^{(1)}\right)-g\left(\nabla\vec{h}^i\cdot\vec{\gamma}^{(2)}\right)\cdot\vec{k}\right\}dV\end{aligned} \tag{2.51}$$

where $\theta_{p,q,ex}$ is the phase angle of each external force, Here, the external moment should be described based on the origin of body-fixed coordinates.

CHAPTER 3

Numerical implementation

3.1 Boundary integral equation (BIE)

In 3-diemnsional wave-body interaction, the boundary integral equation with potential flow assumption has been used widely. Its basic form is expressed as follows:

$$C(P)\phi_S^{(m)}(P)+\iint_{S_T}\phi_S^{(m)}(Q)\frac{\partial G(P,Q)}{\partial n_Q}dS(Q)=\iint_{S_T}G(P,Q)\frac{\partial \phi_S^{(m)}(Q)}{\partial n_Q}dS(Q) \tag{3.1}$$

where $P = (X,Y,Z)$ means a field point; $Q = (X',Y',Z')$ means a source point; $C(P)$ means the solid angle at the field point P; S_T is entire computational domain ($S_F+S_B+S_D+S_C$).

3.2 Higher-order boundary element method (HOBEM)

Boundary integral equation could be solved analytically or numerically by numerous ways. In the light of a general geometry of body model, numerical integration is conducted with Green function which is called boundary element method (BEM). In this study, the boundary integral equation is discretised numerically by quadrilateral panel to solve boundary-value problem. At first, the integral domain is segmented into each quadrilateral panel. It is written by

$$C(P)\phi_S^{(m)}(P)+\sum_{j=1}^{N_T}\iint_{e_j}\phi_S^{(m)}(Q)\frac{\partial G(P,Q)}{\partial n_Q}dS(Q)=\sum_{j=1}^{N_T}\iint_{e_j}G(P,Q)\frac{\partial \phi_S^{(m)}(Q)}{\partial n_Q}dS(Q) \tag{3.2}$$

In HOBEM, the velocity potential is approximated to summation of the value at each node by bi-quadratic shape function in the panel. It is expressed in this form.

$$\phi_S^{(m)} = \sum_{i=1}^{9} N_i(u,v)\phi_{S_i}^{(m)} \tag{3.3}$$

where N_i is shape function

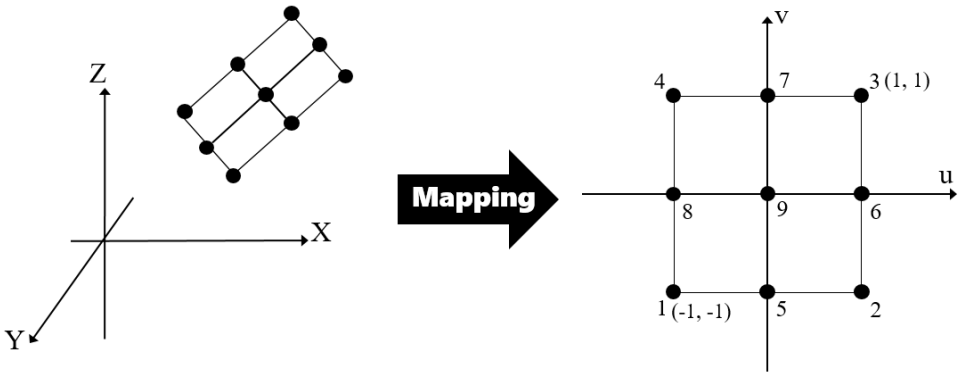

Fig. 3.1 Mapping from inertial coordinates to local coordinates on a panel

Here, the velocity potential could be interpolated in the local coordinates which was mapped from inertial coordinates (*See* Fig. 3.1). In this coordinates, each shape function has following form.

$$\begin{aligned}
&N_1(u,v) = \frac{(u-1)(v-1)uv}{4}, N_2(u,v) = \frac{(u+1)(v-1)uv}{4}, N_3(u,v) = \frac{(u+1)(v+1)uv}{4} \\
&N_4(u,v) = \frac{(u-1)(v+1)uv}{4}, N_5(u,v) = \frac{(1-u^2)(v-1)v}{2}, N_6(u,v) = \frac{(u+1)(1-v^2)u}{2} \\
&N_7(u,v) = \frac{(1-u^2)(v+1)v}{2}, N_8(u,v) = \frac{(u-1)(1-v^2)u}{2}, N_9(u,v) = (1-u^2)(1-v^2)
\end{aligned} \tag{3.4}$$

Substituting Eq. (3.3) into boundary integral equation Eq. (3.2), each integration is composed of shape function and velocity potential on the node with Green's function. It is as follows:

$$\begin{aligned}
&C(P)\phi_S^{(m)}(P) + \sum_{j=1}^{N_T} \iint_{e_j} \sum_{i=1}^{9} N_i(u,v)\phi_{S_i}^{(m)}(Q) \frac{\partial G(P,Q)}{\partial n_Q} dS(Q) \\
&= \sum_{j=1}^{N_T} \iint_{e_j} G(P,Q) \sum_{i=1}^{9} N_i(u,v) \frac{\partial \phi_{S_i}^{(m)}(Q)}{\partial n_Q} dS(Q)
\end{aligned} \tag{3.5}$$

The integration of shape function with Green's function can be obtained provided geometry of all boundaries is given. Thus, velocity potential can go out from the integration. It is written by

$$\begin{aligned} C(P)\phi_S^{(m)}(P) + \sum_{j=1}^{N_T}\sum_{i=1}^{9}\phi_{S_i}^{(m)}\iint_{e_j} N_i(u,v)\frac{\partial G(P,Q)}{\partial n_Q}dS(Q) \\ = \sum_{j=1}^{N_T}\sum_{i=1}^{9}\frac{\partial \phi_{S_i}^{(m)}(Q)}{\partial n_Q}\iint_{e_j} G(P,Q)N_i(u,v)dS(Q) \end{aligned} \tag{3.6}$$

The evaluation of integration is conducted by using different ways depending on strength of the singularity. The detail description of evaluation for each integration and solid angle of HOBEM is described in Zhang (2018).

3.3 Green's function

In potential flow solver, several kinds of Green's function have been used. In time-domain simulation, we adopted Rankine source as a Green's function. It is defined in this form.

$$G(P,Q) = \frac{1}{R_1} + \frac{1}{R_2} \tag{3.7}$$

where $$\begin{cases} R_1 = \sqrt{(X-X')^2 + (Y-Y')^2 + (Z-Z')^2} \\ R_2 = \sqrt{(X-X')^2 + (Y-Y')^2 + (Z+Z'+2H)^2} \end{cases}$$

The bottom condition is automatically satisfied by adding image source R_2. Using symmetric property of body geometry and velocity potential, only half-domain in total surface is considered for the simulation. After applying boundary conditions to the integral equation and collecting unknown and known values at each boundary on the left- and right-hand sides respectively, a matrix form is obtained in the following form:

$$\begin{bmatrix} A_1 & A_2 \end{bmatrix} \begin{Bmatrix} \phi_S^{(m)}\big|_{S_{B_0}} \\ \dfrac{\partial \phi_S^{(m)}}{\partial n}\Big|_{S_{F_0}} \end{Bmatrix} = \begin{bmatrix} B_1 & B_2 \end{bmatrix} \begin{Bmatrix} \dfrac{\partial \phi_S^{(m)}}{\partial n}\Big|_{S_{B_0}} \\ \phi_S^{(m)}\big|_{S_{F_0}} \end{Bmatrix} \tag{3.8}$$

where *A* and *B* mean influence matrices which include an integral over a discretised panel in terms of the Green function together with shape function, respectively. The velocity potential is obtained by solving Eq. (3.8) at each boundary in the perturbation series.

3.4 Calculation of several derivatives in HOBEM

In the perturbation method, several spatial derivative of velocity potential should be calculated. Many kinds of method have been suggested to obtain derivative of velocity potential. It is well known that the first derivative could be conducted by using derivative of integral equation without any difficulty. It could also be obtained by using shape function because the velocity potential is approximated by mathematical formulation in HOBEM. First derivative of velocity potential is expressed in this form.

$$\begin{pmatrix} \phi_X \\ \phi_Y \\ \phi_Z \end{pmatrix} = \begin{pmatrix} X_u & Y_u & Z_u \\ X_v & Y_v & Z_v \\ n_X & n_Y & n_Z \end{pmatrix}^{-1} \begin{pmatrix} \phi_u \\ \phi_v \\ \phi_n \end{pmatrix} \tag{3.9}$$

On the other hands, it is relatively difficult to obtain second derivative of variable than first derivative of it. If double differentiation for the integral equation is conducted, the singularity is much more increased in Green's function and numerical error is expected due to hyper singularity. To increase the accuracy of second derivative quantities, other methods have been suggested based on boundary integral equation.

For instance, using desingularized BEM and geometry of a body model, first derivative of velocity potential is obtained and then differentiation for the boundary integral equation is conducted to obtain second derivatives of velocity potentials(*e.g.* Shao, 2010). Similar way is also applied on Dirichlet type formulation (Chen and Malenica, 1996; Lee *et al*., 2017). In this method, first derivative of velocity potential is substituted to Dirichlet type equation and it is differentiated to obtain second derivative of velocity potential.

In case HOBEM is adopted, second derivative of shape function could be used directly as same with calculation of first derivative quantities. There are two types of formulation on second derivative as used in Choi *et al*. (2001) and Kim (1996). They are as follows:

$$\begin{pmatrix}\phi_{XX}\\ \phi_{YY}\\ \phi_{XY}\\ \phi_{XZ}\\ \phi_{YZ}\end{pmatrix}=[D]^{-1}\left[\begin{pmatrix}\phi_{uu}\\ \phi_{vv}\\ \phi_{uv}\\ \phi_{nu}\\ \phi_{nv}\end{pmatrix}-\begin{pmatrix}X_{uu} & Y_{uu} & Z_{uu}\\ X_{vv} & Y_{vv} & Z_{vv}\\ X_{uv} & Y_{uv} & Z_{uv}\\ n_{Xu} & n_{Yu} & n_{Zu}\\ n_{Xv} & n_{Yv} & n_{Zv}\end{pmatrix}\begin{pmatrix}\phi_X\\ \phi_Y\\ \phi_Z\end{pmatrix}\right] \tag{3.10}$$

where, $$[D]=\begin{bmatrix} & X_u^2-Z_u^2 & Y_u^2-Z_u^2 & 2X_uY_u & 2X_uZ_u & 2Y_uZ_u\\ & X_v^2-Z_v^2 & Y_v^2-Z_v^2 & 2X_vY_v & 2X_vZ_v & 2Y_vZ_v\\ X_uX_v-Z_uZ_v & Y_uY_\eta-Z_uZ_\eta & X_uY_v+X_\eta Y_u & X_uZ_v+X_vZ_u & Y_uZ_v+Y_\eta Z_u\\ n_ZX_u-n_ZZ_u & n_YX_u-n_ZZ_u & n_YX_u+n_XY_u & n_ZX_u+n_XZ_u & n_ZY_u+n_YZ_u\\ n_ZX_v-n_ZZ_v & n_YX_v-n_Zz_v & n_YX_v+n_XZ_v & n_ZX_v+n_XZ_v & n_ZY_v+n_Yz_v\end{bmatrix}$$

$$\begin{Bmatrix}\phi_{XX}\\ \phi_{XY}\\ \phi_{XZ}\\ \phi_{YY}\\ \phi_{YZ}\end{Bmatrix}=\left\{[S]^T[S]\right\}^{-1}[S]^T\begin{Bmatrix}\phi_{X\xi}\\ \phi_{X\eta}\\ \phi_{Y\xi}\\ \phi_{Y\eta}\\ \phi_{Z\xi}\\ \phi_{Z\eta}\end{Bmatrix}\quad\text{where } S=\begin{pmatrix}X_u & Y_u & Z_u & 0 & 0\\ X_v & Y_v & Z_v & 0 & 0\\ 0 & X_u & 0 & Y_u & Z_u\\ 0 & X_v & 0 & Y_v & Z_v\\ -Z_u & 0 & X_u & -Z_u & Y_u\\ -Z_v & 0 & X_v & -Z_v & Y_v\end{pmatrix} \tag{3.11}$$

The accuracy in second derivative variables on the ship hull surface is checked by using a simple Rankine source ($1/4\pi R$) where the source and field points are arbitrarily located on and outside the body surface. Two numerical results obtained by Eqs. (3.10-11) and the analytic solution for the second derivative of Rankine source on the line of hull surface are depicted in Fig. 3.2.

In the calculation, the numbers of body-surface division used in the *X*- and *Z*-directions are 48 and 8, respectively. It can be seen from this figure that both numerical methods provide good agreement with analytic solution, but judging from the results, the first equation (3.10) provides more stable result than the second equation (3.11). Thus we adopted the first equation in our simulation. These results suggest that when the velocity potential has smooth value, the second-derivative of velocity potential could be obtained accurately by using the shape function in HOBEM.

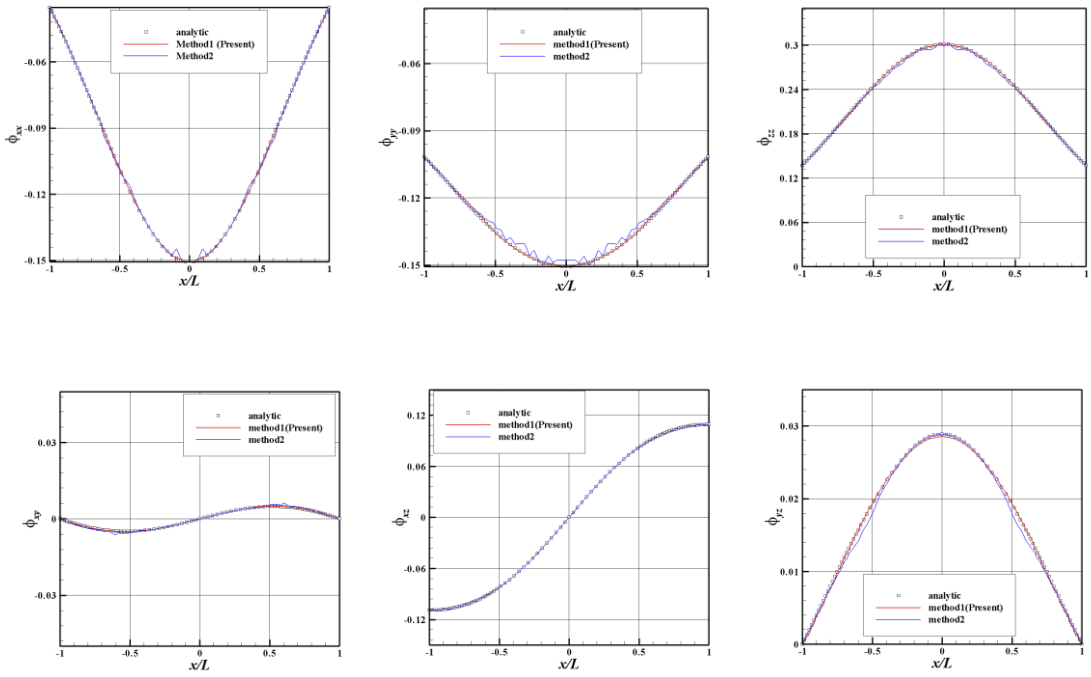

Fig. 3.2 Comparison of second derivatives at source point between numerical methods and analytic solution

It is known that spatial derivative on the free-surface makes numerical instability in Rankine panel method. In the ship forward speed problem, derivative for *X*-direction on a free-surface is calculated by using 3-point upwind scheme which gives more stable solution in the forward speed problem. It is as follows:

$$\frac{\partial \phi}{\partial X} = \frac{X_3^2(\phi_2 - \phi_1) + X_2^2(\phi_2 - \phi_1)}{X_2 X_3 (X_3 - X_2)} \tag{3.12}$$

where X_i and ϕ_i mean the *X*-coordinates and velocity potential at the *i*-th node with assumption ($X_1 = 0$).

3.5 Time-marching scheme

In the time-domain simulation, initial-value problem should be solved. Physical quantities of next time step is predicted by using present values. In our simulation, the explicit Runge-Kutta 4th-order method is adopted. Unsteady velocity potential and wave elevation are updated on free-

surface and body boundary conditions at each time step after determining the coefficients of Runge-Kutta. It is expressed in this form.

$$\left[\phi_{n+1},\zeta_{n+1}\right]=\left[\phi_n,\zeta_n\right]+\frac{1}{6}\left(k_1+2k_1+2k_3+k_4\right)\Delta t \tag{3.13}$$

where k_n: coefficients for Runge-Kutta fourth-order, n : present time step

In the freely-floating body, the calculation of unsteady displacement and velocity of a body model are obtained by using 4th-order Runge-Kutta-Nystrom method. They are expressed in this form (Koo and Kim, 2004).

$$\xi'' = f\left(t,\xi,\xi'\right) \tag{3.14}$$

$$\begin{gathered} k_1=\frac{1}{2}\Delta t f\left(t_n,\xi_n,\xi_n'\right),\ k_2=\frac{1}{2}\Delta t f\left(t_n+\frac{1}{2}\Delta t,\xi_n+K,\xi_n'+k_1\right) \\ k_3=\frac{1}{2}\Delta t f\left(t_n+\frac{1}{2}\Delta t,\xi_n+K,\xi_n'+k_2\right),\ k_4=\frac{1}{2}\Delta t f\left(t_n+\Delta t,\xi_n+L,\xi_n'+2k_3\right) \end{gathered} \tag{3.15}$$

$$\text{where } K=\frac{1}{2}\Delta t\left(\xi_n'+\frac{1}{2}k_1\right),\ L=\Delta t\left(\xi_n'+k_3\right)$$

Using obtained acceleration in the equation of motion, velocity and displacements are updated every time step.

In the initial time steps, Ramp function (Γ) is applied over the several wave periods (T_e) to prevent sudden increase of a response. The function is written by

$$\Gamma=\begin{cases} 0.5\left(1.0-\cos\left(\dfrac{t}{2T_e}\pi\right)\right) & \left(t\le nT_e\right) \\ 1.0 & \left(t>nT_e\right) \end{cases} \tag{3.16}$$

3.6 Type of grid on free-surface

In Rankine panel method, panel mesh exists on both body and free-surface boundaries. The free-surface mesh has two kinds of shape (*See* Fig.3.3); *i.e.* oval and rectangular types of grid. Each shape has advantage and disadvantage.

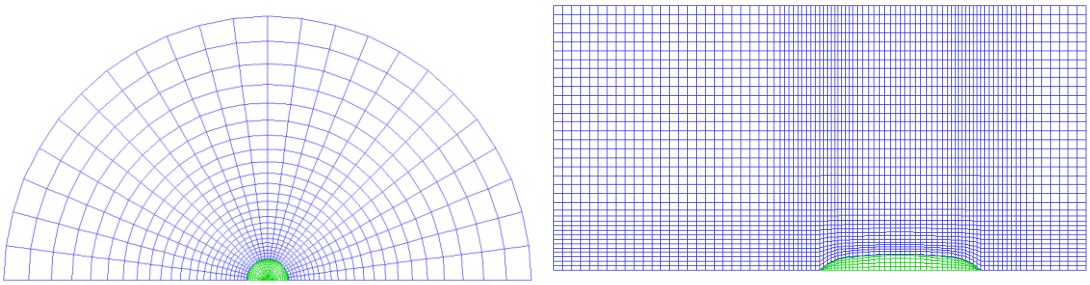

Fig. 3.3 Top view of computation region and panels on the oval/rectangular type free-surface

It is known that generally the oval type grid is more efficient and on the other hands, the rectangular type grid needs more number of mesh but it is more stable than oval type grid. In our simulation, axis-symmetric body is calculated on the oval type free-surface and other general bodies such as ship, barge models are simulated on rectangular type of grid.

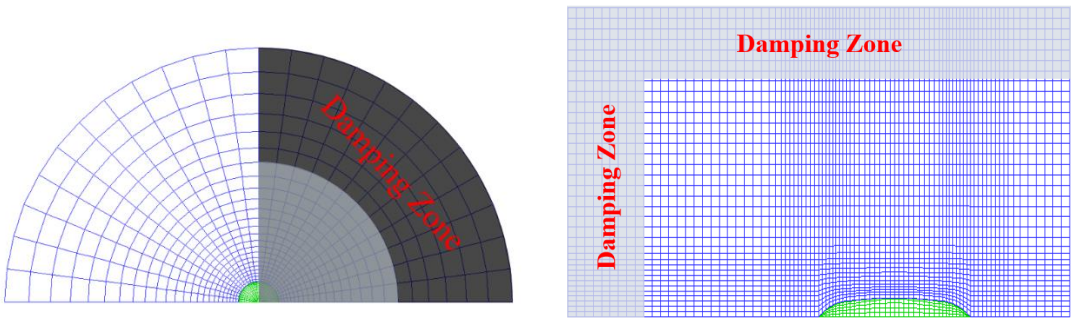

Fig. 3.4 Numerical damping beach at each free-surface type

3.7 Numerical damping beach

In time-domain simulation, the radiation condition is satisfied by using numerical damping scheme to prevent making reflected waves. The general damping zone of each type of grid is shown in the Figure 3.4. In the zero forward speed problem, the artificial damping is installed the edge of free-surface. On the other hands, a ship model with forward speed has damping beach only edge of horizontal direction and downstream region on the free-surface. In damping zone, the artificial damping is added on kinematic free-surface boundary conditions. It is as follows:

$$\frac{\partial \zeta_s^{(m)}}{\partial t} + \vec{V} \cdot \nabla \zeta_s^{(m)} = \frac{\partial \phi_s^{(m)}}{\partial Z} - \left(\frac{\partial \zeta_I^{(m)}}{\partial t} - \frac{\partial \phi_I^{(m)}}{\partial Z} \right) - \vec{V} \cdot \nabla \zeta_I^{(m)} + f_m - 2\nu \zeta_s^{(m)} + \frac{\nu^2}{g} \phi_s^{(m)} \qquad (3.17)$$

$$\text{where } \nu = \begin{cases} \alpha\omega \left(\frac{r - r_0}{L_R} \right)^2 & (r > r_0) \\ 0 & (r \le r_0) \end{cases}$$

and α is strength of damping and L_R is the length of damping zone

3.8 Numerical filter

Simulations of wave-body interaction could have various instabilities especially on the free-surface. As one of the instabilities, the free-surface has the so-called saw-tooth behaviour. Using a low-pass filter is a simple way to prevent this kind of instability. However, the numerical filter could affect the result if the strength and operation frequency are high. In this simulation, the three-point low-pass filter (Shao and Faltinsen, 2010) is applied to the wave elevation to reduce the effect of a filter. The equation adopted is as follows:

$$\bar{\zeta}_j = c\zeta_{j-1} + (1-2c)\zeta_j + c\zeta_{j+1} \qquad (3.18)$$

where j is a node number of collocation point used in the numerical filter and $\bar{\zeta}$ is a new wave elevation after filtering. The strength of numerical filter (c) is decided by considering the wave period and time step size, and the value of c is fixed equal to 0.025 in all simulations. Numerical filter is operated once per 10 time steps for the linear wave elevation and once per 5 time steps for the non-linear wave elevation.

CHAPTER 4

Numerical study by time-domain analysis in monochromatic waves

4.1 Introduction

In this chapter, direct time-domain simulation by using developed HOBEM code and modal approach is implemented for the analysis of the wave-body interaction at different situations of monochromatic waves. Since the second-order springing of an elastic body is complex to be solved directly, the numerical simulation is conducted step by step.

In chapter 4.2, necessary convergence study is introduced before numerical calculation. The generalized mode approach is applied on both rigid and elastic bodies. In chapter 4.3, the wave-body interaction of a rigid body without forward speed is conducted and it is extended to forward speed problem in chapter 4.4. In the last, the numerical study is applied on an elastic body without/with forward speed in chapter 4.5 & 4.6, respectively.

4.2 Convergence study

Convergence study is important for the validation of new code and it should be performed systematically. Before conducting numerical calculation, convergence study is conducted on hemisphere, vertical cylinder in zero forward speed problem and Wigley1 model in forward speed problem. As one of the most important factors in time-domain Rankine panel method, 3 components are considered for convergence study such as computational domain size, time step size, mesh size (He and Kashiwagi, 2014).

4.2.1 Computational domain size

Convergence study for the length of free-surface domain is implemented. During this study, both first-order and second-order quantities are confirmed for computational domain size. The free-surface length is one of the important parameters which could affect the simulation results. Especially there are additional forcing terms composed of several quadratic products in the second-order free-surface boundary condition. It is known that the exact evaluation of free-surface integral in the second-order boundary-value problem is crucial and difficult work. In the present research, we adopted a simple Rankine source as the Green function with rectangular/oval type free surface which is shown in Fig. 3.3. It makes the free-surface integration readily be evaluated. However, the region of integration is definite, thus sufficient extent of the free surface should be given.

In all cases in zero forward speed problem, length of damping zone size is fixed on half of total free-surface length on oval type free-surface. Figure 4.1 is the second-order hydrodynamic force at different free-surface domain size. This figure shows that the result is different depending on computational domain size. It seems that enough length of free-surface should be adopted. During this study, over 2.0 wave lambda of free-surface length is used for simulation in case oval type of grid is chosen.

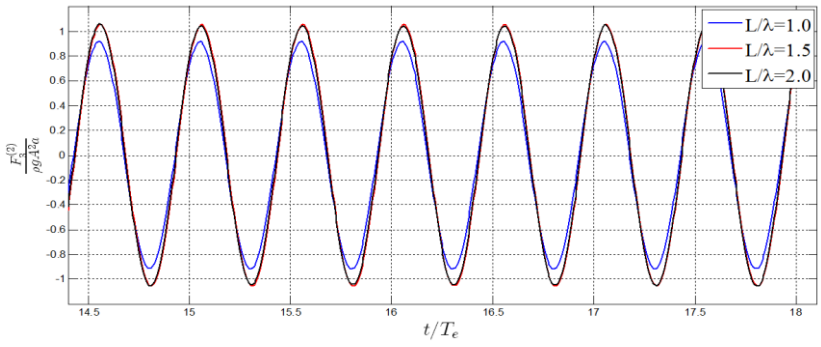

Fig. 4.1 Sensitivity of second-order hydrodynamic force to free-surface length for hemisphere

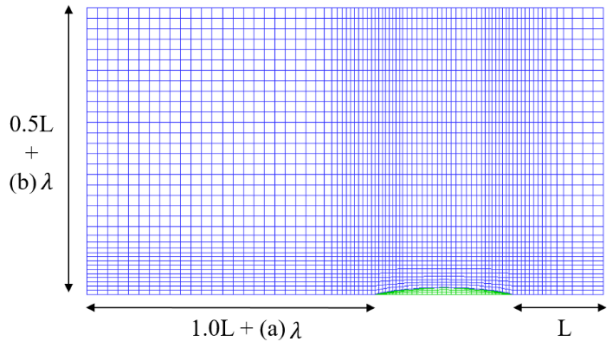

Fig. 4.2 Top view of computation region and rectangular panels on free surface

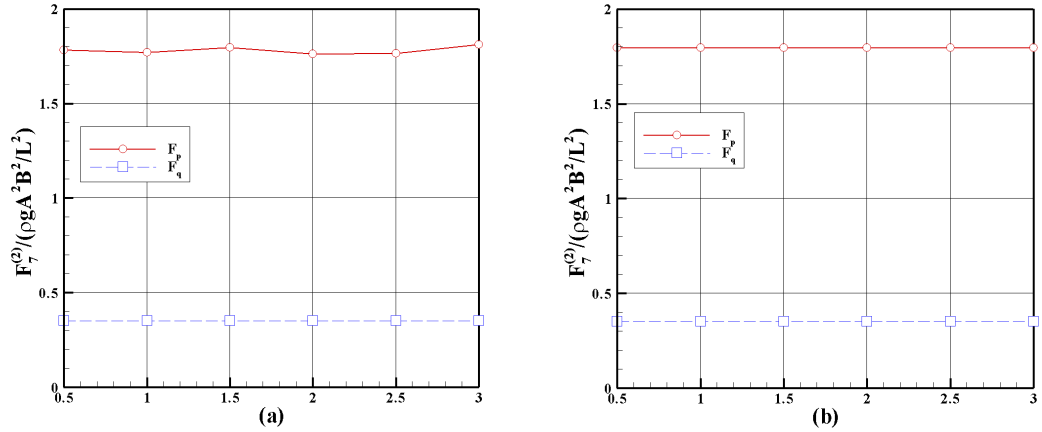

Fig. 4.3 Second-order hydrodynamic force at different free-surface length (wave frequency: 5.5 rad/s, at Fn = 0.2)

In the forward speed problem, we checked both longitudinal and lateral lengths of the free surface from the ship model. Figure 4.3 is the second-order hydrodynamic force when different free-surface lengths are used. The left figure shows the influence of the longitudinal free-surface length (a) defined in Fig. 4.2, and likewise the right figure shows the influence of the lateral free-surface length (b). The result shows that the second-order velocity-potential force (F_p) has continuously small oscillation depending on the longitudinal free-surface length and the quadratic-product force (F_q) composed of linear solutions does not change. On the other hand, the lateral free-surface length does not give any effect on both quadratic-product force and second-order velocity-potential force. From these confirmations, we adopted 1.5 for the values of (a) and (b) as the free-surface length. Here, a numerical damping beach for satisfying the radiation condition is

installed for 0.5 and 1.0 wave length (λ) in the lateral and longitudinal directions, respectively, from the edge of free-surface region.

4.2.2 Time step size

Large time step makes numerical result be unstable and it may not give convergent result. Fig. 4.4 shows second-order hydrodynamic force at different time step size. Compared to the free-surface length, it does not show large sensitivity. However, there is little difference between results. In this study, $\Delta t/T_e = 200$ is used for all cases.

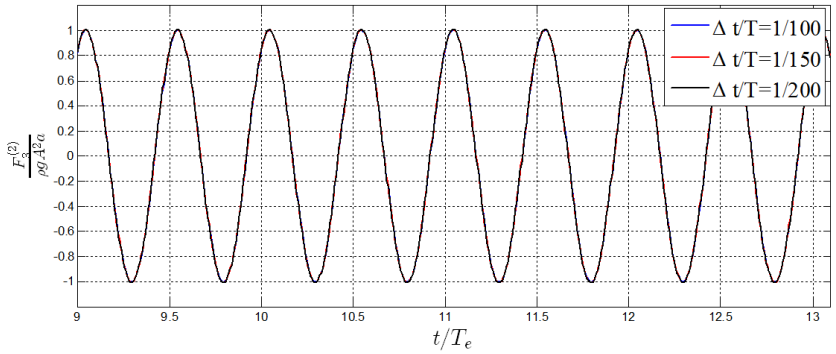

Fig. 4.4 Sensitivity of second order hydrodynamic force to time step for hemisphere

4.2.3 Mesh size

Table 4.1 A list of number of body and free-surface panel

Model	No. of Body panel	No. of Free-surface panel
Test Mesh1	75	270
Test Mesh2	120	400
Test Mesh3	300	900
Hemisphere	300	900
Vertical circular cylinder	400~1000	1000~1200

It is well known that the second-order forces are more sensitive to the number of panels on both body and free-surface boundaries. The sensitivity test at a short wave region is conducted with different panel size. In the higher-order boundary element method (HOBEM), body and free-surface boundaries share several nodes on the intersection waterline. Thus, the increase in the number of body-surface panels also increases the number of free-surface panels. Table 1 shows a list of number of mesh used in convergence study at zero speed problem and Fig. 4.5 is the result

of second-order hydrodynamic force at different mesh size. It shows fast convergence for panel mesh and Mesh3 gives enough convergent result for second-order hydrodynamic force. In this study, 300 body panels and 900 free-surface panels are used for hemisphere in half domain and more many number of mesh is used for vertical circular cylinder to remove an error by mesh problem.

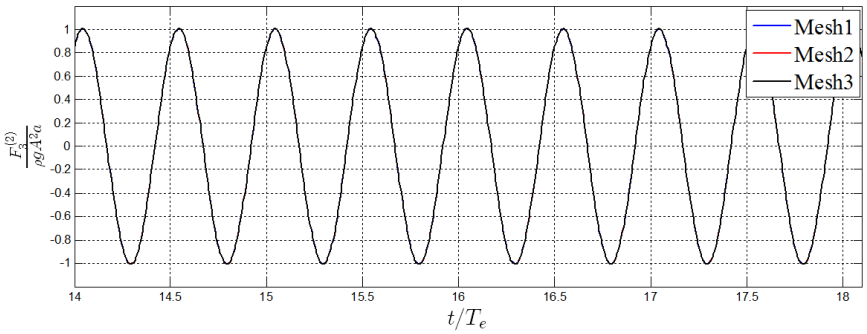

Fig. 4.5 Sensitivity of second order hydrodynamic force to mesh size for hemisphere

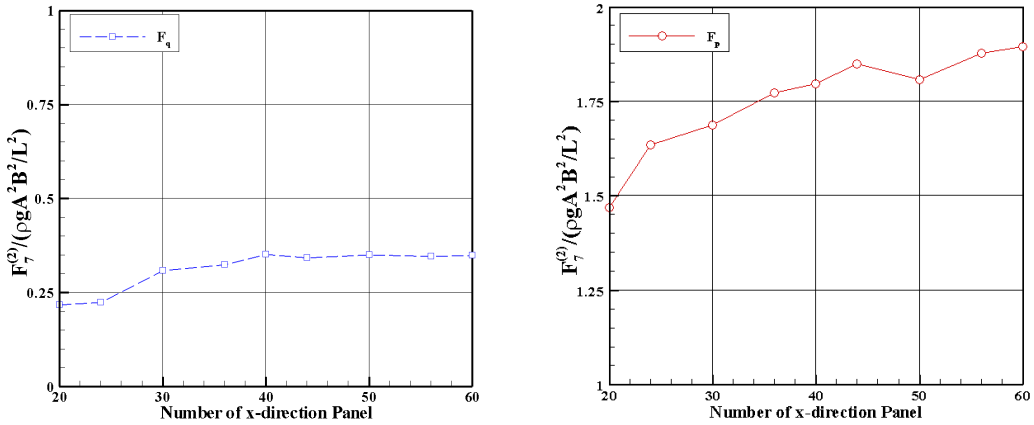

Fig. 4.6 Second-order hydrodynamic force at different number of panels (wave frequency: 5.5 rad/s, at *Fn* = 0.2)

In the forward speed problem, effect of panel mesh is more sensitive than zero forward speed problem. The result of second-order hydrodynamic force at different number of panels is denoted on figure 4.6. The left is the result of quadratic-product force of linear quantities (F_q). It shows that 40 panels for the longitudinal direction gives almost converged result. However, in the right figure for the second-order velocity-potential force (F_p), the result is not converged even with 40 panels in the longitudinal direction. Since the second-order velocity potential is influenced by the free-surface and body-surface panels and both boundaries include second-derivatives of the

velocity potential which have crucial effect on accuracy, the force is much more sensitive to the number of panels on the boundaries. Although we could not obtain fully converged result on the second-order velocity-potential force, we used a large number of panels with where the quadratic-product force shows a converged result.

4.3 Numerical study without forward speed (rigid model)

As a first validation process, linear & second-order hydrodynamic forces for the rigid body motion are confirmed by comparing with classical results. In zero forward speed problem, wave-body interaction at different conditions such as fixed & forced oscillating & freely floating are simulated and the numerical result is discussed.

4.3.1 Fixed body

1) Hemisphere

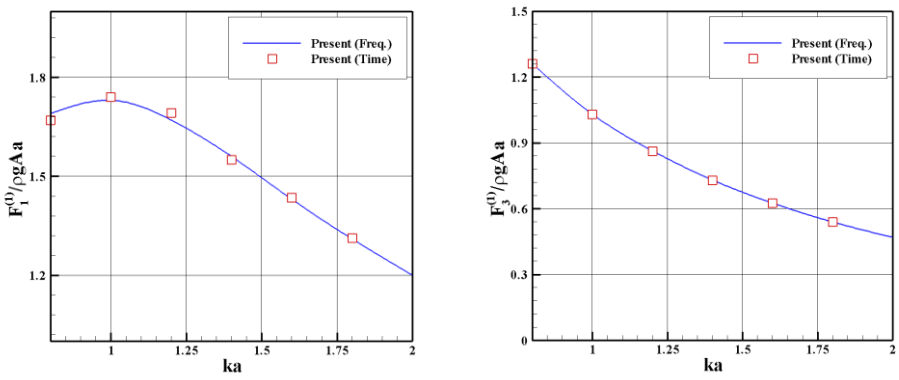

Fig. 4.7 The amplitude of linear surge & heave exciting forces for fixed hemisphere ($H = 3a$)

A fixed hemisphere is studied for sum-frequency hydrodynamic force in the second-order. The water depth is $H=3a$ (a: Radius of hemisphere) and before comparing with sum-frequency hydrodynamic forces, linear quantity is first checked. Figure 4.7 is surge and heave linear wave exciting forces for fixed hemisphere. It shows a good agreement with result of another frequency-domain in-house code.

The second-order diffraction problem on a fixed hemisphere is studied by several researchers. In this study, the result of Kim and Yue (1990), Shao and Faltinsen (2010) are compared with the present result. As mentioned in chapter 2, second-order hydrodynamic force could be divided two

components at diffraction problem. First component is caused by second order velocity potential (F_p). Another component is quadratic product of linear quantities (F_q).

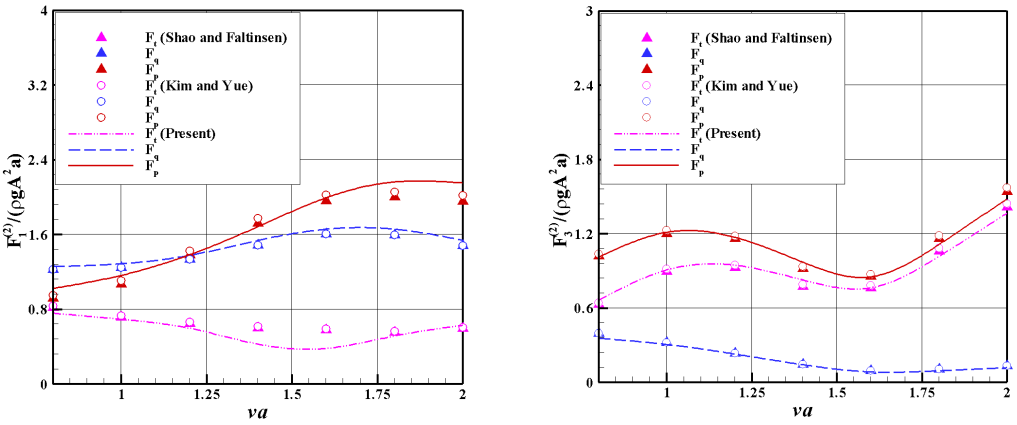

Fig. 4.8 The amplitude of sum-frequency surge & heave forces for fixed hemisphere ($H = 3a$)

Figure 4.8 is non-dimensional amplitude of surge and heave sum-frequency hydrodynamic force on a fixed hemisphere. It shows second-order velocity potential component is substantial in sum-frequency hydrodynamic force. Especially short wave length region, contribution of second order velocity potential becomes larger. Both second-order velocity potential and quadratic product of linear quantities forces show a good agreement with other papers.

2) Vertical cylinder

Vertical cylinder is frequently used for the validation study of developed code in hydrodynamic field because there are many kinds of solution in both linear and non-linear variables. The eigen-function expansion method is particularly often used for different situations such as bottom mounted or surface piercing column, multi-column, and so forth. Present numerical result is compared with that of bottom-mounted and truncated vertical cylinders.

First, fixed truncated vertical cylinder which has same draft (d) with radius (a) is considered and water depth (H) is chosen to 2 radius (a). The linear wave exciting and drift force results are compared with that of Kinoshita *et al.* (1997), Shao (2010). In Kinoshita *et al.* (1997), the result is obtained by numerical method based on BEM. Figure 4.9 is the amplitude of non-dimensional surge and heave linear wave exciting forces and shows a good agreement with other results. In

sequence, Figure 4.10 is the amplitude of non-dimensional surge drift force. It also shows a good agreement overall frequencies.

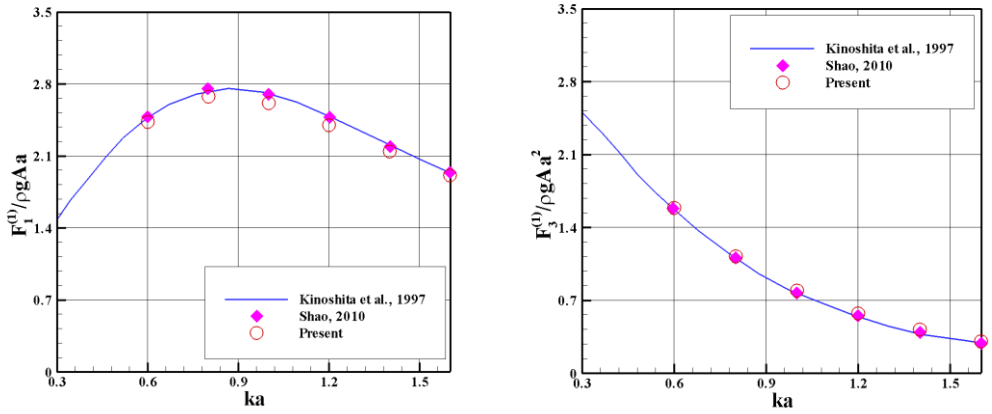

Fig. 4.9 The amplitude of linear surge & heave wave forces for vertical circular cylinder (*H=2a*, *d=a*)

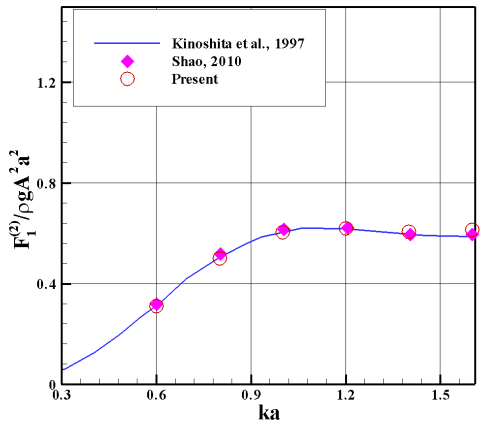

Fig. 4.10 The amplitude of surge drift force for vertical circular cylinder (*H = 2a*, *d = a*)

The double-frequency force in the second-order quantities is also confirmed on a bottom-mounted vertical cylinder. The result is compared with that of Kim & Yue (1990), Choi (2013). In Kim and Yue (1990), the result is obtained by ring source Green function semi-analytically. In Choi (2013), the velocity potential is obtained by using eigen-function expansion and the integration of surface is conducted by semi-analytic way. The left and right in Figure 4.11 show the sum-frequency force of draft(*d*)/radius(*a*) are 4 and 10 bottom-mounted vertical cylinders, respectively. All kinds of second-order forces show a good agreement with other results.

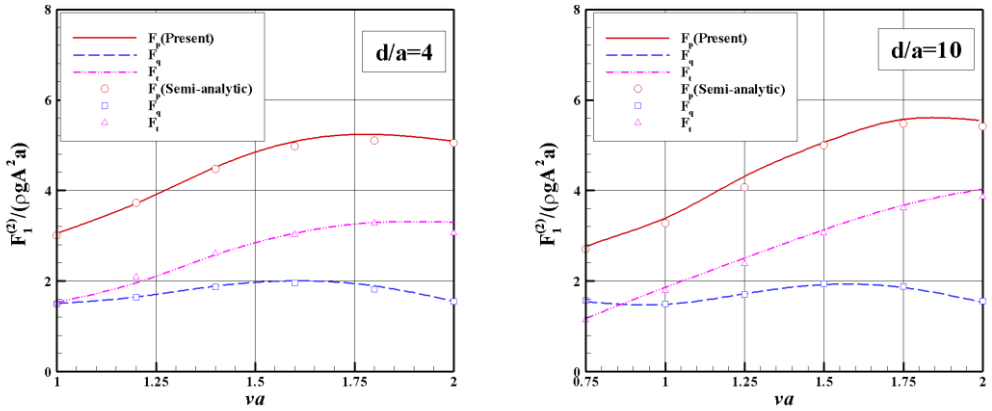

Fig. 4.11 Second-order hydrodynamic forces on rigid vertical cylinder (*d*/*a* is 4 and 10)

From the numerical study of diffraction problem, we could confirm that the second-order hydrodynamic force on a fixed body could be calculated with good accuracy by using time-domain HOBEM.

4.3.2 Forced oscillating body

1) Hemisphere

As already shown in diffraction problem, a first-order quantity is confirmed before obtaining a second-order quantity. Added mass and damping coefficients are obtained by using forced oscillating body. Using orthogonal property of trigonometric function, time-domain results are transformed to hydrodynamic coefficients (*e.g.* Zhou *et al*., 2013). This procedure is briefly as follows:

The total force acting on the body surface can be written in this form (Koo and Kim, 2006)

$$F_i(t) \cong -a_{ij}\ddot{\xi}_j - b_{ij}\dot{\xi}_j - c_{ij}\xi_j \tag{4.1}$$

After multiplying hydrodynamic force with either acceleration or velocity, the integration over the one period is conducted. It is as follows:

$$\int_0^{T_e} \left(a_{ij}\ddot{\xi}_j^{\,2} + c_{ij}\xi_j\ddot{\xi}_j \right) dt = -\int_0^{T_e} F_i(t)\ddot{\xi}_j dt \tag{4.2}$$

$$\int_0^{T_e} b_{ij}\dot{\xi}_j^{\,2} dt = -\int_0^{T_e} F_i(t)\dot{\xi}_j dt \tag{4.3}$$

In forced oscillating simulation, body has sinusoidal acceleration, velocity, motion such as

$$\xi_j = -A_j \cos \omega t,\ \dot{\xi}_j = A_j \omega \sin \omega t,\ \ddot{\xi}_j = A_j \omega^2 \cos \omega t \tag{4.4}$$

Substituting Eq. (4.4) to Eq. (4.2) and (4.3), the added mass and radiation damping coefficient could be determined by orthogonal property of trigonometric function. It is as follows:

$$a_{ij} = -\frac{1}{\pi A_j \omega}\int_0^{T_e} F_i(t)\cos \omega t dt + \frac{c_{ij}}{\omega^2},\ b_{ij} = -\frac{1}{\pi A_j}\int_0^{T_e} F_i(t)\sin \omega t dt \tag{4.5}$$

As a numerical model, a hemisphere is also chosen for added mass and radiation damping coefficients. The results are compared with analytic solution (Hulme, 1982). Fig. 4.12 and Fig. 4.13 denote surge, heave added mass and radiation damping coefficients. They show a good agreement with analytic solution.

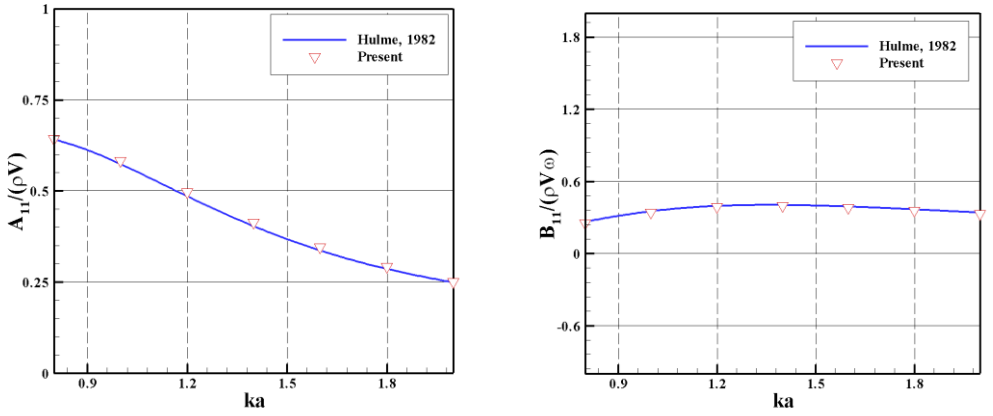

Fig. 4.12 Non-dimensional surge added mass & radiation damping coefficients of a hemisphere

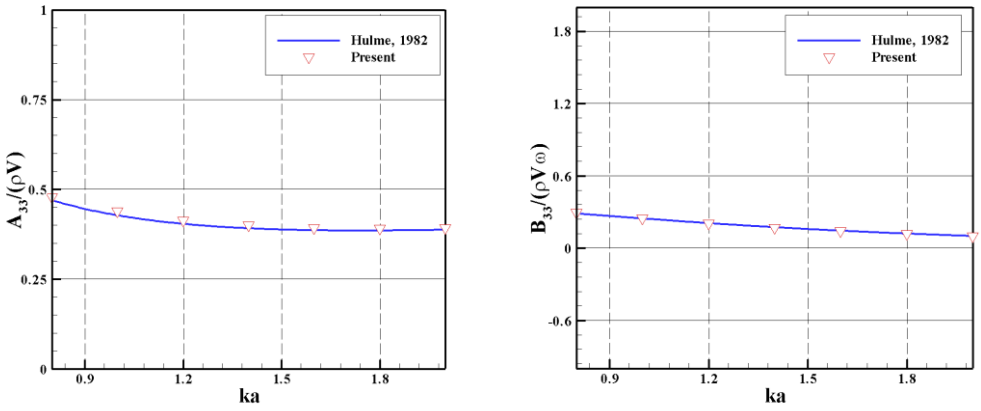

Fig. 4.13 Non-dimensional heave added mass & radiation damping coefficients of a hemisphere

2) Truncated vertical cylinder

Truncated vertical circular cylinder is also chosen as a second-order radiation problem. The water depth (H) is 1.5 radius (a) and draft (d) is set on 0.5 radius (a). Teng *et al*. (2002), Duan *et al*. (2015b) used same model for comparison of second-order hydrodynamic force under forced oscillating body. Second-order hydrodynamic force of radiation problem is also decomposed into two components; *i.e.* F_p and F_q as same with diffraction problem. Fig. 4.14 and Fig. 4.15 show double-frequency vertical hydrodynamic forces due to harmonic oscillating heave and surge motions. Each component of second order hydrodynamic forces is compared with that of other published papers. Overall results show favourable agreement in both surge and heaving body.

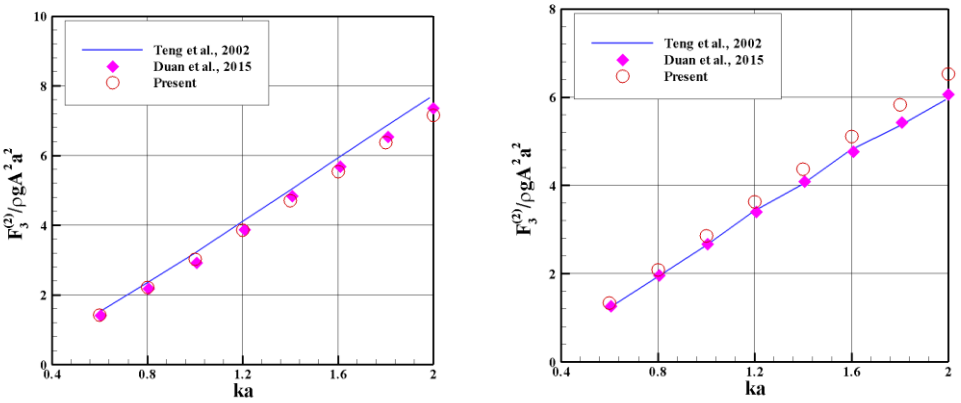

Fig. 4.14 Sum-frequency heave hydrodynamic force due to second order velocity potential (F_p) & quadratic product of linear quantities (F_q) on a forced oscillating heaving cylinder

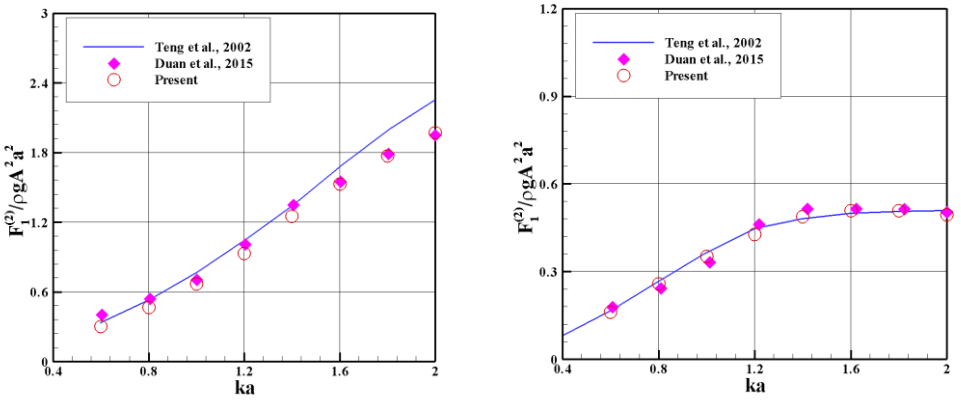

Fig. 4.15 Sum-frequency heave hydrodynamic force due to second order velocity potential (F_p) & quadratic product of linear quantities (F_q) on a forced oscillating surging cylinder

However, the problem including second derivative of velocity potential have been one of difficult numerical problems. It is well known that linear seakeeping analysis of a ship with forward speed has second derivative of double body velocity potential so called m_j-term and second-order radiation problem of stationary structure also has second derivative of unsteady velocity potential on body boundary condition. Accuracy problems of second derivative quantities have been brought by several researchers (*e.g.* Zhao and Faltinsen, 1989; Nakos, 1990; Shao and Faltinsen, 2010). Thus, many different schemes have been developed to avoid calculation of second derivative itself. In the forward speed problem, Tuck's theorem is generally used to avoid second derivative of double body velocity potential (Ogilvie and Tuck, 1969). In second-order radiation force, similar mathematical formulation is also suggested. For example, Teng *et al*. (2002), Lee (1995) obtained second-order unsteady velocity potential without second derivative of velocity potential on body surface by taking Stokes theorem on boundary integral equation. Shao and Faltinsen (2010) also used body-fixed coordinate method not to perform the Taylor expansion on body boundary condition. They also insisted that if the structure has sharp corners with interior angle less than 180 degree, the second derivative of velocity potential in Bernoulli equation fails to converge due to singularity of the flow.

Although the second derivative quantities on body boundary could make a little error, the effect seems not so large at least in the second-order force of the forced oscillating body. Other hydrodynamic forces could also be obtained with good accuracy in time-domain Rankin panel method.

4.3.3 Freely-floating body

As a last section, the motion and force of a freely-floating body has been considered. In the direct time-domain simulation, a freely-floating body continues to drift for wave-direction in horizontal motions because there is no restoring force for these motions. In this study, soft spring is installed at surge, sway, yaw motions to prevent continuous drift of a body. The steady state result of the horizontal motion is obtained after several period of the simulation by using Fourier transform. It is well known that duration period of Ramp function at initial time make different drift of horizontal motion. Fig. 4.16 shows the comparison of the horizontal motion with different duration period of Ramp function without soft spring. It shows long duration time of Ramp

function could reduce the drift of a freely-floating body. Fig. 4.17 shows the comparison of the horizontal motion with different period of soft spring. Here, low period means strong restoring force which could be confirmed at the following definition.

$$c_i = \frac{(m_i + a_i)}{(2\pi / T_s)^2} \tag{4.6}$$

where Ts : Period of soft spring

Since large strength of soft spring affects the result of horizontal motion, it should be careful to choose for strength of it.

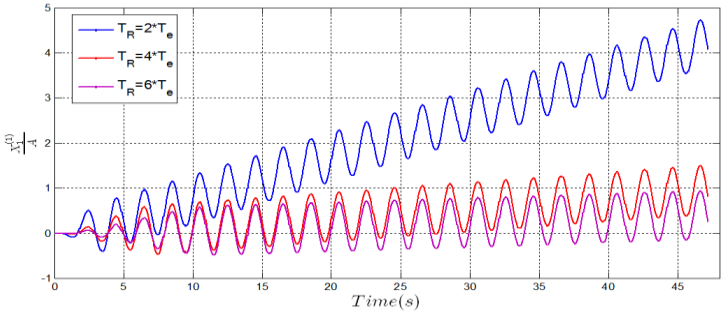

Fig. 4.16 Comparison of horizontal motion with different duration period of Ramp function

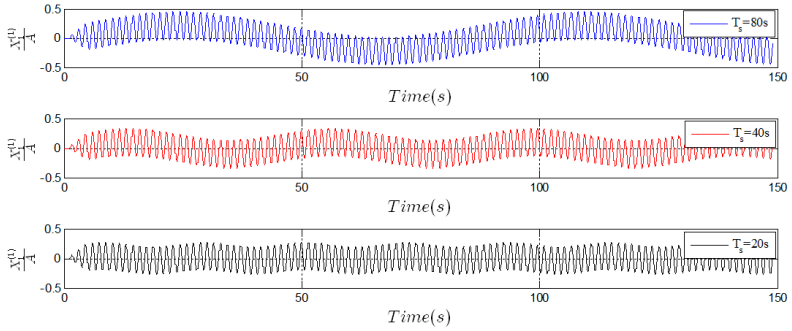

Fig. 4.17 Comparison of horizontal motion with different soft spring period

As a validation model, a freely-floating hemisphere is adopted again. The water depth is set on 1 wave lambda (λ) and numerical results are compared with that of Pinkster (1980) and the experiment result of Kudou (1977). In this simulation, time derivative of velocity potential in hydrodynamic force is calculated by two methods. First method is using finite difference scheme (backward) for the velocity potential. Second method is obtaining so called acceleration potential by using BEM solver for the time derivative of velocity potential simultaneously. Boundary-value problem for time derivative of velocity potential is solved by using Eq. (4.7) and body boundary condition is re-obtained on acceleration potential.

$$\alpha(P)\phi_t(P) + \iint_{S_T} \phi_t \frac{\partial G}{\partial n_q} dS(Q) = \iint_{S_T} G \frac{\partial \phi_t}{\partial n_q} dS(Q) \tag{4.7}$$

$$\nabla \phi_t^{(1)} \cdot \vec{n} = \ddot{\vec{\tau}} \cdot \vec{n} \tag{4.8}$$

In both methods, iteration loop for hydrodynamic force & acceleration is not used. Figure 4.18 is surge, heave RAO on a freely-floating hemisphere. It shows that second method is more similar with result of Pinkster (1980). Because of improved linear quantities, the mean drift force also shows more similar result with experiment data as shown in Fig 4.19.

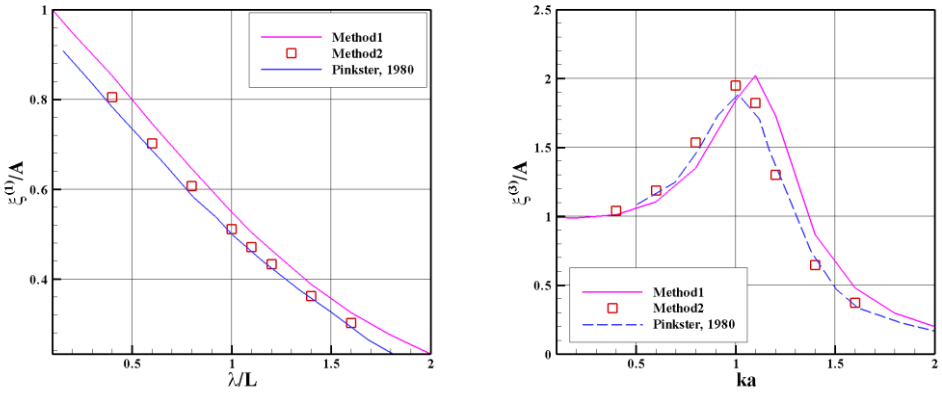

Fig. 4.18 Surge and heave response amplitude operator of freely floating hemisphere (*H* = λ)

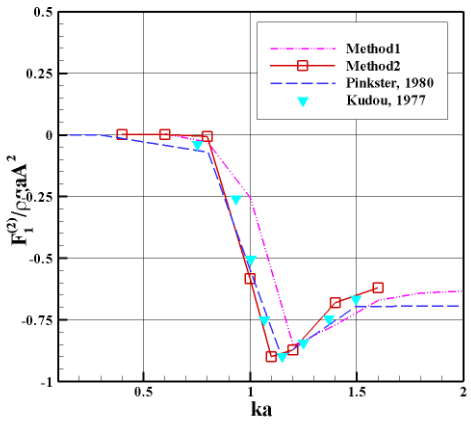

Fig. 4.19 Surge mean drift of freely floating hemisphere (*H* = λ)

Next, double-frequency hydrodynamic force is also calculated at the same condition with diffraction problem. The result is compared with semi-analytic solution of Kim and Yue (1990) and another in-house frequency-domain code which is based on wave Green function HOBEM.

Figure 4.20 shows the second-order force from quadratic product of linear quantities (F_q) on a freely-floating hemisphere. Left and right figures mean surge and heave direction forces, respectively. Although there is a little difference near the resonance, overall results agree well with other semi-analytic and frequency-domain results.

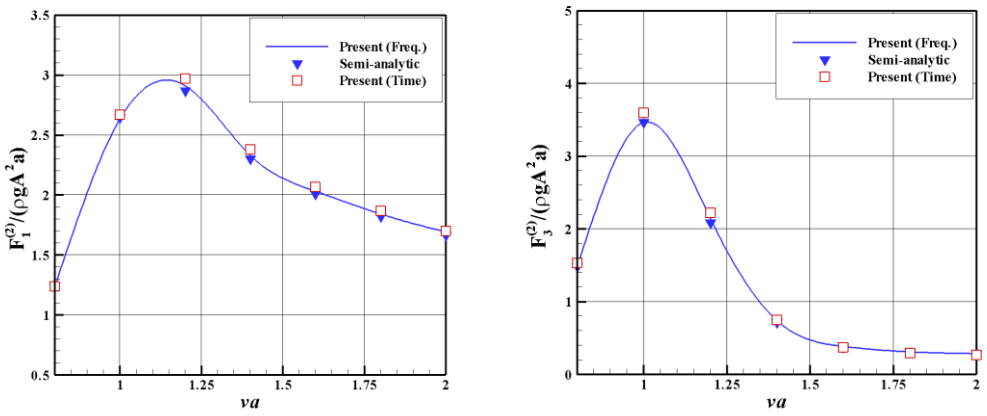

Fig. 4.20 Quadratic product of linear quantities (F_q) on freely-floating hemisphere. Left figure means surge direction force and right figure is heave direction force ($H=3a$)

The contribution of second-order velocity potential (F_p) in the second-order hydrodynamic force is also compared with frequency-domain in-house code whose detail will be explained at next chapter. Fig. 4.21 shows that the second-order velocity potential force at each surge and heave direction. In the left figure, the surge force shows a good agreement each other. On the other hands, heave direction force shows remarkable difference near resonance region.

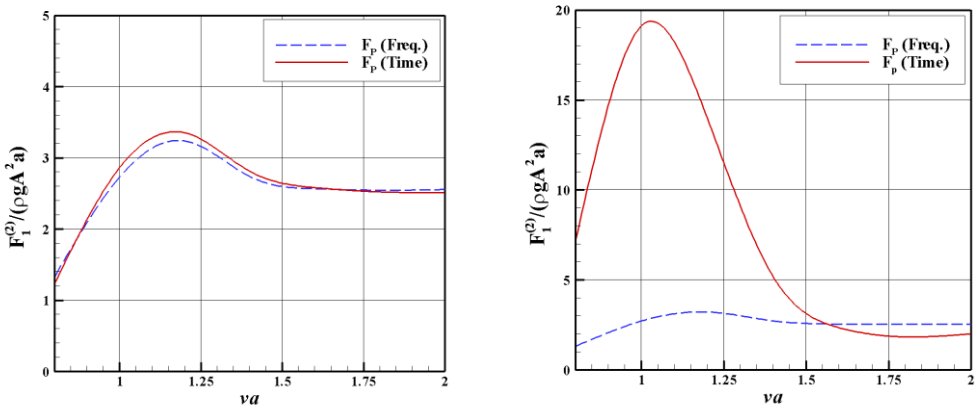

Fig. 4.21 Non-dimensional total second order velocity potential force (F_p) on freely-floating hemisphere. Left figure means surge direction force and right figure is heave direction force ($H=3a$).

There might be possible two reasons of the difference except inaccuracy of linear quantities. The first is numerical inaccuracy in the second derivatives of velocity potential which needed in the second-order body boundary condition as mentioned previous section. The second-derivative term is coupled with body motion on second-order boundary condition. In the light of the fact that difference dramatically increases as body motion increases, second derivative quantities on body surface seem sensitive. Another reason may be due to truncated free-surface region adopted in the Rankine panel method. This truncated free-surface problem was not prominent in the second-order diffraction/radiation problems of fixed or forced oscillating body simulations.

4.3.4 Summary

From the study of a rigid body at zero forward speed, it seems that second-order velocity potential could be obtained with good accuracy in diffraction problem. When the body has motion, there exists second derivative of velocity potential and it causes an error in second-order hydrodynamic force. Especially in the freely-floating condition, an error could appear near resonance region due to inaccuracy of second-derivative on body boundary condition and strong coupling of non-homogeneous components on free-surface boundary. It is also confirmed that the acceleration potential could improve the result of free-body simulation and the calculation of second-order velocity potential force.

4.4 Numerical study with forward speed (rigid model)

The forward speed problem with rigid body assumption is considered in this section. Using previous researches conducted by experiment or another numerical simulation, the validation study of developed code is implemented on a rigid ship model.

4.4.1 Simulated ship model

The ship model considered in forward speed problem is slender & blunt modified Wigley models (Kashiwagi, 2013) and Wigley1 model (Journee, 1992) whose hull shape has relatively simple as shown in Figure 4.22. They can also be expressed in a mathematical form with the following equation:

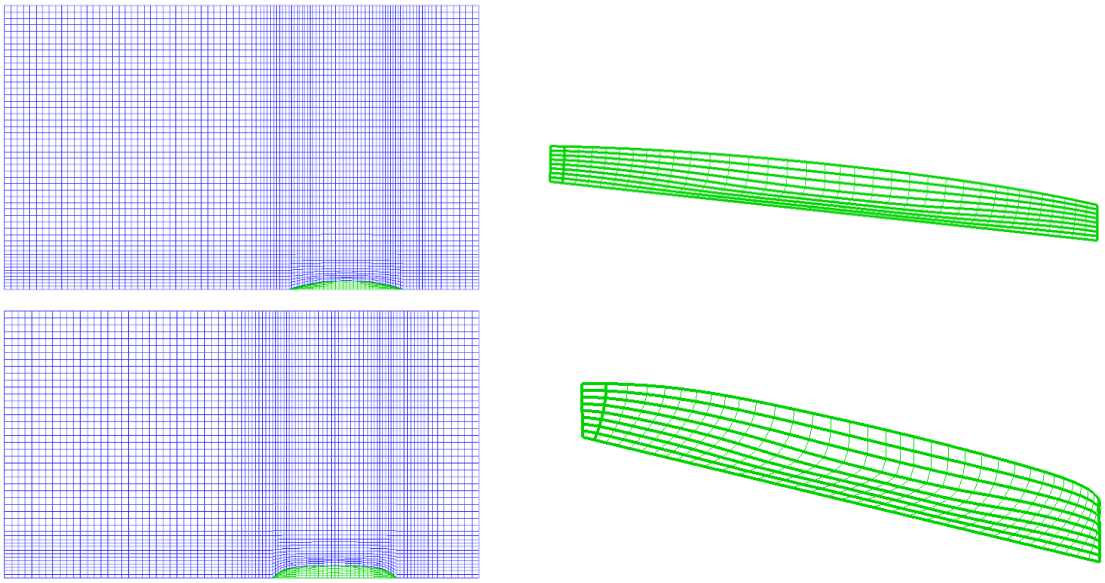

Fig. 4.22 Slender and blunt modified models

1) Slender modified Wigley & Wigley1 ship model

$$\eta = \left(1-\varsigma^2\right)\left(1-\psi^2\right)\left(1+0.2\psi^2\right)+\varsigma^2\left(1-\varsigma^8\right)\left(1-\psi^2\right)^4 \tag{4.9}$$

2) Blunt modified Wigley ship model

$$\eta = \left(1-\varsigma^2\right)\left(1-\psi^2\right)\left(1+0.6\psi^2+0.2\psi^4\right)+\varsigma^2\left(1-\varsigma^8\right)\left(1-\psi^2\right)^4 \tag{4.10}$$

where $\psi = 2x/L,\ \eta = 2y/B,$ and $\varsigma = z/d$

Principal dimensions of the ship model are shown in Table 4.2. The Froude number (F_n) is fixed to 0.2 in all simulations and 0.3 is additionally considered on the Wigley1 model.

Considering numerical accuracy in the body boundary condition which includes several higher-order derivatives of double body velocity potential, we adopted the so-called Neumann-Kelvin assumption in all simulations. Hence, the double body velocity potential and its derivatives are not included in this study.

Table 4.2 Principal dimensions of ship models

Principal dimension	Blunt modified Wigley	Slender modified Wigley	Wigley1
Length (L)	2.5 m	2.0 m	3.0 m
Breadth (B)	0.5 m	0.3 m	0.3 m
Draft (d)	0.175 m	0.125 m	0.1875 m
Center of gravity (OG)	-0.03 m	-0.0404 m	-0.0175 m
C_B	0.635	0.56	0.563

4.4.2 Linear diffraction & radiation problem of ship models

Before obtaining motion response, diffraction/radiation problems are considered on slender/blunt modified Wigley models. Figures 4.23 and 4.24 are hydrodynamic coefficients and wave exciting forces of blunt modified Wigley ship and Figure 4.25 and 4.26 are same variables of slender modified Wigley ship. These results are compared with that of experiment and numerical result of EUT (He and Kashiwagi, 2014). Figures show that time-domain HOBEM results give a good agreement with other results.

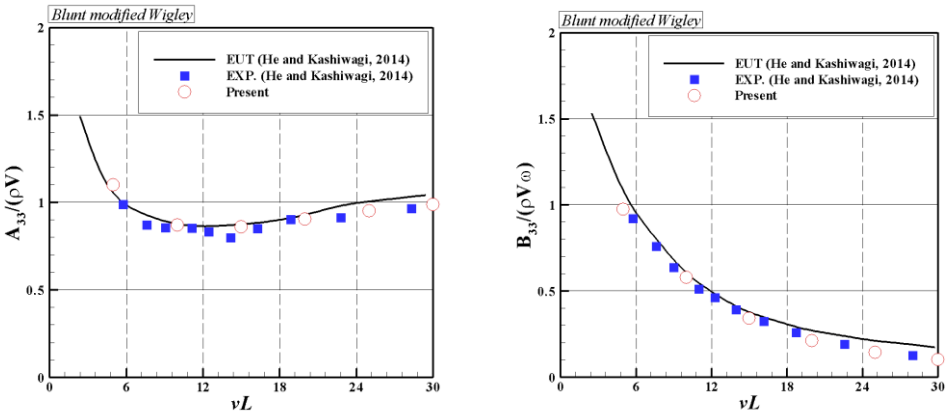

Fig. 4.23 Heave added mass & damping coefficient of blunt modified Wigley ship (*Fn* = 0.2)

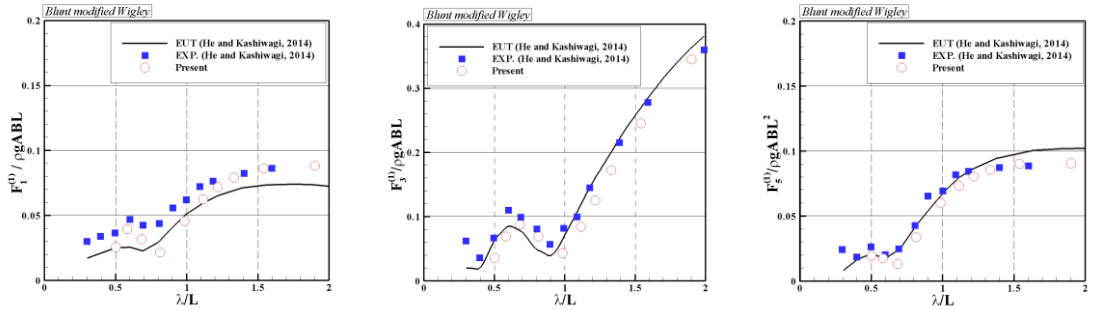

Fig. 4.24 Wave exciting force of blunt modified Wigley ship (*Fn* = 0.2, β = 180º)

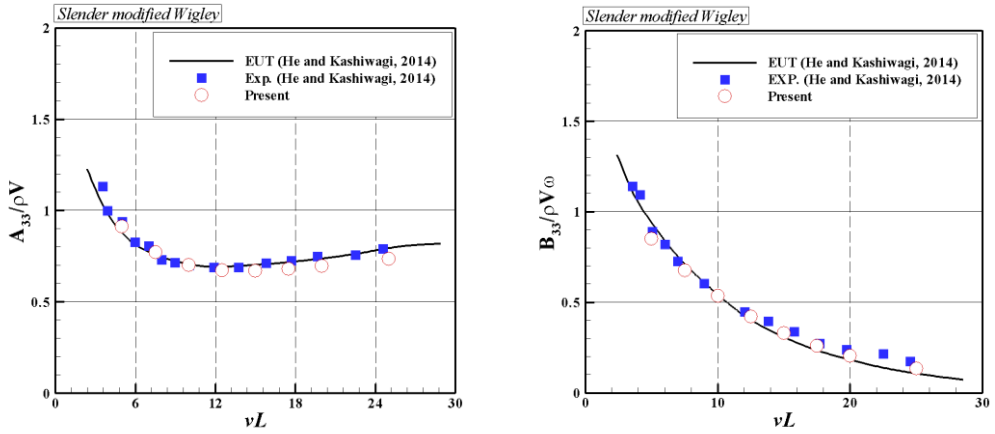

Fig. 4.25 Heave added mass & damping coefficient of slender modified Wigley ship (*Fn* = 0.2)

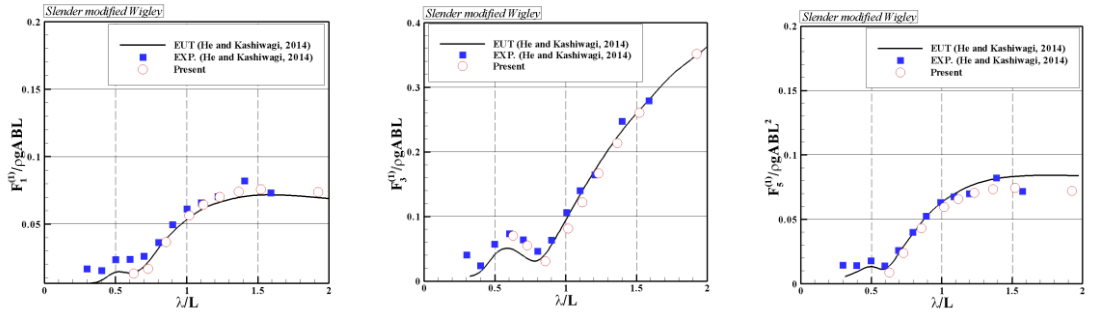

Fig. 4.26 Wave exciting force of slender modified Wigley ship (*Fn* = 0.2, β = 180º)

4.4.3 Freely-floating ship models

Using the equation of motion, motion response of Wigley ship models is calculated. After obtained acceleration in the equation of motion, velocity & motion of a ship model are calculated by using Runge-Kutta-Nystrom method at each time step. Artificial spring is installed to avoid continuous drift phenomenon. Long duration of Ramp function period at initial time steps is also used to reduce drifting for horizontal direction.

First, the motion responses of both slender & blunt modified Wigley models are calculated and compared with other result of the experiment and different numerical results such as EUT, NSM, 3-D RPM as shown in Kashiwagi (2013).

Fig. 4.27 is the surge, heave, pitch motion responses of blunt modified Wigley model. It seems that HOBEM gives fair agreement with other results but vertical motions are relatively underestimated at low frequency regions.

Figure 4.28 is same kinds of motion response in slender modified Wigley model. In heave motion, HOBEM result is more similar with that of A=0.025m experiment than A=0.01m case. In the heave & pitch motions, present result has better agreement with that of 3-D RPM than blunt model's response case. Referred RPM code adopted double body flow assumption, thus it seems that slender modified Wigley ship has smaller effect of steady disturbed potential than blunt modified Wigley ship.

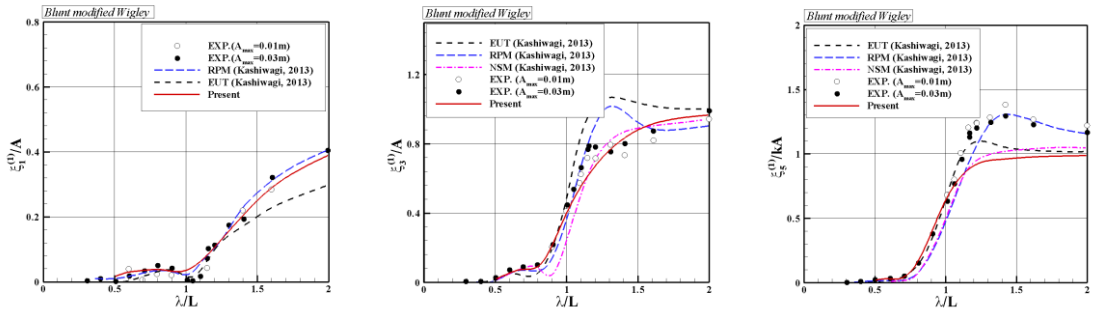

Fig. 4.27 Motion response of blunt modified Wigley model [Surge,Heave,Pitch] (*Fn* = 0.2, β = 180°)

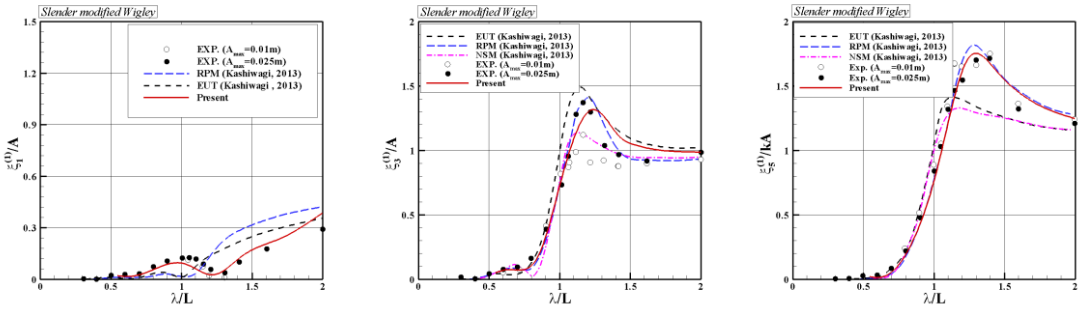

Fig. 4.28 Motion responses of slender modified Wigley model [Surge,Heave,Pitch] (*Fn* = 0.2, β = 180º)

At the last, Wigley1 model is used as a validation. This model has the most slender hull shape among numerical models in this study. Vertical motions are compared with that of experiment (Journee, 1992) and other 3-D RPM codes in time-domain (Shao and Faltinsen, 2012; Joncquez, 2009).

Figure 4.29 and 4.30 show motion responses at different Froude number 0.2 and 0.3, respectively in head waves. We could confirm that the vertical motions increase as forward speed increases. It also seems that NK assumption slightly overestimates the motion responses near resonance especially due to simplified m_j-terms without steady disturbed flow effect.

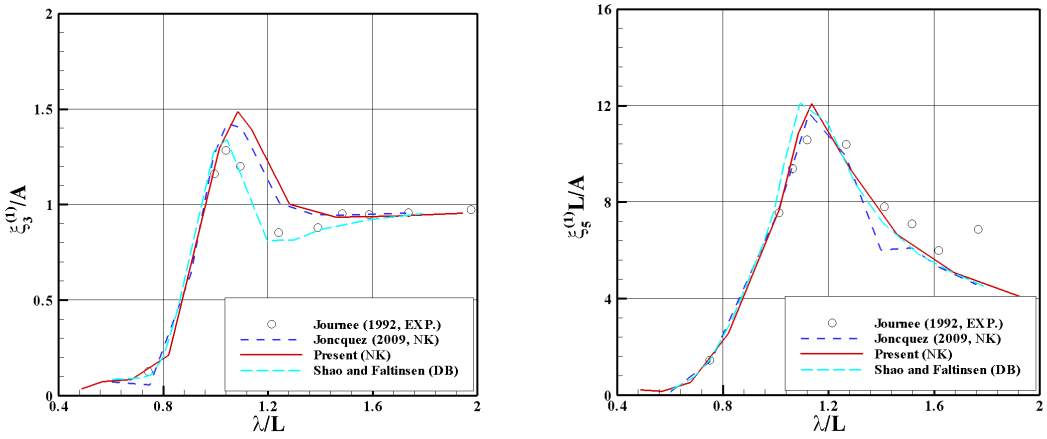

Fig. 4.29 Motion response of Wigley1 model [Heave, Pitch] (*Fn* = 0.2, β = 180º)

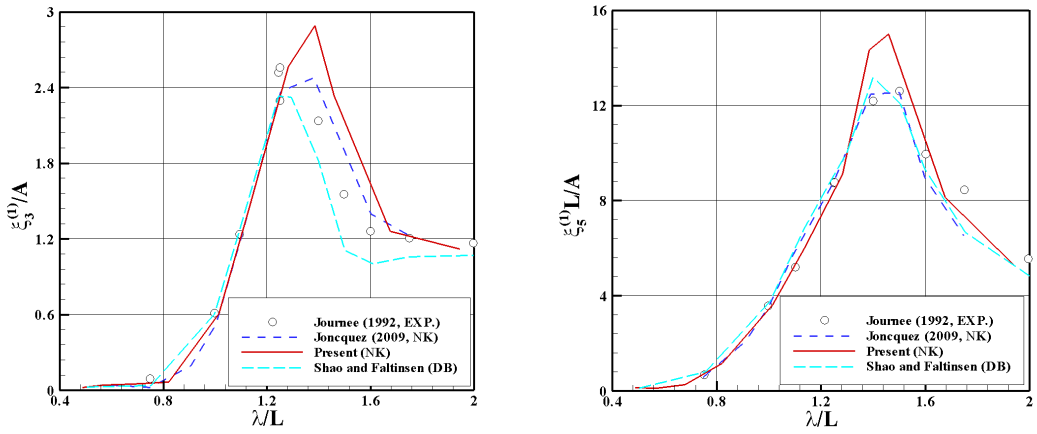

Fig. 4.30 Motion response of Wigley1 model [Heave, Pitch] (*Fn* = 0.3, β = 180º)

Using linear variables, quadratic product of linear quantities could be calculated and the steady force can be obtained by measuring the average value of it. As a validation of quadratic forces, the steady force is compared with published data. In particular, the surge steady force is called wave induced added resistance which has been particularly researched in the seakeeping problem by many researchers.

From the several decades, numerous methods to predict exact added resistance of a ship have been suggested. Since the steady force could be calculated by not only pressure integration but also momentum conservation theorem which is so called far-field method, several formulations to calculate steady force in waves have been developed. For instance, Maruo (1960) derived the formulation of steady force by using far-field method based on Kochin function. Gerritsma and Beukelman (1972) suggested radiated wave energy method based on momentum conservation theorem. Using Parseval's theorem, Kashiwagi (1995) also derived similar formulation in the frame of far-field method and calculated wave induced steady force based on enhanced unified theory (EUT). Using wave elevations near the ship hull, the added resistance is calculated by Okushu (1980) in the cylindrical coordinate system. Kashiwagi (2013) suggested general formulation of unsteady wave pattern analysis in Cartesian coordinate and measured wave pattern in experiments.

In Kashiwagi (2013), he compared several methods and discussed some components of added resistance in waves. His results are compared with present time-domain simulation based on pressure integration method in generalized modes. As same with zero forward speed problem, the translational mode is substituted to modal vector in generalized mode's formulation.

Figure 4.31 shows wave induced added resistance of two modified Wigley models. Left figure is the result of slender modified Wigley model and the right figure is that of blunt modified Wigley model. In slender model, it shows favourable agreement with other results though it is underestimated than others. However, blunt model shows rather poor agreement with other results. It seems that the underestimated vertical motion might be one of main reason and steady flow effect is larger than slender models as same with the linear motion response case.

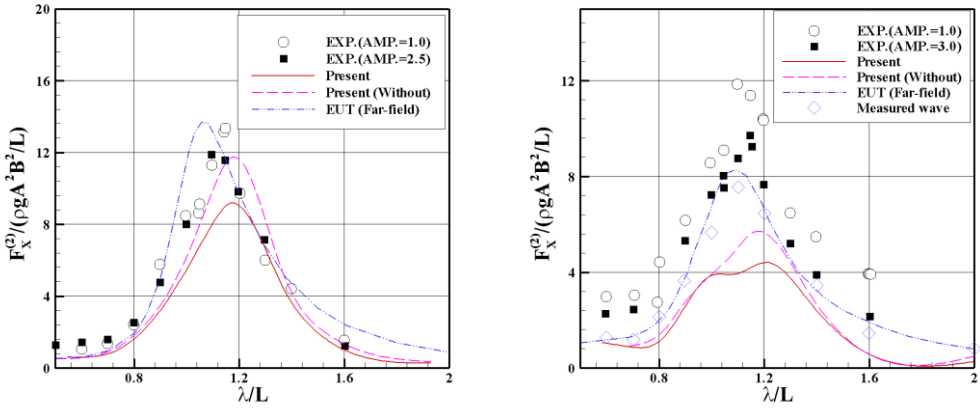

Fig. 4.31 Added resistance of slender & blunt modified Wigley model (*Fn* = 0.2, β = 180º)

In the last, the steady force for rigid body motions of Wigley1 ship model is compared with experiment and another time-domain RPM results (Joncquez, 2009) in different forward speed.

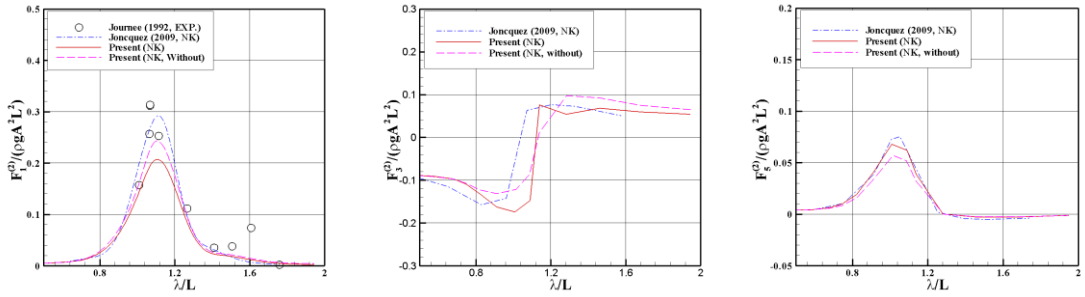

Fig. 4.32 Steady force of Wigley1 model [Surge, Heave, Pitch] (*Fn* = 0.2, β = 180º)

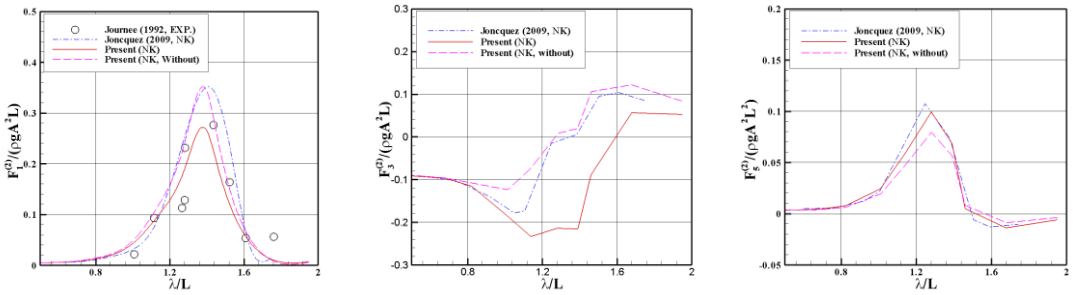

Fig. 4.33 Steady force of Wigley1 model [Surge, Heave, Pitch] (*Fn* = 0.3, β = 180º)

Figure 4.32 and 4.33 show the steady force at Froude number 0.2 and 0.3 in head waves. Present simulations show a little smaller value than other results especially near resonance region. One of reason might be come from the inaccuracy in calculation for the second derivative of unsteady velocity potential on body surface. Thus, we denoted the result without second-derivative of unsteady velocity potential together in figures. The existence of second derivative of unsteady velocity potential reduces the value of surge direction force and other heave and pitch direction forces increase especially near resonance region in this model. If we considers the fact that these ship models are relatively slender and we are using NK assumption, we could figure out that the difficulty of exact calculation of second-order force with forward speed as discussed by previous researchers (*e.g.* Shao and Faltinsen, 2012; Lee *et al*., 2017).

4.4.4 Summary

In NK assumption, several simple ship models are used in the validation process. The motion responses show a good agreement except rather blunt ship model and overestimates peak values near resonance frequency in slender models. The mean drift force is also confirmed by calculating quadratic product of linear quantities. The results show favourable agreement in slender models and rather poor agreement is confirmed in blunt models. It is confirmed that second derivative of velocity potential is more sensitive in forward speed problem though the ship hull is simple and slender. More detail study should be given for estimation of second-order hydrodynamic force with forward speed by using various methods.

4.5 Numerical study without forward speed (elastic model)

From this section, we consider the responses of an elastic body. Before solving forward speed problem, the numerical study is conducted on zero forward speed problem. Since there are many other researches on stationary body, the developed codes are compared with these published results. After structural model what used in this study is introduced, numerical results on fixed and floating bodies are calculated and discussed.

4.5.1 Simulated structural model

The floating body is treated as a simple beam to calculate the hydroelastic response. The Euler-Bernoulli & Timoshenko beam equations are used for the structure model. Since the head wave condition is considered, only the vertical bending mode is included as the elastic responses. Hence, the modal vector can be defined as follows:

$$h_1^j = -\frac{\partial w_j}{\partial X}\left(Z - Z^N\right),\ \ h_2^j = 0,\ \ h_3^j = w_j \tag{4.11}$$

1) Euler-Bernoulli beam theory

The dynamic Euler-Bernoulli beam equation could be written in this form.

$$m_s \frac{d^2\tau_3}{dt^2} + EI\frac{d^4\tau_3}{dX^4} = f \tag{4.12}$$

Using the method of weighted residuals, the beam equation could be transformed to following equation.

$$\sum_{j=1}^{n}\xi_j(t)\int_{-L/2}^{L/2} w_i(X)\left[m_s\xi_j\frac{d^2w_j(X)}{dt^2} + EI\xi_j\frac{d^4w_j(X)}{dX^4}\right]dX = \int_{-L/2}^{L/2} w_i(X) f\left(X,t\right)dX \tag{4.13}$$

Using defined modal mass and stiffness matrices, Eq. (4.13) could be summarized in this form.

$$\sum_{j=1}^{n}\left[M_{ij}\ddot{\xi}_j(t) + K_{ij}\xi_j(t)\right] = F_i(t) \tag{4.14}$$

From the equation, the mode shape of the beam model could be obtained by solving the eigen-value problem. The homogeneous solution of Euler-Bernoulli beam can be readily obtained by

assuming the free-free end condition and the time harmonic oscillation. The final symmetric and anti-symmetric mode shapes can be expressed as follows:

$$w_{2j}(q) = \frac{1}{2}\left(\frac{\cos \kappa_{2j} q}{\cos \kappa_{2j}} + \frac{\cosh \kappa_{2j} q}{\cosh \kappa_{2j}} \right) \tag{4.15}$$

$$w_{2j+1}(q) = \frac{1}{2}\left(\frac{\sin \kappa_{2j+1} q}{\sin \kappa_{2j+1}} + \frac{\sinh \kappa_{2j+1} q}{\sinh \kappa_{2j+1}} \right) \tag{4.16}$$

where q is the non-dimensional coordinates ($2X/L$) , and j=0 and 1 denote the rigid modes; namely heave and pitch motions, respectively. The factor κ_j (which is the j-th eigenvalue related to the elastic natural frequency) can be calculated numerically, satisfying the following eigen-value equation (Newman, 1994).

$$(-1)^j \tan \kappa_j + \tanh \kappa_j = 0 \tag{4.17}$$

The modal mass and stiffness matrices can be obtained from the sectional mass (m_s). In this study, the sectional mass and flexural rigidity are assumed constant along the ship length (L). In this case, the modal mass and stiffness matrices are simply expressed in the following form.

$$\left.\begin{aligned} \mathrm{M}_{ij} &= m_s \int_{-L/2}^{L/2} w_i(X) w_j(X) dX = \frac{m_s L}{4}\delta_{ij} \quad \text{for} \quad i, j \geq 7 \\ \mathrm{M}_{11} &= \mathrm{M}_{33} = m_s L,\ \mathrm{M}_{55} = \frac{1}{12} m_s L^2 \end{aligned}\right\} \tag{4.18}$$

$$\mathrm{K}_{ij} = EI \int_{-L/2}^{L/2} \frac{\partial^2 w_i(X)}{\partial X^2} \frac{\partial^2 w_j(X)}{\partial X^2} dX = 4 \frac{EI}{L^3} \kappa_{j-5}^4 \delta_{ij} \tag{4.19}$$

2) Timoshenko beam theory

Considering shear stress in section area, the rotation in-plane at each section could be considered. Timoshenko beam equation is derived by taking into account the shear effect for Euler-Bernoulli beam.

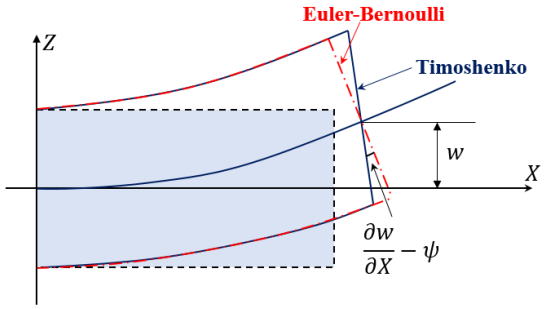

Fig. 4.34 Comparison of Euler-Bernoulli beam and Timoshenko beam

Using force & moment equilibrium and constitute equation of Timoshenko beam, free-free end dynamic Timoshenko beam equation could be written in this form (Jensen, 2001).

$$\frac{\partial}{\partial X}\left[EI\left(1+\upsilon\frac{\partial}{\partial t}\right)\frac{\partial \psi}{\partial X}\right]+\mu GA\left(1+\upsilon\frac{\partial}{\partial t}\right)\left(\frac{\partial w}{\partial X}-\psi\right)=m_s r^2\frac{\partial^2\psi}{\partial t^2} \tag{4.20}$$

$$\frac{\partial}{\partial X}\left[\mu GA\left(1+\upsilon\frac{\partial}{\partial t}\right)\left(\frac{\partial w}{\partial X}-\psi\right)\right]-m_s\frac{\partial^2 w}{\partial t^2}=-F \tag{4.21}$$

where visco-elastic stress-strain relationship is assumed, μ is shear coefficient, υ is structural damping, r is radius of gyration.

Using modal superposition method, both vertical & angular displacements in Timoshenko beam model could be expressed by summation of modal function and amplitude. It is as follows:

$$\psi(X,t)=\sum_{i=1}^{N}\xi_i(t)\alpha^i(X) \tag{4.22}$$

$$w(X,t)=\sum_{i=1}^{N}\xi_i(t)h_3^i(X) \tag{4.23}$$

To obtain modal function at each mode, orthogonality and normalization of modal functions are used for eigenvalue analysis. The following orthogonal relation is given as follows:

$$\int_{-L/2}^{L/2}\left[m_s r^2\alpha^i\alpha^j+m_s h_3^i h_3^j\right]dX=\delta_{ij} \tag{4.24}$$

$$\int_{-L/2}^{L/2}\left\{\alpha^i\left(EI\frac{\partial\alpha^j}{\partial X}\right)+\alpha^i\mu GA\left(\frac{\partial h_3^j}{\partial X}-\alpha^j\right)+h_3^i\left[\mu GA\left(\frac{\partial h_3^j}{\partial X}-\frac{\partial\alpha^j}{\partial X}\right)\right]\right\}dX=0 \tag{4.25}$$

Substituting Eq. (4.22) and (4.23) to Eq. (4.20) and (4.21) and using orthogonal relation Eq. (4.24) and (4.25), the equation of motion could be expressed as follows (Jensen, 2001):

$$\frac{\partial^2 \xi_j}{\partial t^2} + \upsilon\omega_{n_j}^2 \frac{\partial \xi_j}{\partial t} + \omega_{n_j}^2 \xi_j = \int_{-L/2}^{L/2} h_3^j(X) f(X,t) dX \tag{4.26}$$

If each cross-sectional variable has different value, the modal function is generally calculated by using FEM. In this study, Stodola method is used to obtain the modal function (Jensen, 2001).

4.5.2 Bottom-mounted elastic vertical cylinder

Table 4.3 Principal dimensions of bottom-mounted elastic cylinder

Principal dimensions	Original model	Present model
Radius of cylinder (a)	10 *m*	1 *m*
Draft of cylinder (*d*)	200 *m*	20 *m*
Water depth (*H*)	200 *m*	20 *m*
Distributed mass (*md*)	0.322×10^8 *kg*	0.322×10^5 *kg*
Concentrated mass (m_0)	0.643×10^8 *kg*	0.643×10^5 *kg*
Flexural rigidity (*EI*)	0.211×10^{14} *kg* m^3/s^2	0.211×10^9 *kg* m^3/s^2

To confirm the excitation force for the elastic response, we performed several computations for an elastic vertical cylinder with superstructure. The model used to calculate the linear and second-order horizontal deflections in (Newman, 1994; Choi, 2013) is selected in the present simulation. The principal dimensions of this model are 10 m in radius (*a*), 200 m in draft (*d*) and flexural rigidity is $EI/m_0 H^3 = 0.41\ s^{-2}$. Summation of the mass distribution (*md*) is half of submerged mass and a concentrated mass (m_0) is added on the top of the cylinder.

In our simulation, the radius (*a*) of model is non-dimensionalized, thus it has 1.0 as described on the Table 4.3 This elastic cylinder has free-fixed condition at each edge and its mode shape is demonstrated in the Figure 4.35. Described mode shape is obtained by using Jacobian polynomial function which is admissible since it satisfies geometric boundary condition. The equation is expressed as follows:

$$h_1^j(Z) = q^2 P_{j-1}(q), \quad q = 1 + \frac{Z}{H} \tag{4.27}$$

$$P_n(q) = \sum_{m=0}^{n} (-1)^m \frac{(4+2n-m)!}{m!(n-m)!(4+n-m)!} q^{n-m} \tag{4.28}$$

where

$$P_0 = 1$$
$$P_1 = 6q - 5$$
$$P_2 = 28q^2 - 42q + 15$$
$$P_3 = 120q^3 - 252q^2 + 168q - 35$$

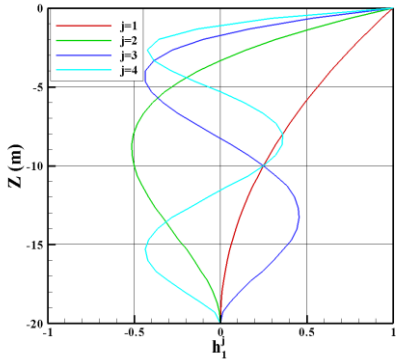

Fig. 4.35 The mode shape of a bottom-mounted elastic cylinder

Both of the linear and second-order forces and responses are calculated for the elastic cylinder. In addition, linear quantities and their quadratic-product force are obtained. These results are compared with semi-analytical results obtained by the eigen function expansion method (Choi, 2013). In the zero speed problem, the quadratic product of linear quantities of each mode could be decomposed into four components. They are as follows:

$$\vec{F}^{(2)} = \frac{1}{2}\rho g \oint_{W.L} \left(\zeta^{(1)} - \tau_3^{(1)}\right)^2 \vec{n} dl \qquad \text{(I)}$$

$$-\rho \iint_{S_{B_0}} \frac{1}{2} \nabla\phi^{(1)} \cdot \nabla\phi^{(1)} \vec{n} dS \qquad \text{(II)}$$

$$-\rho \iint_{S_{B_0}} \left(\vec{\tau}^{(1)} \cdot \nabla\right) \frac{\partial \phi^{(1)}}{\partial t} \vec{n} dS \qquad \text{(III)} \tag{4.29}$$

$$-\rho \iint_{S_{B_0}} \left(g\tau_3^{(1)} + \frac{\partial \phi^{(1)}}{\partial t} \right) \left\{ \left(\nabla \cdot \vec{\tau}^{(1)}\right) \vec{n} - \nabla \vec{\tau}^{(1)} \cdot \vec{n} \right\} dS \qquad \text{(IV)}$$

Figure 4.36 shows the result of each component in the quadratic product of linear quantities for the first mode and we can confirm good agreement with semi-analytical and present numerical results at each component. Summation of three components in Eq. (4.29) and the second-order velocity-potential force are also shown in Fig. 4.37. The left figure is the quadratic-product force and the right figure is the second-order velocity-potential force. The summation of each component of quadratic-product force has a good agreement with semi-analytic solution. However, the second-order velocity-potential force by the time-domain simulation shows that the difference increases as it approaches near linear resonance wave frequency where a noticeable underestimated force is obtained compared to semi-analytical solution.

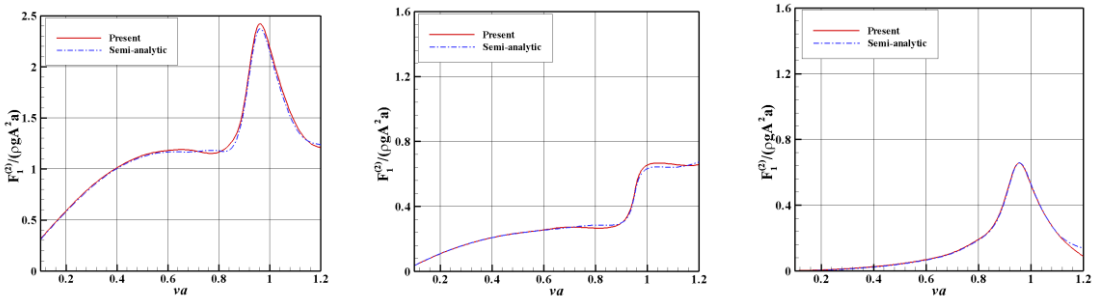

Fig. 4.36 Component of quadratic product force of the first mode (I, II, III from the left)

We deduce possible reasons why the results are different from semi-analytical solution except inaccuracy of linear quantities. It is almost same with the previous conclusion of rigid body dynamics for freely-floating body. The first is numerical inaccuracy in the second derivatives needed in the second-order body boundary condition. Another reason may be due to truncated free-surface region adopted in the Rankine panel method.

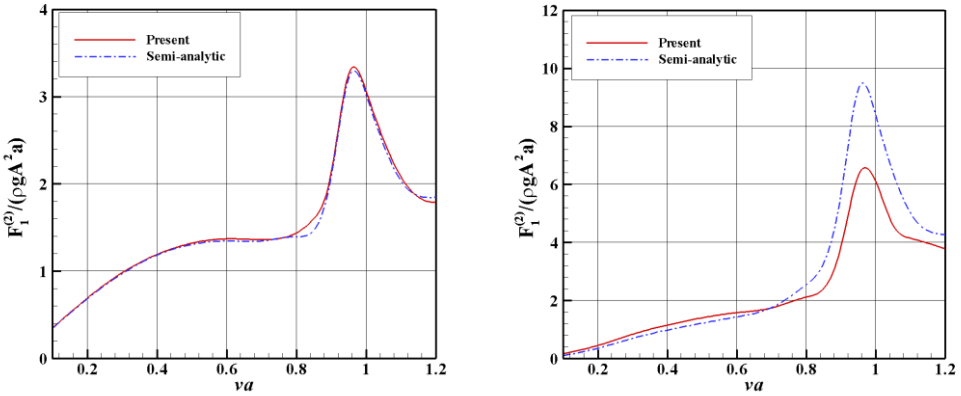

Fig. 4.37 The second-order forces due to quadratic product of linear quantities (F_q, left figure) and second-order velocity potential (F_p, right figure) of the first mode

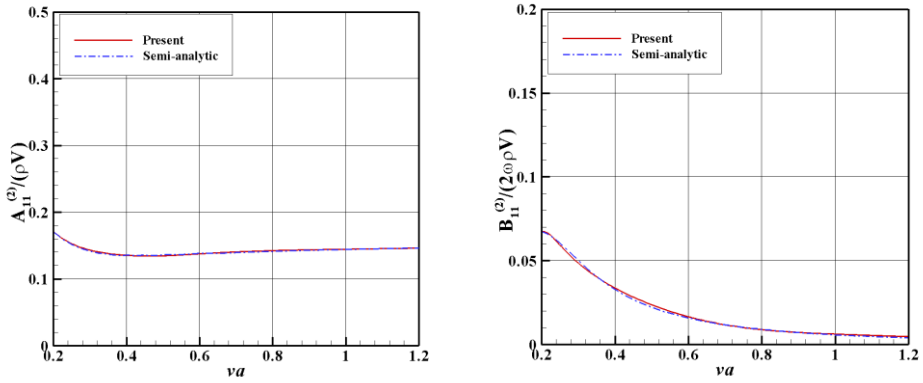

Fig. 4.38 Comparison of second-order added mass (A_{11}) and damping coefficient (B_{11}) of the first mode

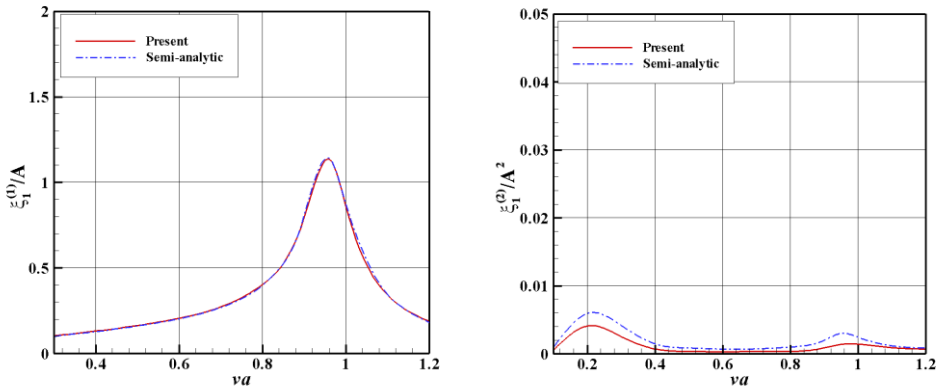

Fig. 4.39 Comparison of linear and second-order hydroelastic responses of the first mode

To obtain the second-order response, second-order hydrodynamic coefficients are calculated. Using the forced oscillating simulation with second-order motion, the second-order added mass and damping coefficients are obtained. Fig. 4.38 shows an example of the added mass and damping coefficients of the first mode, which are in good agreement with semi-analytical solutions. Using the motion equation, linear and second-order hydroelastic responses are obtained. The left and right figures in Fig. 4.39 are the linear and second-order hydroelastic responses of the first mode, respectively. The linear results show a good agreement with each other. The second-order response shows a little different value only near the resonance due to difference in the second-order external forces. The second-order resonance is confirmed near half of the natural

frequency but the response amplitude operator (RAO) is relatively very small in this mode overall wave frequencies.

4.5.3 Elastic floating barge

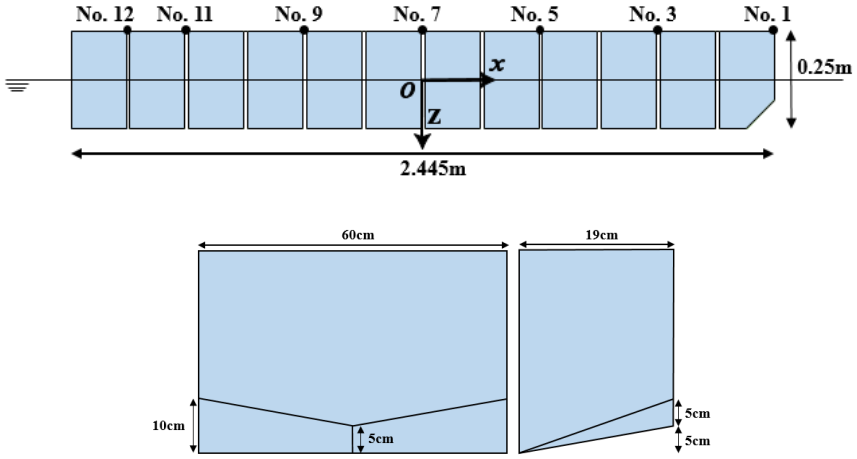

Fig. 4.40 Elastic barge model from side and plan view and shape of first floater

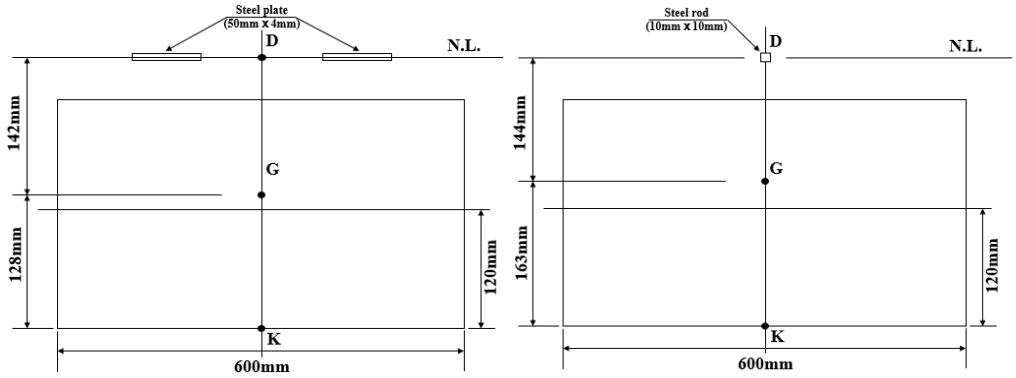

Fig. 4.41 Plan view of Malenica (left) & Remy (right) model

Deformable stationary barge is used to confirm the numerical result on a floating elastic body. Two experiments for same barge model have been performed by Malenica *et al*. (2003) and Remy *et al*. (2006). In this dissertation, we call each model used in experiment Malenica and Remy model, respectively. The shape of barge model is shown in Figure 4.40. The barge is composed of 12 floaters which have 0.19 *m* length, 0.6 *m* breadth, 0.25 *m* depth and 0.12 *m* draft. Each floater has 0.015 *m* gap to prevent collapse of bodies so the total length of model is 2.445 *m*. The first floater has slightly modified.

Structural part is a little difference due to connector of body. In Malenica model, floater is connected by two steel plates which have 6 *mm* × 50 *mm* size. In Remy model, plates are changed to a steel rod which has 10 *mm* × 10 *mm* size to consider both vertical and torsional bending modes as shown in Figure 4.41. Principal dimension of structure part is described in Table 4.4. In the experiment, each section's front part has optical sensor, thus the displacement is measured on top of a floater by these sensors.

Table 4.4 Principal dimension of each barge model

Principle dimension	Malenica model	Remy model
Mass (*m*)	171.77 *kg*	
Center of Gravity (*KG*)	0.128 *m*	0.163 *m*
Radius of Gyration (K_{yy}/L)	0.294	
Flexural rigidity (*EI*)	360.5 Nm^2	175 Nm^2

1) Malenica model

Among the hydroelastic response, vertical displacement of Malenica model in head wave is calculated at 1,3,5,7,9,11 sections (*See* Fig. 4.40). The result is compared with experiment and numerical result of Kim *et al*. (2009). They calculated the results by using direct coupling with time domain Rankine panel and one-dimensional FEM.

The vertical RAOs of each point are denoted in the Figure 4.42. The result of different beam model shows almost same value except resonance region and Timoshenko beam model gives a little smaller resonance frequency. However, both results show a good agreement with experiment and another numerical result. In this model, the resonance region of vibration was not measured at experiment. Although the resonance frequency of two-node vibration has almost same frequency around 8.5 rad/s, the result shows that there is some difference near resonance frequency.

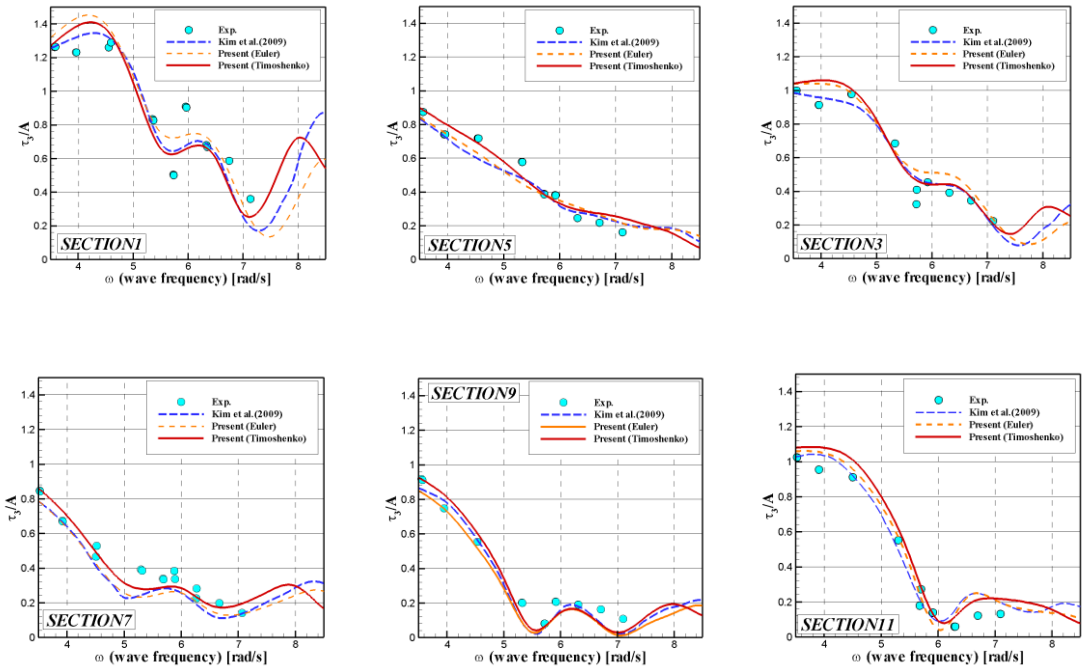

Fig. 4.42 Comparison for vertical displacement of each point for Malenica model (head waves)

2) Remy model

In Remy model, the experiment is implemented several times in both regular and irregular waves with different heading angles. The average of results at irregular waves are given after using Fourier transformation. As conducted in Malenica model's experiment, the motion is measured on top of each floater but measured point 11 moves to section 12. In this study, head wave's vertical displacement is selected in the experiment result. Since there is also only averaged value in Remy *et al*. (2006), we used experiment data denoted in Kim *et al.* (2009) and their numerical is also compared together. The comparison of RAO result is shown in Figure 4.43. It seems that present result shows favourable agreement with other results overall frequencies. However, the numerical result is sensitive near resonance region.

In this experiment, resonance frequency of elastic response is included in measured frequency of experiment. Euler beam model's result shows that there are some differences with experiment especially near 7.5rad/s due to difference of resonance for elastic response. In Timoshenko beam, natural frequency is slightly moved to lower frequency region for both models thus it gives more similar results near resonance region. However, numerical results are overestimated at resonance frequency. The difference is larger at both tips of barge model than other sections. In both tips of

barge, there exist several vertical modes simultaneously and two-node vertical mode is also relatively large. Hence, the vertical displacement is more sensitive than other sections. The reason of difference might be come from not exact hydrodynamic modelling and structural damping.

As a validation process of developed generalized modes, the second-order quantities are additionally calculated. However, it is difficult to find the sum-frequency result in second-order hydrodynamic force. The mean drift force is considered as a comparison variable and the flexibility effect is confirmed.

If there is no elastic motion, it could be calculated by classical second-order formulation so called Pinkster formulation on stationary structure (Pinkster, 1980). The generalized mode formulation is first confirmed with Eq. (4.29) and another numerical result (Park *et al*., 2016) on a rigid body assumption. Figure 4. 44 shows the surge mean drift force of barge model. Left figure shows that generalized mode formulation has a perfect agreement with classical formulation as proven in Appendix A. Right figure also shows that each component also gives a good agreement with another numerical result.

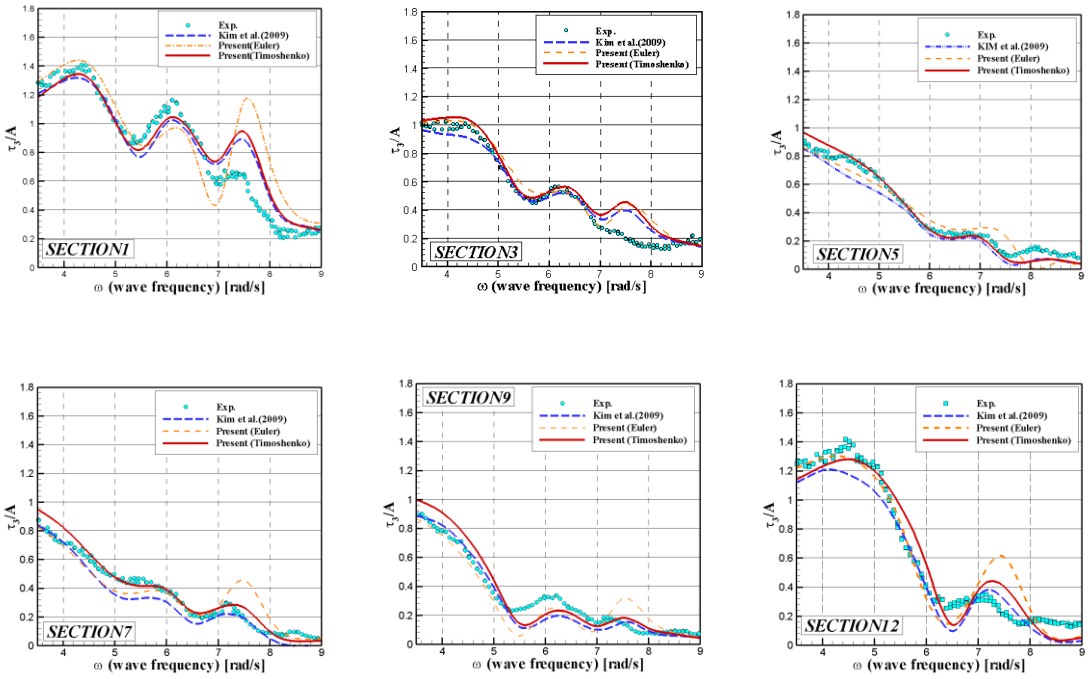

Fig. 4.43 Comparison for vertical displacement of each point for Remy model (head waves)

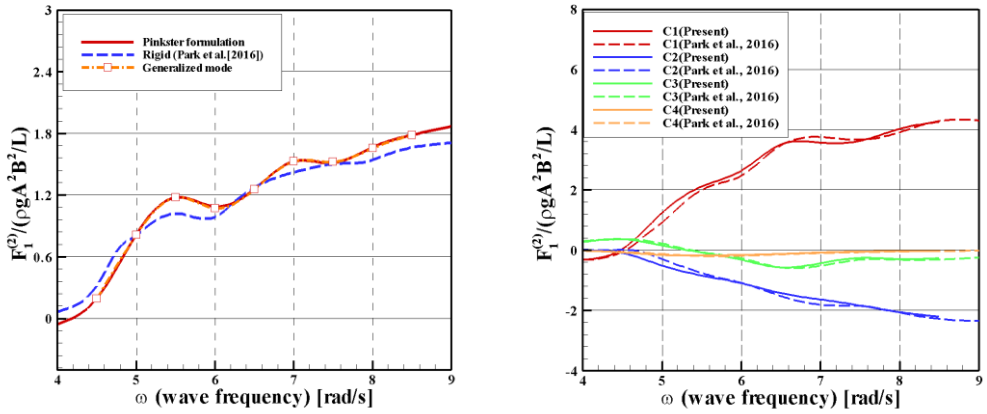

Fig. 4.44 Mean drift force of floating rigid barge (head waves)

In Fig. 4.45, both Malenica model (EI=360.5Nm^2) and Remy model (EI=175Nm^2)'s surge mean drift forces are compared with that of rigid body model. In low frequency region, the result shifts to high frequency region when the flexural rigidity decreases due to reduction of relative vertical wave elevation by hydroelastic response as shown in the right figure. In high frequency region, the result increases drastically near resonance region due to excitation of elastic response. We could also confirm component 4 is slightly increased than rigid body overall frequencies due to hydroelastic response.

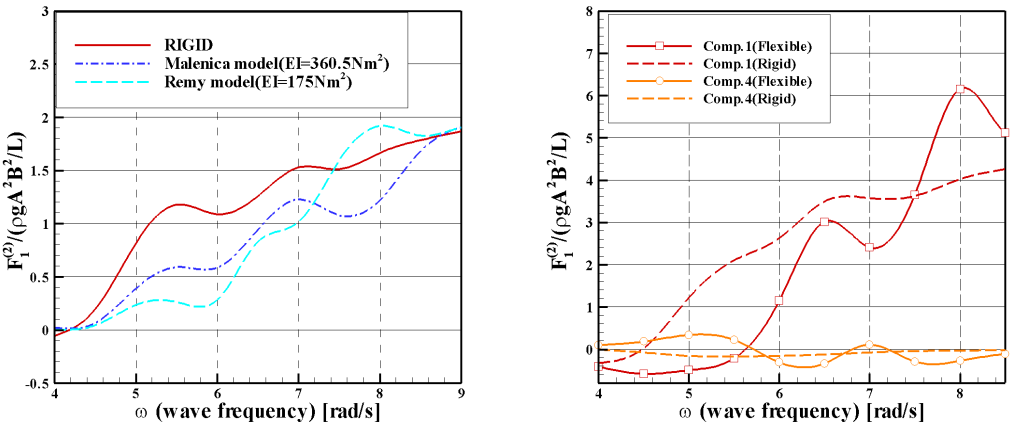

Fig. 4.45 Mean drift force of an elastic barge at different flexural rigidity (Malenica and Remy model) and comparison of component 1, 4 on Remy model

4.5.4 Summary

In the zero forward speed problem, the hydroelastic response of an elastic body is calculated. Linear hydroelastic response is obtained with good accuracy in both bottom-mounted cylinder and very flexible floating barge models. However, the motion is little sensitive near resonance region and overestimated than experiment's results. To improve the response near resonance, more exact modelling should be conducted. The mean drift force on elastic barge is also checked. The generalized mode formulation shows a good agreement with classical equations. The effect of elastic response on mean drift force is also well confirmed. However, the second-order velocity potential force at free-motion does not show good agreement as same with rigid body motion case.

4.6 Numerical study with forward speed (elastic model)

As a final step, numerical study on hydrodynamic force with consideration of both elasticity and forward speed is conducted. The flexibility and forward speed effect on linear & second-order hydrodynamic force are discussed.

4.6.1 Linear hydrodynamic response of elastic Wigley1 model

Several linear hydrodynamic responses of an elastic Wigley1 ship model in head waves are calculated by changing the flexural rigidity. Three structure models are artificially determined to confirm the hydroelastic response.

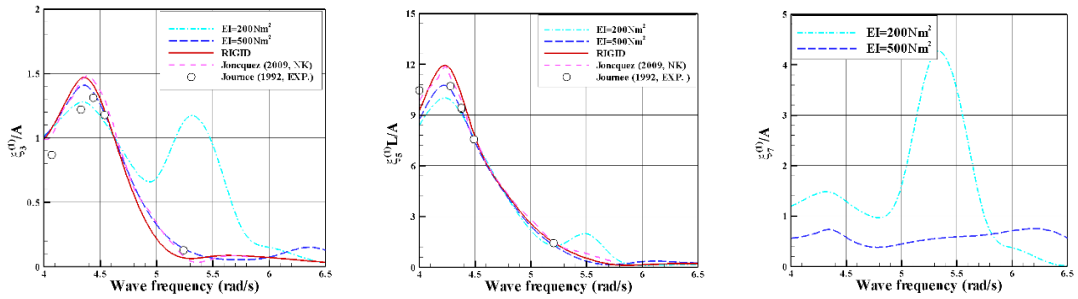

Fig. 4.46 Linear responses in heave, pitch, and two-node vertical bending mode of Wigley1 ship model in head waves (*Fn* = 0.2)

Figure 4.46 shows linear vertical responses in head waves at three different modes. Another time-domain result using Neumann-Kelvin assumption (Joncquez, 2009) and experimental results (Journee, 1992) are also included in this figure. The right figure for the 2-node vertical bending mode shows that the elastic ship with EI=200 Nm^2 has resonance phenomenon at wave frequency 5.5. The other heave and pitch motions are influenced near the frequency of elastic resonance especially in the heave motion, and also we can see slight decrease in amplitude as the flexural rigidity decreases except at resonance region.

In the linear wave-body interaction, we can see the body boundary condition (Eq. (2.22)) has a divergence term of displacement $\nabla \cdot \vec{\tau}^{(1)}$ which only exists in a deformable body. We confirmed the effect of this term for the linear response in head waves. However, there is almost no change in the linear response with/without this divergence term, and therefore it seems that this term has no substantial effect on the hydrodynamic response. This divergence term exists as shown in Fig. 4.47 but the value is too small (about 0.1% of total value in linear body boundary) to affect the response.

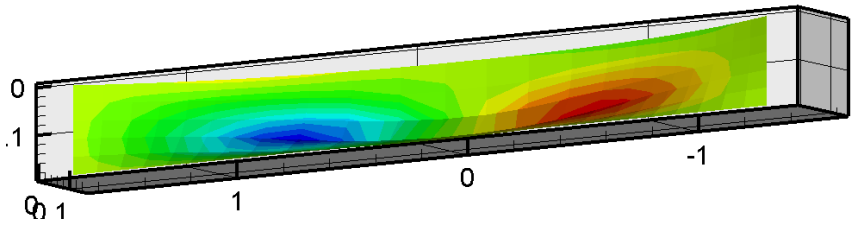

Fig. 4.47 The divergence of displacement in the linear body boundary condition

4.6.2 The effect of flexibility on quadratic product forces for ship model

The effect of flexibility on the quadratic product of linear quantities is checked for a freely-floating body. Double frequency wave forces are obtained by changing the flexural rigidity of the ship model. Fig. 4.48 shows that all forces at three different motion modes decrease as the flexural rigidity decreases except around the region of resonant wave frequency and the effect of flexibility is relatively small on two-node vertical bending mode.

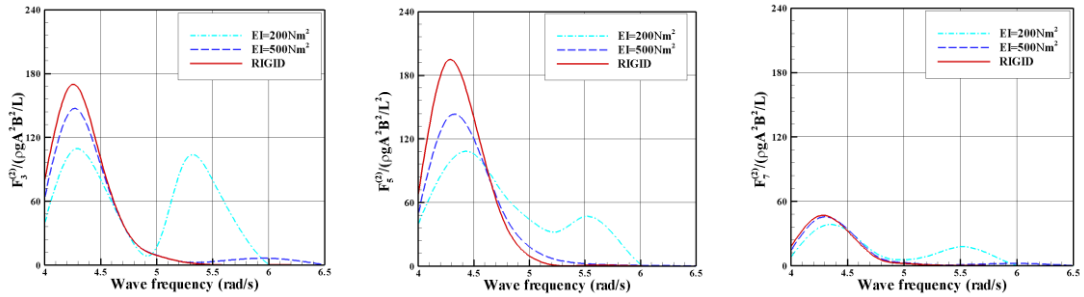

Fig. 4.48 Double frequency wave loads by quadratic product of linear quantities (F_q) for heave, pitch, and two-node vertical bending of Wigley1 ship model in head waves (Fn = 0.2)

In the force due to quadratic product of linear quantities, the steady force can be calculated by taking the time average of the force. Fig. 4.49 shows the steady forces in surge, heave, and pitch of the ship model. In this figure, computed results for the rigid model by another time-domain simulation using the Neumann-Kelvin assumption (Joncquez, 2009) and the measured results only at surge (Jouernee, 1992) direction are also included as same with rigid body case. The surge steady force, which is called the added resistance in waves, shows the same tendency as double-frequency forces discussed earlier with regard to the effect of flexibility. We can see also from this figure that the heave steady force increases as the flexural rigidity decreases in a low frequency region and the effect of flexibility for the pitch steady moment is relatively small.

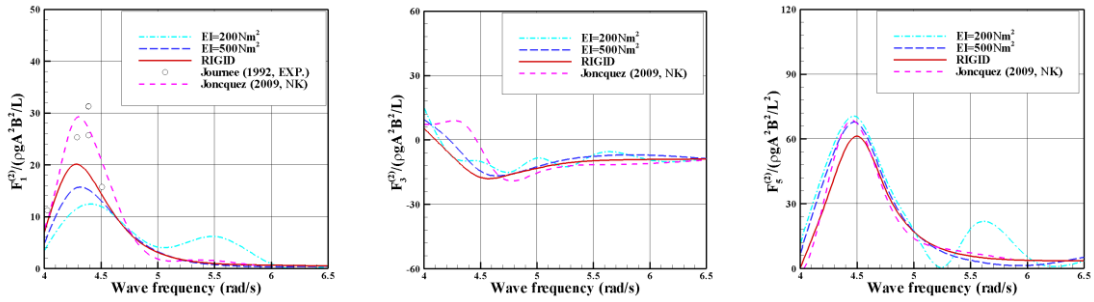

Fig. 4.49 The steady force for surge, heave, and pitch of Wigley1 ship in head waves (Fn = 0.2)

4.6.3 The effect of forward speed and flexural rigidity on second-order excitation forces

Due to uncertainty in the calculation of second-order velocity potential on a freely-floating body in the Rankine panel method, we fixed unsteady rigid body motions. The generalized second-

order velocity-potential force for the two-node vertical bending mode is calculated with elastic mode response.

In this condition, the forward speed effect is checked by changing the Froude number from 0.12 to 0.20. The left figure in Fig. 4.50 shows that the velocity-potential force increases as the Froude number increases in the low-frequency region but the force changes little in short-wavelength regions. In the same condition, the effect of flexural rigidity is also confirmed. The right figure of Fig. 4.50 shows that the second-order velocity-potential force increases as the flexural rigidity decreases due to the increase of elastic response.

The total second-order forces with different flexural rigidity are shown in Fig. 4.51. It seems that the effect of flexibility on the quadratic-product force is larger than that on the second-order velocity-potential force. As shown in the right figure, the quadratic-product force for a very flexible ship becomes much larger than the velocity-potential force near the resonance region. Considering the flexural rigidity of usual ships, however, it could be deduced that the second-order velocity-potential force is predominant on the generalized non-linear excitation force for hydroelastic response.

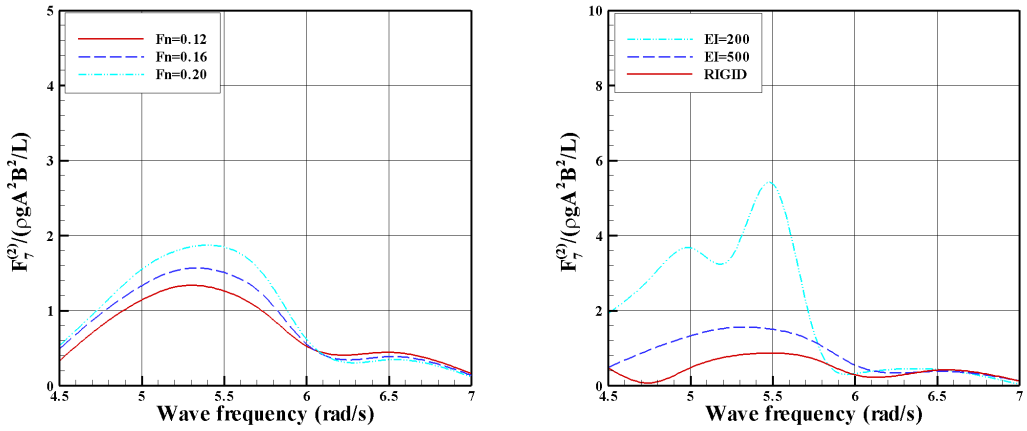

Fig. 4.50 Second-order velocity-potential force for two-node vertical bending of Wigley1 ship model in head waves with different forward speed and flexural rigidity (unsteady rigid body motion is fixed)

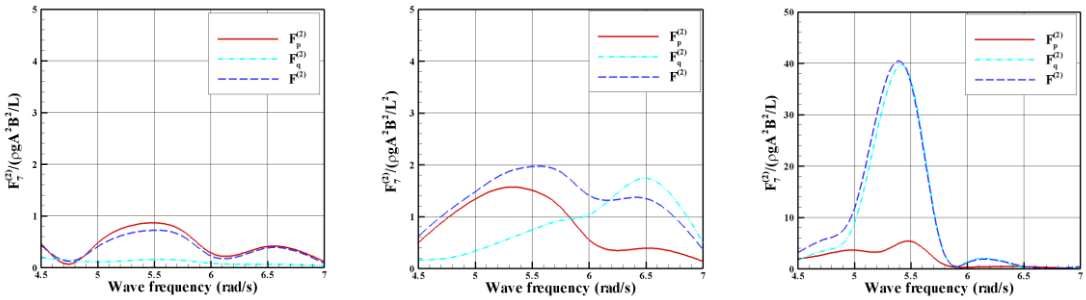

Fig. 4.51 Double-frequency wave loads for two-node vertical bending of rigid (left), *EI* = 500 (middle), and *EI* = 200 (right) Wigley1 ship model in head waves (*Fn* = 0.16, unsteady rigid body motion is fixed)

4.6.4 Summary

The linear and second-order hydrodynamic forces and responses with forward speed on an elastic body are calculated. In the linear motion, the divergence term which only exists in elastic body has no substantial effect and the vertical rigid motion is influenced by elastic bending mode. In the second-order, several quantities are checked by changing forward speed, flexural rigidity and so forth. The effect of flexural rigidity on second-order force is similar with zero forward speed case. The importance of second-order velocity potential force is also confirmed. However, it is calculated with some limitation of Rankine panel method on the free body motion in waves. Thus, much further investigations should be conducted in detail.

CHAPTER 5

Numerical study by frequency-domain analysis in bichromatic waves

5.1 Introduction

In this chapter, wave-body interaction of an elastic body is extended for bichromatic waves without forward speed. The steady state assumption is adopted additionally thus frequency-domain analysis is performed by using wave Green function in HOBEM. Several mathematical formulations to calculate second-order hydrodynamic force in bichromatic waves are explained additionally in the chapter 5.2. Among second-order hydrodynamic forces, detail way to calculate second-order velocity potential force is considered in chapter 5.3. In the last, several numerical results in bichromatic waves are demonstrated.

5.2 Mathematical formulation in bichromatic waves

5.2.1 Boundary-value problem

As mentioned in chapter 2, boundary condition should be defined to solve boundary-value problem. Provided that bottom and radiation conditions are automatically satisfied, other instantaneous free-surface and body boundary conditions in stationary structure are written as follows:

$$\frac{\partial^2 \Phi}{\partial t^2} + g\frac{\partial \Phi}{\partial Z} = -2\nabla\Phi\cdot\nabla\frac{\partial \Phi}{\partial t} - \frac{1}{2}\nabla\Phi\cdot\nabla\left(\nabla\Phi\cdot\nabla\Phi\right) \quad \text{on } S_F \tag{5.1}$$

$$\frac{\partial \Phi}{\partial n} = \vec{n}\cdot\dot{\vec{\tau}} \quad \text{on } S_B \tag{5.2}$$

In bichromatic waves, the linear velocity potential is defined in this form.

$$\Phi^{(1)}(\mathbf{x},t) = \mathrm{Re}\left\{\sum_{j=1}^{2}\phi_j^{(1)}e^{i\omega_j t}\right\} \tag{5.3}$$

$$\text{where}\quad \phi_j^{(1)} = A_j^{(1)}\left(\phi_I^{(1)} + \phi_S^{(1)}\right) + \sum_{i=1}^{N}\xi_i^{(1)}\phi_i^{(1)}$$

The solution of linear velocity potential is very well known and can be obtained by using numerous analytical, numerical ways. In the frame work of weakly non-linear assumption, each variables such as velocity potential, motion, force, etc. is approximated on the value of mean surface in perturbation series. Using Taylor expansion, the second-order boundary conditions are approximated on each mean surface. They are expressed in this form.

1) Free-surface boundary condition

$$\frac{\partial^2\Phi^{(2)}}{\partial t^2} + g\frac{\partial\Phi^{(2)}}{\partial Z} = Q_F \qquad \text{on } Z=0 \tag{5.4}$$

$$\text{where } Q_F = -2\nabla\Phi^{(1)}\cdot\nabla\frac{\partial\Phi^{(1)}}{\partial t} + \frac{1}{g}\frac{\partial\Phi^{(1)}}{\partial t}\left(\frac{\partial^3\Phi^{(1)}}{\partial t^2\partial Z} + g\frac{\partial^2\Phi^{(1)}}{\partial Z^2}\right)$$

2) Body-surface boundary condition

$$\frac{\partial\Phi^{(2)}}{\partial n} = \vec{n}\cdot\dot{\vec{\tau}}^{(2)} + \mathrm{Q}_B \qquad \text{on } \mathrm{S}_{B_0} \tag{5.5}$$

$$\text{where } Q_B = \vec{n}\left(\dot{\vec{\gamma}}^{(2)}\right) - \vec{n}\cdot\left[\vec{\tau}^{(1)}\cdot\nabla\nabla\Phi^{(1)}\right] + \left\{\left(\nabla\cdot\vec{\tau}^{(1)}\right)\vec{n} - \left[\nabla\vec{\tau}^{(1)}\right]^T\cdot\vec{n}\right\}\cdot\left\{\dot{\vec{\tau}}^{(1)} - \nabla\Phi^{(1)}\right\}$$

In the frequency-domain analysis, the second-order velocity potential can be decomposed into three parts as same with linear wave-body interaction problem. It is as follows:

$$\Phi^{(2)} = \Phi_I^{(2)} + \Phi_S^{(2)} + \Phi_R^{(2)} \tag{5.6}$$

Among several components, scattering velocity potential contains all non-homogeneous terms on both free- & body- surfaces. Thus its boundary condition is expressed in this form.

$$\frac{\partial^2\Phi_S^{(2)}}{\partial t^2} + g\frac{\partial\Phi_S^{(2)}}{\partial Z} = Q_F - Q_{F_I} \qquad \text{on } \mathrm{Z}=0 \tag{5.7}$$

$$\frac{\partial \Phi_S^{(2)}}{\partial n} = -\frac{\partial \Phi_I^{(2)}}{\partial n} + \mathrm{Q}_B \qquad \text{on } \mathrm{S}_{B_0} \tag{5.8}$$

The non-homogeneous component makes second-order boundary-value problem be difficult to be solved. Especially non-homogeneous component on the free-surface is regarded as an added oscillating pressure and makes several property of second-order velocity potential (Newman, 1990).

5.2.2 Wave Green function

Before calculating second-order quantities, linear velocity potential should be calculated exactly. In the frequency-domain, it is obtained by using HOBEM based on wave Green function. As well known, the wave Green function has several kinds of form. After conducting the eigen-function expansion on the water depth, the wave Green function could be expressed by series expansion (John, 1950). It is as follows:

$$\begin{aligned} G = & \frac{1}{\pi}\sum_{n=1}^{\infty}\frac{k_n^2}{\nu - H\left(k_n^2+\nu^2\right)}\frac{\cos k_n\left(Z+H\right)}{\cos k_n H}\frac{\cos k_n\left(Z^{'}+H\right)}{\cos k_n H}K_0\left(k_n R\right) \\ & + \frac{i}{2}\sum_{n=1}^{\infty}\frac{k^2}{\nu + H\left(k^2-\nu^2\right)}\frac{\cosh k\left(Z+H\right)}{\cosh kH}\frac{\cosh k\left(Z^{'}+H\right)}{\cosh kH}H_0\left(kR\right) \end{aligned} \tag{5.9}$$

$$\text{where } \omega^2 = -gk_n \tan k_n h$$

Substituting the wave Green function to the integral equation, the velocity potential on the body & free-surface boundaries could be obtained in this form.

$$C_i\left(\vec{X}\right)\phi_i\left(\vec{X}\right) = \begin{cases} \sum_{j=1}^{NP}\left\{\left[S_{ij}\right]-\left[DE_{ij}\right]\right\} & \text{for radiation} \\ \phi_{Ii}\left(\vec{X}\right) - \sum_{j=1}^{NP}\left[DE_{ij}\right] & \text{for diffraction} \end{cases} \tag{5.10}$$

where
$$\left[S_{ij}\right] = \iint_{S_j}\frac{\partial \phi}{\partial n_q}G\left(\vec{X},\vec{X}^{'}\right)dS\left(Q\right)$$
$$\left[DE_{ij}\right] = \iint_{S_j}\phi\frac{\partial G}{\partial n_q}\left(\vec{X},\vec{X}^{'}\right)dS\left(Q\right)$$
, NP : body panel number

5.2.3 Generalized hydrodynamic force in bichromatic waves

Several second-order quantities in bichromatic waves are decomposed into sum- and difference – frequency components. They are as follows:

$$\Phi^{(2)} = \mathrm{Re}\sum_j\sum_l\left\{\phi^{(2)+}e^{i(\omega_j+\omega_l)t}\right\} + \mathrm{Re}\sum_j\sum_l\left\{\phi^{(2)-}e^{i(\omega_j-\omega_l)t}\right\} \tag{5.11}$$

$$\left[Q_F, Q_B\right] = \mathrm{Re}\sum_j\sum_l\left\{\left[Q_F^+, Q_B^+\right]e^{i(\omega_j+\omega_l)t}\right\} + \mathrm{Re}\sum_j\sum_l\left\{\left[Q_F^-, Q_B^-\right]e^{i(\omega_j-\omega_l)t}\right\} \tag{5.12}$$

$$\left[P, \tau\right] = \mathrm{Re}\sum_j\sum_l\left\{\left[p_{jl}^+, \tau_{jl}^+\right]e^{i(\omega_j+\omega_l)t}\right\} + \mathrm{Re}\sum_j\sum_l\left\{\left[p_{jl}^-, \tau_{jl}^-\right]e^{i(\omega_j-\omega_l)t}\right\} \tag{5.13}$$

$$F_{ijl}^{(2)} = \mathrm{Re}\sum_j\sum_l\left\{F_{ijl}^{(2)+}e^{i(\omega_j+\omega_l)t}\right\} + \mathrm{Re}\sum_j\sum_l\left\{F_{ijl}^{(2)-}e^{i(\omega_j-\omega_l)t}\right\} \tag{5.14}$$

In the second-order wave-body interaction problem, difference frequency components are important for several situations such as slowly varying force on the moored vessels or low-frequency resonance phenomenon. In this study, however, we are focusing on springing problem thus the sum-frequency components are only considered.

As described in chapter 2, each force is redefined by using inner product of modal vector and pressure in the generalized modes. We can rewrite it in this form.

$$F_{ijl}^{(2)+} = \iint_{S_B} p_{jl}^+\left(\vec{h}^i \cdot \vec{N}\right)_{jl} ds \tag{5.15}$$

Approximating the pressure and inner product on mean body surface, the second-order generalized force could also be obtained in bichromatic waves. Using the classical way, the second-order hydrodynamic force is analysed by summation of three following forces.

$$F_{ijl}^{(2)+} = F_{p_{ijl}}^{(2)+} + F_{q_{ijl}}^{(2)+} + F_{res_{ijl}}^{(2)+} \tag{5.16}$$

$$F_{res_{ijl}}^{(2)+} = C_{ik}\xi_{kjl}^{(2)} \tag{5.17}$$

$$F_{p_{ijl}}^{(2)+} = -i\rho\left(\omega_j + \omega_l\right)\iint_{S_{B0}}\phi^{(2)+}\left(\vec{h}^i \cdot \vec{n}\right)dS \tag{5.18}$$

$$
\begin{aligned}
F_{q_{ijl}}^{(2)+} = & -\frac{\rho g}{2}\int_{WL}\left(\zeta_j^{(1)}-\tau_{3j}^{(1)}\right)\left(\zeta_l^{(1)}-\tau_{3l}^{(1)}\right)\frac{\left(\vec{h}^i\cdot\vec{n}\right)}{\sin\beta}dl \\
& +\rho\iint_{S_{B_0}}\left(\frac{1}{2}\nabla\phi_j^{(1)}\cdot\nabla\phi_l^{(1)}+i\omega_l\vec{\tau}_j^{(1)}\cdot\nabla\phi_l^{(1)}+g\gamma_{3jl}\right)\left(\vec{h}^i\cdot\vec{n}\right)dS \\
& +\rho\iint_{S_{B_0}}\left(i\omega_j\phi_j^{(1)}+g\tau_{3j}^{(1)}\right)\left\{\nabla\vec{h}^i\cdot\vec{\tau}_l^{(1)}+\left(\nabla\cdot\vec{\tau}_l^{(1)}\right)\vec{h}^i-\nabla\vec{\tau}_l^{(1)}\cdot\vec{h}^i\right\}\cdot\vec{n}dS \\
& +\rho g\iint_{S_{B_0}} z\left\{\begin{array}{l}\left(\nabla\cdot\vec{\gamma}_{jl}^{(2)}\right)\vec{h}^i-\nabla\vec{\gamma}_{jl}^{(2)}\cdot\vec{h}^i+\nabla\vec{h}^i\cdot\vec{\gamma}_{jl}^{(2)} \\ +\left(\nabla\vec{h}^i\cdot\vec{\tau}_j^{(1)}\right)\cdot\nabla\vec{\tau}_l^{(1)}+\vec{h}^i\cdot\left(\frac{\partial\vec{\tau}_j^{(1)}}{\partial y}\times\frac{\partial\vec{\tau}_l^{(1)}}{\partial z},\frac{\partial\vec{\tau}_j^{(1)}}{\partial z}\times\frac{\partial\vec{\tau}_l^{(1)}}{\partial x},\frac{\partial\vec{\tau}_j^{(1)}}{\partial x}\times\frac{\partial\vec{\tau}_l^{(1)}}{\partial y}\right)\end{array}\right\}\cdot\vec{n}dS
\end{aligned}
\tag{5.19}
$$

Second-order boundary-value problem should be solved to obtain second-order restoring (F_{res}) & velocity potential force (F_p). On the other hands, another force (F_q) consists of linear quantities.

5.3 Evaluation of second-order velocity potential force

Instead of solving second-order boundary condition, the second-order velocity potential force could be calculated by using only linear quantities. Molin (1979) suggested so called indirect method by applying the Haskind relation to the second-order boundary condition. This method is starting from the following integral equation.

$$
\iint_{S_B}\left(\phi_s\frac{\partial\psi_i^{\pm}}{\partial n}-\psi_i^{\pm}\frac{\partial\phi_s}{\partial n}\right)dS+\iint_{S_F}\left(\phi_s\frac{\partial\psi_i^{\pm}}{\partial n}-\psi_i^{\pm}\frac{\partial\phi_s}{\partial n}\right)dS=0 \tag{5.20}
$$

Here, bottom and far-field radiation conditions are satisfied and become zero. ψ_i is so called *assistant velocity potential* which satisfies following boundary conditions

$$
-\left(\omega_j\pm\omega_l\right)^2\psi_i^{\pm}+g\frac{\partial\psi_i^{\pm}}{\partial Z}=0 \qquad \text{on } Z=0 \tag{5.21}
$$

$$
\frac{\partial\psi_i^{\pm}}{\partial n}=n_i \qquad \text{on } S_{B_0} \tag{5.22}
$$

Substituting second-order boundary condition into Eq. (5.20), the second-order scattering velocity potential has following relation

$$\iint_{S_{B_0}} \phi_s \frac{\partial \psi_i^{\pm}}{\partial n} dS = -\iint_{S_{B_0}} \psi_i^{\pm} \left(\frac{\partial \phi_I^{(2)}}{\partial n} + Q_B^{\pm} \right) dS - \frac{1}{g} \iint_{S_{F_0}} \left(Q_F^{\pm} - Q_{F_{II}}^{\pm} \right) \psi_i^{\pm} dS \tag{5.23}$$

Thus, the sum-frequency scattering velocity potential force can be expressed in this form

$$\begin{aligned} F_{p_{ijl}}^{(2)+} = & -i\rho\left(\omega_j + \omega_l\right) \iint_{S_{B_0}} \left(\left(\vec{h}^i \cdot \vec{n}\right) \phi_I^{(2)+} - \psi_i^+ \frac{\partial \phi_I^{(2)+}}{\partial n} \right) dS \\ & - i\rho\left(\omega_j + \omega_l\right) \iint_{S_{B_0}} \psi_i^+ Q_B^+ dS - i\rho \frac{\left(\omega_j + \omega_l\right)}{g} \iint_{S_{F_0}} \left(Q_F^+ - Q_{F_{II}}^+ \right) \psi_i^+ dS \end{aligned} \tag{5.24}$$

This formulation includes several non-homogeneous components and it should be evaluated by both body and free-surface integration. It has been decomposed into several components (Kim and Yue, 1990). They are as follows:

$$f_{p-BB}^{i+} = -i\rho\omega^+ \iint_{S_{B_0}} \left(\left(\vec{h}^i \cdot \vec{n}\right) \phi_I^{(2)+} - \psi_i^+ \frac{\partial \phi_I^{(2)+}}{\partial n} \right) dS - \frac{i\rho\omega^+}{g} \iint_{S_{F_0}} \left(Q_F^+ - Q_{F_{II}}^+ \right) \psi_i^+ dS \tag{5.25}$$

$$f_{BB}^{i+} = -i\rho\omega^+ \iint_{S_{B_0}} \left(\psi_i^+ Q_B^+ \right) dS \tag{5.26}$$

Each component shows the contribution from non-homogeneous terms of body & free-surface boundaries. The detail evaluation of each integration is explained at following sections.

5.3.1 The incident wave part

The second-order incident wave velocity potential could be obtained by satisfying the free-surface boundary and sea bottom (*Z*=-*H*) condition. As a result, it could be obtained analytically (Bowers, 1980) by substituting the linear incident wave velocity potential on the following free-surface boundary condition.

$$\frac{\partial^2 \Phi_I^{(2)}}{\partial t^2} + g \frac{\partial \Phi_I^{(2)}}{\partial Z} = Q_{F_I} \qquad \text{on } Z = 0 \tag{5.27}$$

$$\text{where } Q_{F_I} = -2\nabla\Phi_I^{(1)} \cdot \nabla \frac{\partial \Phi_I^{(1)}}{\partial t} + \frac{1}{g} \frac{\partial \Phi_I^{(1)}}{\partial t} \left(\frac{\partial^3 \Phi_I^{(1)}}{\partial t^2 \partial Z} + g \frac{\partial^2 \Phi_I^{(1)}}{\partial Z^2} \right)$$

After solving above equation with sea bottom condition, the second-order incident velocity potential is derived in this form.

$$\phi_I^{+(2)} = \frac{A_j A_l}{2} ig\left(\gamma_{jl}^{+} + \gamma_{lj}^{+}\right) \frac{\cosh k^{+}\left(Z+H\right)}{\cosh k^{+} H} e^{-ik^{+}\left(X\cos\beta + Y\sin\beta\right)} \tag{5.28}$$

where $\gamma_{jl}^{+} = \frac{1}{2\omega_j} \frac{k_j^2\left(1-\tanh^2 k_j H\right) + 2k_j k_l\left(1-\tanh k_j H \tanh k_l H\right)}{\nu^{+} - k^{+}\tanh k^{+} H}$, $\nu^{+} = \frac{\left(\omega_j + \omega_l\right)^2}{g}$,

$k^{+} = k_j + k_l$

5.3.2 The body part

The body surface integration is expressed by using symmetric form. It is as follows:

$$f_{BB}^{i+} = -i\rho\omega^{+} \iint_{S_{B_0}} \left(\psi_i^{+} Q_B^{+}\right) dS = -i\rho\omega^{+} \iint_{S_{B_0}} \frac{1}{2}\left(q_{B_{jl}}^{+} + q_{B_{lj}}^{+}\right) \psi_i^{+} dS \tag{5.29}$$

The body part includes integration of body non-homogeneous component. In non-homogeneous term, there is one second derivative of velocity potential. Using shape function of HOBEM, we could evaluate second derivative value accurately provided the geometry is not so complex. Another way is to use following Stokes theorem to avoid the calculation of second-derivative itself.

$$\iint_{S_{B_0}} \left\{\psi\left(\nabla\times\vec{F}\right) + \left(\nabla\psi\right)\times\vec{F}\right\}\cdot\vec{N} dS = \oint_{WL} \psi\vec{F}\cdot\vec{T} dl \tag{5.30}$$

where ***T*** is unit tangent vector

On an elastic body, the second derivative of velocity potential term is expressed in this form.

$$\begin{aligned}\iint_{S_{B_0}} \vec{n}\cdot\left[\psi_i^{+}\vec{\tau}_j^{(1)}\cdot\nabla\nabla\phi_l^{(1)}\right] dS = &-\iint_{S_{B_0}} \psi_i^{+}\left(\nabla\cdot\vec{\tau}_j^{(1)}\right)\left(\nabla\phi_l^{(1)}\cdot\vec{n}\right) dS + \iint_{S_{B_0}} \left\{\psi_i^{+}\left(\nabla\phi_l^{(1)}\cdot\nabla\vec{\tau}_j^{(1)}\right)\cdot\vec{n}\right\} dS \\ &- \iint_{S_{B_0}} \left\{\nabla\psi_i^{+}\times\left(\nabla\phi_l^{(1)}\times\vec{\tau}_j^{(1)}\right)\right\}\cdot\vec{n} dS + \oint_{WL} \psi_i^{+}\left(\nabla\phi_l^{(1)}\times\vec{\tau}_j^{(1)}\right)\cdot\vec{T} dl\end{aligned} \tag{5.31}$$

Thus, the body surface integral could be rewritten without second derivative. It is as follows:

$$\iint_{S_{B_0}} q^+_{B_{jl}} \psi_i^+ dS = \frac{1}{2}\iint_{S_{B_0}} \psi_i^+ \vec{n}\cdot\left(\dot{\vec{\gamma}}^{(2)}_{jl}\right) + \psi_i^+ \left\{\left(\nabla\cdot\vec{\tau}_l^{(1)}\right)\vec{n} - \left[\nabla\vec{\tau}_l^{(1)}\right]^T\cdot\vec{n}\right\}\cdot\left\{i\omega_j\vec{\tau}_j^{(1)} - \nabla\phi_j^{(1)}\right\} \mathrm{dS}$$
$$+\frac{1}{2}\iint_{S_{B_0}} \psi_i^+\left(\nabla\cdot\vec{\tau}_j^{(1)}\right)\left(\nabla\phi_l^{(1)}\cdot\vec{n}\right)dS - \frac{1}{2}\iint_{S_{B_0}}\left\{\psi_i^+\left(\nabla\phi_l^{(1)}\cdot\nabla\vec{\tau}_j^{(1)}\right)\cdot\vec{n}\right\}dS \qquad (5.32)$$
$$+\frac{1}{2}\iint_{S_{B_0}}\left\{\nabla\psi_i^+\times\left(\nabla\phi_l^{(1)}\times\vec{\tau}_j^{(1)}\right)\right\}\cdot\vec{n}dS - \frac{1}{2}\oint_{WL}\psi_i^+\left(\nabla\phi_l^{(1)}\times\vec{\tau}_j^{(1)}\right)\cdot\vec{T}dl$$

This modified integral form of the body part could be conducted numerically without any difficulty.

5.3.3 The free-surface part

The free-surface integration is the most difficult part to be evaluated and important in second-order velocity potential force. As a first step in evaluation of free-surface integral, the radius (R_s) which does not have the *local-wave* is determined (*See* Fig. 5.1). Next, each region is integrated by different methods. In the near-field region ($r < R_S$), the integration is conducted numerically and in the far-field region ($r > R_S$), the integration is approximated mathematically by using series expansion and defined functions. The detail method is described as follows:

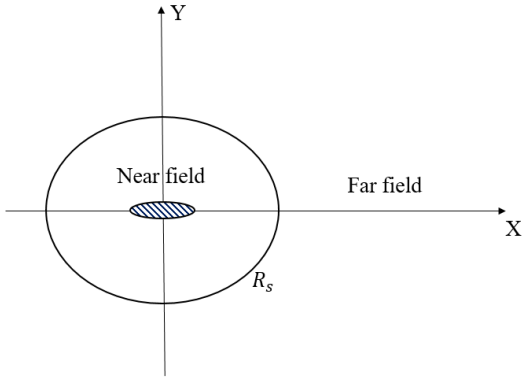

Fig. 5.1 The division of free-surface integral region (Top view)

1) Integration of near-field free-surface

The free-surface integral of near-field is computed numerically. The free-surface integral is expressed by using symmetric form.

$$-\frac{i\omega^+}{g}\iint_{S_{F_{in}}}\left(Q_F^+ - Q_{F_{II}}^+\right)\psi_i^+ dS = -\frac{i\omega^+}{2g}\iint_{S_{F_{in}}}\left(q_{F_{jl}}^+ + q_{F_{lj}}^+ - q_{F_{II_{jl}}}^+ - q_{F_{II_{lj}}}^+\right)\psi_i^+ dS \tag{5.33}$$

Using free-surface boundary condition *i.e.* $\frac{\partial\phi_j^{(1)}}{\partial Z} = \nu_j\phi_j^{(1)}$, free-surface integral could be written by

$$\iint_{S_{F_{in}}} q_{F_{jl}}^+\psi_i^+ dS = \iint_{S_{F_{in}}}\left\{\phi_j^{(1)}\phi_l^{(1)}\lambda_{jl} + \frac{i\omega_l\phi_l^{(1)}}{2}\frac{\partial^2\phi_j^{(1)}}{\partial Z^2} - i\omega_l\left(\frac{\partial\phi_j^{(1)}}{\partial X}\frac{\partial\phi_l^{(1)}}{\partial X} + \frac{\partial\phi_j^{(1)}}{\partial Y}\frac{\partial\phi_l^{(1)}}{\partial Y}\right)\right\}\psi_i^+ dS$$
$$\text{where} \quad \lambda_{jl} = -i\left(\frac{\omega_l\nu_j^2}{2} + \omega_l\nu_j\nu_l\right) \tag{5.34}$$

In this integral, there is also a second derivative term of velocity potential. Using 2-dimensional Gauss theorem on free-surface as used in Kim (1991), second derivative term could be removed.

$$\iint_{S_{F_{in}}}\phi_j^{(1)}\frac{\partial_2\phi_l^{(1)}}{\partial Z^2}\psi_i^+ dS = -\int_{WL+R_s}\phi_j^{(1)}\left(\frac{\partial\phi_l^{(1)}}{\partial X}n_X + \frac{\partial\phi_l^{(1)}}{\partial Y}n_Y\right)\psi_i^+ dl$$
$$+\iint_{S_{F_{in}}}\left(\frac{\partial\phi_j^{(1)}}{\partial X}\frac{\partial\phi_l^{(1)}}{\partial X} + \frac{\partial\phi_j^{(1)}}{\partial Y}\frac{\partial\phi_l^{(1)}}{\partial Y}\right)\psi_i^+ + \phi_j^{(1)}\left(\frac{\partial\phi_l^{(1)}}{\partial X}\frac{\partial\psi_i^+}{\partial X} + \frac{\partial\phi_l^{(1)}}{\partial Y}\frac{\partial\psi_i^+}{\partial Y}\right)dS \tag{5.35}$$

Thus, the free-surface integral could be rewritten in this form

$$\iint_{S_{F_{in}}} q_{F_{jl}}^+\psi_i^+ dS = -\int_{WL+R_s}\frac{i\omega_k\phi_l^{(1)}}{2}\left(\frac{\partial\phi_j^{(1)}}{\partial X}n_x + \frac{\partial\phi_j^{(1)}}{\partial Y}n_y\right)\psi_i^+ dl + \iint_{S_{F_{in}}}\frac{i\omega_l\phi_l^{(1)}}{2}\left(\frac{\partial\phi_j^{(1)}}{\partial X}\frac{\partial\psi_i^+}{\partial X} + \frac{\partial\phi_j^{(1)}}{\partial Y}\frac{\partial\psi_i^+}{\partial Y}\right)dS$$
$$+\iint_{S_{F_{in}}}\left\{-\frac{i\omega_l}{2}\left(\frac{\partial\phi_l^{(1)}}{\partial X}\frac{\partial\phi_j^{(1)}}{\partial X} + \frac{\partial\phi_l^{(1)}}{\partial Y}\frac{\partial\phi_j^{(1)}}{\partial Y}\right) + \phi_j^{(1)}\phi_l^{(1)}\lambda_{jl}\right\}\psi_i^+ dS \tag{5.36}$$

2) Integration of far-field free-surface

In the far-field free-surface region, the integration has infinite region and the integrand has value in the far-field region due to slowly decaying property, thus direct numerical integration is very difficult to give good accuracy. Instead of numerical integration, we could evaluate free-surface integral by using far-field approximation of several linear variables.

Before conducting series expansion, velocity potential is expressed mathematically by using asymptotic formulation. The incident wave velocity potential is approximated by using Fourier-Bessel expansion in this form.

$$\begin{aligned}\phi_I &= \frac{igA}{\omega}\frac{\cosh(k(Z+H))}{\cosh(kH)}\sum_{n=0}^{\infty}\varepsilon_n(-1)^n J_n(kR)\cos n(\theta-\beta) \\ &= \frac{igA}{\omega}\frac{\cosh(k(Z+H))}{\cosh(kH)}\sum_{n=0}^{\infty}J_n(kr)\left[A_n^c\cos n\theta + A_n^s\sin n\theta\right]\end{aligned} \tag{5.37}$$

$$\text{where } \begin{pmatrix}A_n^c\\A_n^s\end{pmatrix} = \frac{igA}{\omega}\varepsilon_n(-1)^n\begin{pmatrix}\cos n\beta\\ \sin n\beta\end{pmatrix} \text{ and } \varepsilon_0 = 1, \varepsilon_n = 2(n\geq 1)$$

The disturbed velocity potentials can be obtained by solving following integration.

$$\begin{aligned}\phi &= \iint_S \sigma(r',\theta')G(r,\theta;r',\theta')dS \\ \text{where, } \sigma &= \frac{1}{4\pi}\left(\frac{\partial\phi}{\partial n} - \phi\frac{\partial}{\partial n}\right)\end{aligned} \tag{5.38}$$

To evaluate the integration, the wave Green function in far-field is first approximated in this form

$$G \approx -2\pi i\frac{k^2}{k^2H - v^2H + v}\cosh k(Z+H)\cosh(Z'+H)H_0(kR) \tag{5.39}$$

To expand above equation, Graf's addition theorem is used in a Fourier-Bessel series. As a result, the field and source points are separated in the Green function. It could be rewritten by

$$G \approx 2\pi i\frac{k^2}{k^2H - v^2H + v}\cosh k(Z+H)\cosh(Z'+H)J_n(kr')H_n(kr)\cos n(\theta-\theta') \tag{5.40}$$

After substituting Eq. (5.40) into Eq. (5.38), radiation & diffraction velocity potentials could be expressed by using generalized *Kochin* function (B_n). It is as follows:

$$\phi_B = \sum_{n=0}^{\infty}H_n(kr)\left[B_n^c\cos n\theta + B_n^s\sin n\theta\right] \tag{5.41}$$

$$\text{where } \begin{pmatrix}B_n^c\\B_n^s\end{pmatrix} = 2\pi i\frac{k^2}{k^2H - v^2H + v}\varepsilon_n\iint_{S_B}\sigma(r',\theta')\frac{\cosh(k(z'+H))}{\cosh(kH)}J_n(kr')\begin{pmatrix}\cos n\theta'\\ \sin n\theta'\end{pmatrix}dS$$

Using defined variables, far-field free-surface integration has been conducted by numerous integration ways. In this study, we evaluated the integral by using same way suggested by Newman (1991). Since we used indirect method, the far-field variable of assistant velocity potential which is expressed as ***C*** is simply added on the equation. In this dissertation, we just repeat the evaluation procedure of far-field free-surface integration in Newman (1991) and more detail explanation is written in the paper. The far-field integration is divided into three components as follows:

$$\iint_{S_{F_{out}}} \left(Q^{+}_{F_{BBjl}} + Q^{+}_{F_{IBjl}} + Q^{+}_{F_{BIjl}} \right) \psi_i^{+} dS \tag{5.42}$$

To simplify the procedure of integration, only disturbed velocity potential (Q_{FBB}) is first considered. The free-surface integral could be rewritten in the cylindrical coordinate system. It is as follows:

$$\iint_{S_{F_{out}}} \left(Q^{+}_{F_{BBjl}} \right) \psi_i^{+} dS = \frac{i}{4} \iint_{S_{F_{out}}} \left\{ \begin{array}{l} -2\left(\omega_j + \omega_l\right)\left(\dfrac{\partial \phi_j^{(1)}}{\partial r}\dfrac{\partial \phi_l^{(1)}}{\partial r} + \dfrac{1}{r^2}\dfrac{\partial \phi_j^{(1)}}{\partial \theta}\dfrac{\partial \phi_l^{(1)}}{\partial \theta} + \nu_j \nu_l \phi_j^{(1)} \phi_l^{(1)} \right) \\ + \dfrac{\omega_j}{g}\phi_j^{(1)}\left(-\omega_l^2 \nu_l \phi_l^{(1)} + g k_l^2 \phi_l^{(1)} \right) + \dfrac{\omega_l}{g}\phi_l^{(1)}\left(-\omega_j^2 \nu_j \phi_j^{(1)} + g k_j^2 \phi_j^{(1)} \right) \end{array} \right\} \psi_i^{+} dS \tag{5.43}$$

Substituting defined far-field variables into Eq. (5.43), it is expressed in this form.

$$= \frac{i}{4} \iint_{S_{F_{out}}} \left[\begin{array}{l} -2\left(\omega_j + \omega_l\right) k_j k_l \\ \times \sum_{m=0}^{\infty}\sum_{n=0}^{\infty} H_m^{'}\left(k_j r\right) H_n^{'}\left(k_l r\right) \left[B_{mj}^{c} \cos m\theta + B_{mj}^{s} \sin m\theta \right] \left[B_{nl}^{c} \cos n\theta + B_{nl}^{s} \sin n\theta \right] \\ -2\left(\omega_j + \omega_l\right) \dfrac{mn}{r^2} \\ \times \sum_{m=0}^{\infty}\sum_{n=0}^{\infty} H_m\left(k_j r\right) H_n\left(k_l r\right) \left[-B_{mj}^{c} \sin m\theta + m B_{mj}^{s} \cos m\theta \right] \left[-B_{nl}^{c} \sin n\theta + B_{nl}^{s} \cos n\theta \right] \\ + \left[\omega_l \left(k_j^2 - \nu_j^2 \right) + \omega_j \left(k_l^2 - \nu_l^2 \right) - 2\left(\omega_j + \omega_l\right) \nu_j \nu_l \right] \\ \times \sum_{m=0}^{\infty}\sum_{n=0}^{\infty} H_m\left(k_j r\right) H_n\left(k_l r\right) \left[B_{mj}^{c} \cos m\theta + B_{mj}^{s} \sin m\theta \right] \left[B_{nl}^{c} \cos n\theta + B_{nl}^{s} \sin n\theta \right] \end{array} \right] \\ \times \sum_{u=0}^{\infty} H_u\left(k_k r\right) \left[C_{uk}^{c} \cos u\theta + C_{uk}^{s} \sin u\theta \right] dS \tag{5.44}$$

Using following recurrence relation of Hankel function, it is rewritten by

$$H_v^{'} = \frac{1}{2}\left(H_{v-1} - H_{v+1}\right), \quad 2v\frac{H_v}{z} = H_{v-1} + H_{v+1} \tag{5.45}$$

$$\begin{aligned} &= \frac{i}{4}\iint_{S_{F_{out}}} \left[\begin{array}{l} -2\left(\omega_j + \omega_l\right)\dfrac{k_j k_l}{4}\left(\begin{array}{l} \displaystyle\sum_{m=0}^{\infty}\sum_{n=0}^{\infty}\left\{ \begin{array}{l} \left(H_{m-1}H_{n-1} - H_{m-1}H_{n+1} + H_{m+1}H_{n+1} - H_{m+1}H_{n-1}\right) \\ \times\left[B_{mj}^{c}\cos m\theta + B_{mj}^{s}\sin m\theta\right]\left[B_{nl}^{c}\cos n\theta + B_{nl}^{s}\sin n\theta\right] \end{array} \right\} \\ +\displaystyle\sum_{m=0}^{\infty}\sum_{n=0}^{\infty}\left\{ \begin{array}{l} \left(H_{m-1}H_{n-1} + H_{m-1}H_{n+1} + H_{m+1}H_{n+1} + H_{m+1}H_{n-1}\right) \\ \times\left[-B_{mj}^{c}\sin m\theta + B_{mj}^{s}\cos m\theta\right]\left[-B_{nl}^{c}\sin n\theta + B_{nl}^{s}\cos n\theta\right] \end{array} \right\} \end{array} \right) \\ +\left\{ \begin{array}{l} \left(\omega_j\left(k_l^2 - v_l^2\right) + \omega_l\left(k_j^2 - v_j^2\right) - 2\left(\omega_j + \omega_l\right)v_l v_j\right) \\ \times\displaystyle\sum_{m=0}^{\infty}\sum_{n=0}^{\infty}H_m\left(k_j\rho\right)H_n\left(k_l\rho\right)\left[B_{mj}^{c}\cos m\theta + B_{mj}^{s}\sin m\theta\right]\left[B_{nl}^{c}\cos n\theta + B_{nl}^{s}\sin n\theta\right] \end{array} \right\} \end{array} \right] \\ &\times\sum_{u=0}^{\infty}H_u\left(k_k\rho\right)\left[C_{uk}^{c}\cos u\theta + C_{uk}^{s}\sin u\theta\right]dS \end{aligned} \tag{5.46}$$

Since the variable is described in cylindrical coordinate system, the free-surface integral could be evaluated by separating integration variables; *i.e.* azimuthal and radial directions. Thus the equation could be rewritten by

$$\begin{aligned} &= \frac{i}{4}\int_{R_s}^{\infty} \left[\begin{array}{l} -2\left(\omega_j + \omega_l\right)\dfrac{k_j k_l}{4}\left\{ \begin{array}{l} \displaystyle\sum_{m=0}^{\infty}\sum_{n=0}^{\infty}\sum_{u=0}^{\infty}\left[\begin{array}{l} \left\{H_{m-1}H_{n-1} - H_{m-1}H_{n+1} + H_{m+1}H_{n+1} - H_{m+1}H_{n-1}\right\}H_u \\ \times\left(\begin{array}{l} B_{mj}^{c}B_{nl}^{c}C_{uk}^{c}\lambda_{mnu}^{+} + B_{mj}^{s}B_{nl}^{s}C_{uk}^{c}\lambda_{mnu}^{-} \\ B_{mj}^{c}B_{nl}^{s}C_{uk}^{s}\lambda_{num}^{-} + B_{mj}^{s}B_{nl}^{c}C_{uk}^{s}\lambda_{umn}^{-} \end{array} \right) \end{array} \right] \\ +\displaystyle\sum_{m=0}^{\infty}\sum_{n=0}^{\infty}\sum_{u=0}^{\infty}\left[\begin{array}{l} \left\{H_{m-1}H_{n-1} + H_{m-1}H_{n+1} + H_{m+1}H_{n+1} + H_{m+1}H_{n-1}\right\}H_u \\ \times\left(\begin{array}{l} B_{mj}^{c}B_{nl}^{c}C_{uk}^{c}\lambda_{mnu}^{-} + B_{mj}^{s}B_{nl}^{s}C_{uk}^{c}\lambda_{mnu}^{+} \\ -B_{mj}^{c}B_{nl}^{s}C_{uk}^{s}\lambda_{umn}^{-} - B_{mj}^{s}B_{nl}^{c}C_{uk}^{s}\lambda_{num}^{-} \end{array} \right) \end{array} \right] \end{array} \right\}rdr \\ +\left\{ \begin{array}{l} \left\{\omega_j\left(k_l^2 - v_l^2\right) + \omega_l\left(k_j^2 - v_j^2\right) - 2\left(\omega_j + \omega_l\right)v_l v_j\right\} \\ \times\displaystyle\sum_{m=0}^{\infty}\sum_{n=0}^{\infty}\sum_{u=0}^{\infty}H_m H_n H_u\left(\begin{array}{l} B_{mj}^{c}B_{nl}^{c}C_{uk}^{c}\lambda_{mnu}^{+} + B_{mj}^{s}B_{nl}^{s}C_{uk}^{c}\lambda_{mnu}^{-} \\ B_{mj}^{c}B_{nl}^{s}C_{uk}^{s}\lambda_{num}^{-} + B_{mj}^{s}B_{nl}^{c}C_{uk}^{s}\lambda_{umn}^{-} \end{array} \right) \end{array} \right\} \end{array} \right] \end{aligned} \tag{5.47}$$

Here, upper & lower lines in parenthesis (*BBC*) mean $\cos u\theta$ & $\sin u\theta$ components, respectively and integration of trigonometric function for the azimuthal direction is defined in this form.

$$\int_0^{2\pi} \cos m\theta \cos n\theta \cos u\theta d\theta = \frac{\pi}{\varepsilon_u}\left[\delta_{u,|m-n|} + \delta_{u,m+n}\right] \equiv \lambda^{+}_{mnu} \tag{5.48}$$

$$\int_0^{2\pi} \sin m\theta \sin n\theta \cos u\theta d\theta = \frac{\pi}{\varepsilon_u}\left[\delta_{u,|m-n|} - \delta_{u,m+n}\right] \equiv \lambda^{-}_{mnu} \tag{5.49}$$

$$\int_0^{2\pi} \cos m\theta \sin n\theta \sin u\theta d\theta = \frac{\pi}{\varepsilon_u}\left[\delta_{m,|u-n|} - \delta_{m,u+n}\right] \equiv \lambda^{-}_{num} \tag{5.50}$$

$$\int_0^{2\pi} \sin m\theta \cos n\theta \sin u\theta d\theta = \frac{\pi}{\varepsilon_u}\left[\delta_{n,|u-m|} - \delta_{n,u+m}\right] \equiv \lambda^{-}_{umn} \tag{5.51}$$

where integration which includes odd number of *sin* function has no value due to symmetric property.

After few mathematical manipulations with defined variables, it could be expressed simpler form. It is as follows:

$$= \frac{i}{8}\int_{R_s}^{\infty}\sum_{m=0}^{\infty}\sum_{n=0}^{\infty}\sum_{u=0}^{\infty}\left[\begin{array}{l}\left\{\Omega_{jl}H_mH_nH_u - \Lambda_{jl}\left(H_{m-1}H_{n-1} + H_{m+1}H_{n+1}\right)H_u\right\} \\ \times\left\{\begin{pmatrix} B^c_{mj}B^c_{nl}C^c_{uk} + B^s_{mj}B^s_{nl}C^c_{uk} \\ B^s_{mj}B^c_{nl}C^s_{uk} - B^c_{mj}B^s_{nl}C^s_{uk}\end{pmatrix}\begin{pmatrix}\lambda^{+}_{mnu} + \lambda^{-}_{mnu} \\ \lambda^{-}_{umn} - \lambda^{-}_{num}\end{pmatrix}\right\} \\ +\left\{\Omega_{jl}H_mH_nH_u + \Lambda_{jl}\left(H_{m-1}H_{n+1} + H_{m+1}H_{n-1}\right)H_u\right\} \\ \times\left\{\begin{pmatrix} B^c_{mj}B^c_{nl}C^c_{uk} - B^s_{mj}B^s_{nl}C^c_{uk} \\ B^c_{mj}B^s_{nl}C^s_{uk} + B^s_{mj}B^c_{nl}C^s_{uk}\end{pmatrix}\begin{pmatrix}\lambda^{+}_{mnu} - \lambda^{-}_{mnu} \\ \lambda^{-}_{umn} + \lambda^{-}_{num}\end{pmatrix}\right\}\end{array}\right] rdr \tag{5.52}$$

where $\Omega^{+}_{jl} = \left(\omega_j\left(k_l^2 - \nu_l^2\right) + \omega_l\left(k_j^2 - \nu_j^2\right) - 2\left(\omega_j + \omega_l\right)\nu_l\nu_j\right)$ and $\Lambda^{+}_{jl} = \left(\omega_j + \omega_l\right)k_jk_l$

In this step, let us consider integral of radial direction in detail. One of difficulty in free-surface integral is come from infinite interval of radial direction. As shown in Eq. (5.52), the integration of radial direction is composed of triple product of Hankel functions. It could be defined in this form.

$$F_{mnu} = \int_{R_s}^{\infty} H_m\left(k_j\rho\right)H_n\left(k_l\rho\right)H_u\left(k_k\rho\right)rdr \tag{5.53}$$

Since this integral has oscillating and slowly decaying properties, the integrand exists at the very far region from the body. It is very difficult to evaluate integration accurately by using direct numerical integration. Instead of using numerical integral, numerous ways such as series expansion are suggested by many researchers. For instance, Newman (1991), Malenica *et al*. (2018) used complex analysis and conducted numerical integration with exponential function in complex region. Kim and Yue (1989) used series expansion based on recurrence relation of Fresnel integral. Chau andTaylor (1992) developed approximation method using another series expansion with minimum error. Choi *et al*. (2001) developed new analytic solution on radial direction after stationary phase approximation on azimuthal direction. In this study, we also used same series expansion of Chau and Taylor (1992). The asymptotic formulation of Hankel function of the second-kind using series expansion is written as follows:

$$H_m(x) = \sqrt{\frac{2}{\pi x}} e^{-i(x-\gamma_m)} \sum_{p=0}^{\infty} (-i)^p \frac{C_{mp}}{x^p} \tag{5.54}$$

where $\gamma_m = \frac{\pi}{2}\left(m+\frac{1}{2}\right)$, $C_{mp} = \frac{\left(4m^2-1\right)\left(4m^2-9\right)\cdots\left[4m^2-(2p-1)^2\right]}{p!8^p}$

$$C_{m0} = 1 \text{ and } C_{mp} = \frac{4m^2-(2p-1)^2}{8p} C_{mp-1}$$

Using above asymptotic formulation, integration which includes triple product of Hankel function could be expressed as follows (Chau and Taylor, 1992; Choi, 2013):

$$F_{mnu} = \sqrt{\frac{2}{\pi k_j}}\sqrt{\frac{2}{\pi k_l}}\sqrt{\frac{2}{\pi k_k}} e^{i(\gamma_m+\gamma_n+\gamma_u)} \sum_{p=0}^{N_m}\sum_{q=0}^{N_n}\sum_{s=0}^{N_u} (-i)^{p+q+s} \frac{C_{mp}}{k_j^p}\frac{C_{nq}}{k_l^q}\frac{C_{us}}{k_k^s} \int_{R_s}^{\infty} \frac{e^{-i(k_j+k_l+k_k)r}}{r^{p+q+s+1/2}} dr \tag{5.55}$$

Chau and Taylor (1992) suggested the maximum series number N_m = m/2+2 to make minimum error of summation. In this study, N_m = m+5 is used as a maximum number and the approximation is conducted on Hankel function of the second-kind. The remained integral is evaluated as follows (Chau and Taylor, 1992):

$$A_n = \int_{R_s}^{\infty} \frac{e^{-i(k_j+k_l+k_k)\rho}}{r^{n+1/2}} dr = \sum_{m=1}^{N} \frac{\Gamma(n+m-1/2)}{\Gamma(n+1/2)} \frac{1}{\left\{-i(k_j+k_l+k_k)\right\}^m} \frac{e^{-i(k_j+k_l+k_k)R_s}}{R_s^{n+m-1/2}} + E_N \tag{5.56}$$

where E_N is a truncation error and it is known that the great number (N) has maximum within $\left(k_j + k_l + k_k\right)R_s - n$.

However, if argument of Hankel function is less than Bessel-order, it could have large imaginary value thus asymptotic form could make some error. In this study, we did integration numerically by using Clenshaw-Curtis integration until argument of the function is larger than Bessel-order. As a validation test, the evaluation of Eq. (5.53) [The test is conducted on Hankel function of the first-kind] using asymptotic formulation and Clenshaw-Curtis integration is conducted. The result is denoted in the Table 5.1 where the integration interval is from 10 to 11 and wave numbers are 1.0. This table shows that asymptotic expansion has little difference with another result at large Bessel-order and Clenshaw-Curtis integration has a good agreement in all Bessel-orders.

Table 5.1 Comparison of integration which has triple Hankel funciton integrand in finite interval

m	n	u	Chau and Taylor (1992)	Asymptotic expansion (Present)	Clenshaw-Curtis (Present)
1	2	3	(0.001886,0.003742)	(0.001886,0.003742)	(0.001886,0.003742)
5	3	6	(-0.006758,0.002120)	(-0.006758,0.002120)	(-0.006758,0.002120)
9	9	12	(-0.011812,-0.034072)	(-0.011812,-0.034072)	(-0.011812,-0.034072)
11	11	14	(0.109891,0.000471)	(0.109891,0.000472)	(0.109891,0.000471)
14	9	17	(-0.361132,0.022987)	(-0.361132,0.022982)	(-0.361132,0.022987)
12	12	15	(-0.040433,-0.246565)	(-0.040430,-0.246566)	(-0.040433,-0.246565)
13	13	17	(-0.240852,0.712168)	(-0.240862,0.712162)	(-0.240852,0.712168)

In Eq.(5.42), there are three types of quadratic forcing term on the free-surface. As used in disturbed velocity potential, the incident wave velocity also could be expressed by using Bessel function or summation of Hankel function and its conjugates. They are defined in this form.

$$G_{mnu} = \int_{R_s}^{\infty} H_m\left(k_j r\right) J_n\left(k_l r\right) H_u\left(k_k r\right) r dr = \int_{R_s}^{\infty} H_m\left(k_j r\right) \frac{\left\{H_n\left(k_l r\right) + H_n^*\left(k_l r\right)\right\}}{2} H_u\left(k_k r\right) r dr \qquad (5.57)$$

$$P_{mnu} = \int_{R_s}^{\infty} J_m\left(k_j r\right) H_n\left(k_l r\right) H_u\left(k_k r\right) r dr = \int_{R_s}^{\infty} \frac{\left\{H_m\left(k_j r\right) + H_m^*\left(k_j r\right)\right\}}{2} H_n\left(k_l r\right) H_u\left(k_k r\right) r dr \qquad (5.58)$$

Using these defined equations, all free-surface integrals of far-field region are expressed as a series expansion in this form.

$$\iint_{S_{F_{out}}} \left(Q^{+}_{F_{BBjl}}\right)\psi_j^{+} dS = \frac{i}{8}\sum_{m=0}^{\infty}\sum_{n=0}^{\infty}\sum_{u=0}^{\infty}\left[\begin{array}{l}\left\{\Omega_{jl}F_{m,n,u} - \Lambda_{jl}\left(F_{m-1,n-1,u} + F_{m+1,n+1,u}\right)\right\}\begin{pmatrix} B^c_{mj}B^c_{nl}C^c_{uk} + B^s_{mj}B^s_{nl}C^c_{uk} \\ B^s_{mj}B^c_{nl}C^s_{uk} - B^c_{mj}B^s_{nl}C^s_{uk}\end{pmatrix}\begin{pmatrix}\lambda^{+}_{mnu} + \lambda^{-}_{mnu} \\ \lambda^{-}_{umn} - \lambda^{-}_{num}\end{pmatrix} \\ +\left\{\Omega_{jl}F_{m,n,u} + \Lambda_{jl}\left(F_{m-1,n+1,u} + F_{m+1,n-1,u}\right)\right\}\begin{pmatrix} B^c_{mj}B^c_{nl}C^c_{uk} - B^s_{mj}B^s_{nl}C^c_{uk} \\ B^c_{mj}B^s_{nl}C^s_{uk} + B^s_{mj}B^c_{nl}C^s_{uk}\end{pmatrix}\begin{pmatrix}\lambda^{+}_{mnu} - \lambda^{-}_{mnu} \\ \lambda^{-}_{umn} + \lambda^{-}_{num}\end{pmatrix}\end{array}\right] \tag{5.59}$$

$$\iint_{S_{F_{out}}} \left(Q^{+}_{F_{BBjl}}\right)\psi_j^{+} dS = \frac{i}{8}\sum_{m=0}^{\infty}\sum_{n=0}^{\infty}\sum_{u=0}^{\infty}\left[\begin{array}{l}\left\{\Omega_{jl}G_{m,n,u} - \Lambda_{jl}\left(G_{m-1,n-1,u} + G_{m+1,n+1,u}\right)\right\}\begin{pmatrix} B^c_{mj}A^c_{nl}C^c_{uk} + B^s_{mj}A^s_{nl}C^c_{uk} \\ B^s_{mj}A^c_{nl}C^s_{uk} - B^c_{mj}A^s_{nl}C^s_{uk}\end{pmatrix}\begin{pmatrix}\lambda^{+}_{mnu} + \lambda^{-}_{mnu} \\ \lambda^{-}_{umn} - \lambda^{-}_{num}\end{pmatrix} \\ +\left\{\Omega_{jl}G_{m,n,u} + \Lambda_{jl}\left(G_{m-1,n+1,u} + G_{m+1,n-1,u}\right)\right\}\begin{pmatrix} B^c_{mj}A^c_{nl}C^c_{uk} - B^s_{mj}A^s_{nl}C^c_{uk} \\ B^c_{mj}A^s_{nl}C^s_{uk} + B^s_{mj}A^c_{nl}C^s_{uk}\end{pmatrix}\begin{pmatrix}\lambda^{+}_{mnu} - \lambda^{-}_{mnu} \\ \lambda^{-}_{umn} + \lambda^{-}_{num}\end{pmatrix}\end{array}\right] \tag{5.60}$$

$$\iint_{S_{F_{out}}} \left(Q^{+}_{F_{IBjl}}\right)\psi_j^{+} dS = \frac{i}{8}\sum_{m=0}^{\infty}\sum_{n=0}^{\infty}\sum_{u=0}^{\infty}\left[\begin{array}{l}\left\{\Omega_{jl}P_{m,n,u} - \Lambda_{jl}\left(P_{m-1,n-1,u} + P_{m+1,n+1,u}\right)\right\}\begin{pmatrix} A^c_{mj}B^c_{nl}C^c_{uk} + A^s_{mj}B^s_{nl}C^c_{uk} \\ A^s_{mj}B^c_{nl}C^s_{uk} - A^c_{mj}B^s_{nl}C^s_{uk}\end{pmatrix}\begin{pmatrix}\lambda^{+}_{mnu} + \lambda^{-}_{mnu} \\ \lambda^{-}_{umn} - \lambda^{-}_{num}\end{pmatrix} \\ +\left\{\Omega_{jl}P_{m,n,u} + \Lambda_{jl}\left(P_{m-1,n+1,u} + P_{m+1,n-1,u}\right)\right\}\begin{pmatrix} A^c_{mj}B^c_{nl}C^c_{uk} - A^s_{mj}B^s_{nl}C^c_{uk} \\ A^c_{mj}B^s_{nl}C^s_{uk} + A^s_{mj}B^c_{nl}C^s_{uk}\end{pmatrix}\begin{pmatrix}\lambda^{+}_{mnu} - \lambda^{-}_{mnu} \\ \lambda^{-}_{umn} + \lambda^{-}_{num}\end{pmatrix}\end{array}\right] \tag{5.61}$$

This series summation should conduct $m \times n \times u$ number of calculations. It could be reduced by using orthogonal property of already defined integral of trigonometric functions. As shown in Eqs. (5.59-61), there are four types of combination made by integration of trigonometric functions. Their results are as follows:

$$\lambda^{+}_{mnu} + \lambda^{-}_{mnu} = \pi\delta_{m,n+u} + \pi\delta_{n,m+u} \tag{5.62}$$

$$\lambda^{-}_{umn} - \lambda^{-}_{num} = \pi\delta_{m,n+u} - \pi\delta_{n,m+u} \tag{5.63}$$

$$\lambda^{+}_{mnu} - \lambda^{-}_{mnu} = \pi\delta_{u,m+n} \tag{5.64}$$

$$\lambda^{-}_{umn} + \lambda^{-}_{num} = \pi\delta_{u,n+m} \tag{5.65}$$

This combination shows that this series expansion *exists only* where ***u=m-n; u=n-m; u=m+n*** as expressed in Figure 5.2.

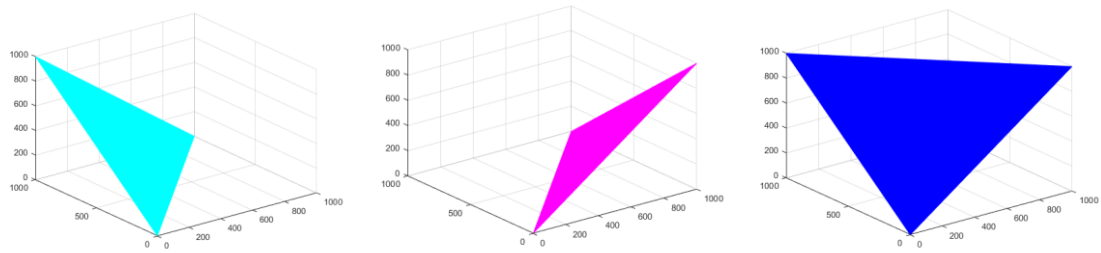

Fig. 5.2 Combination of series numbers which satisfy azimuthal direction of the free-surface integration (each direction in the plot means respectively *m,n,u*)

Using symmetric property of trigonometric function, finally free-surface integral could be expressed in this form.

$$\begin{aligned}
\iint_{S_{F_{out}}}\left(Q^{+}_{F_{jl}}\right)\psi_i^{+}dS = {}& \frac{\pi i}{8}\sum_{m=u}^{N}\left(1+\delta_{mu}\right)\left[U_{mn}\left(F\right)\begin{pmatrix}B^c_{mj}B^c_{nl}C^c_{uk}+B^s_{mj}B^s_{nl}C^c_{uk}\\ B^s_{mj}B^c_{nl}C^s_{uk}-B^c_{mj}B^s_{nl}C^s_{uk}\end{pmatrix}\right]_{n=m-u} \pm \frac{\pi i}{8}\sum_{m=0}^{N-u}\left(1+\delta_{m0}\right)\left[V_{mn}\left(F\right)\begin{pmatrix}B^c_{mj}B^c_{nl}C^c_{uk}+B^s_{mj}B^s_{nl}C^c_{uk}\\ B^s_{mj}B^c_{nl}C^s_{uk}-B^c_{mj}B^s_{nl}C^s_{uk}\end{pmatrix}\right]_{n=m+u} \\
& + \frac{\pi i}{8}\sum_{m=1}^{u-1}\left[W_{mn}\left(F\right)\begin{pmatrix}B^c_{mj}B^c_{nl}C^c_{uk}-B^s_{mj}B^s_{nl}C^c_{uk}\\ B^c_{mj}B^s_{nl}C^s_{uk}+B^s_{mj}B^c_{nl}C^s_{uk}\end{pmatrix}\right]_{n=u-m} + \frac{\pi i}{8}\sum_{m=u}^{N}\left(1+\delta_{mu}\right)\left[U_{mn}\left(G\right)\begin{pmatrix}B^c_{mj}A^c_{nl}C^c_{uk}+B^s_{mj}A^s_{nl}C^c_{uk}\\ B^s_{mj}A^c_{nl}C^s_{uk}-B^c_{mj}A^s_{nl}C^s_{uk}\end{pmatrix}\right]_{n=m-u} \\
& \pm \frac{\pi i}{8}\sum_{m=0}^{N-u}\left(1+\delta_{m0}\right)\left[V_{mn}\left(G\right)\begin{pmatrix}B^c_{mj}A^c_{nl}C^c_{uk}+B^s_{mj}A^s_{nl}C^c_{uk}\\ B^s_{mj}A^c_{nl}C^s_{uk}-B^c_{mj}A^s_{nl}C^s_{uk}\end{pmatrix}\right]_{n=m+u} + \frac{\pi i}{8}\sum_{m=1}^{u-1}\left[W_{mn}\left(G\right)\begin{pmatrix}B^c_{mj}A^c_{nl}C^c_{uk}-B^s_{mj}A^s_{nl}C^c_{uk}\\ B^s_{mj}A^s_{nl}C^s_{uk}+B^s_{mj}A^c_{nl}C^s_{uk}\end{pmatrix}\right]_{n=u-m} \\
& + \frac{\pi i}{8}\sum_{m=u}^{N}\left(1+\delta_{mu}\right)\left[U_{mn}\left(P\right)\begin{pmatrix}A^c_{mj}B^c_{nl}C^c_{uk}+A^s_{mj}B^s_{nl}C^c_{uk}\\ A^s_{mj}B^c_{nl}C^s_{uk}-A^c_{mj}B^s_{nl}C^s_{uk}\end{pmatrix}\right]_{n=m-u} \pm \frac{\pi i}{8}\sum_{m=0}^{N-u}\left(1+\delta_{m0}\right)\left[V_{mn}\left(P\right)\begin{pmatrix}A^c_{mj}B^c_{nl}C^c_{uk}+A^s_{mj}B^s_{nl}C^c_{uk}\\ A^s_{mj}B^c_{nl}C^s_{uk}-A^c_{mj}B^s_{nl}C^s_{uk}\end{pmatrix}\right]_{n=m+u} \\
& + \frac{\pi i}{8}\sum_{m=1}^{u-1}\left[W_{mn}\left(P\right)\begin{pmatrix}A^c_{mj}B^c_{nl}C^c_{uk}-A^s_{mj}B^s_{nl}C^c_{uk}\\ A^c_{mj}B^s_{nl}C^s_{uk}+A^s_{mj}B^c_{nl}C^s_{uk}\end{pmatrix}\right]_{n=u-m}
\end{aligned} \tag{5.66}$$

where $U_{mn}\left(F\right)=\left(\Omega_{jl}F_{m,n,m-n}-\Lambda_{jl}\left[F_{m-1,n-1,m-n}+F_{m+1,n+1,m-n}\right]\right)$

$$V_{mn}\left(F\right)=\left(\Omega_{jl}F_{m,n,n-m}-\Lambda_{jl}\left[F_{m-1,n-1,n-m}+F_{m+1,n+1,n-m}\right]\right)$$

$$W_{mn}\left(F\right)=\left(\Omega_{jl}F_{m,n,m+n}+\Lambda_{jl}\left[F_{m-1,n+1,m+n}+F_{m+1,n-1,m+n}\right]\right)$$

5.4 Numerical result and discussion

To validate the developed numerical code and formulation in the generalized mode, the validation could be conducted for the rigid body motion whose numerical results are obtained by

substituting translational mode into modal vector. Thus second-order generalized hydrodynamic forces for rigid body motion are compared with other results obtained in published paper and each contribution of non-linear body and free-surface part is also confirmed in sequence.

Second-order hydrodynamic force on a fixed and freely-floating hemisphere is calculated. The result is compared with semi-analytic solution of Kim and Yue (1990) and another frequency domain solver *MLINHYDH* which is based on wave Green function HOBEM (Choi *et al*., 2001). In this simulation, boundary radius (R_s) on free-surface is 10 *m* at all frequencies.

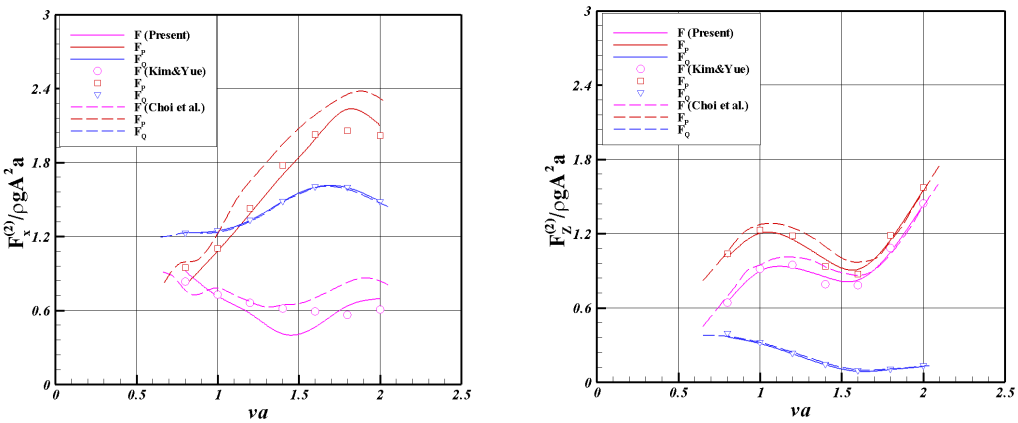

Fig. 5.3 Comparison of surge & heave second-order hydrodynamic forces on a fixed hemisphere (*H* = 3*a*)

Figure 5.3 is the comparison of second-order hydrodynamic forces of a fixed hemisphere and each figure means surge and heave forces. In all results, quadratic product forces show a good agreement. On the other hands, the second-order velocity potential force shows a little difference in surge direction force. In the fixed body, second-order velocity potential force almost obtained from the contribution of free-surface non-linearity and the difference might be come from erupt change of surge radiation velocity potential on free-surface as described in Choi *et al*. (2001).

In sequence, the second-order hydrodynamic force is analysed on the freely-floating body. Provided that the floating body has motion, the non-linearity come from both body and free-surface effects, thus each effect is analysed in detail.

Figure 5.4 shows surge & heave second-order hydrodynamic force from quadratic product (F_q) and body non-linear effect in second-order velocity potential force (F_{BB}). From the obtained results

where the value is large near linear resonance region, it seems that both non-linear forces are quite influenced by the linear motion response. All results could be obtained with good accuracy.

Figure 5.5 shows total second-order hydrodynamic force (F) and free-surface non-linear effect ($F_{p\text{-}BB}$) in second-order velocity potential force at each direction (surge & heave). In numerical results, heave force shows a good agreement but surge direction force also shows a little difference due to free-surface non-linear parts. The reason of difference might be severe oscillation of surge radiation velocity potential on free-surface as same with fixed body. In the high-frequency, second-order velocity potential has large value on this model.

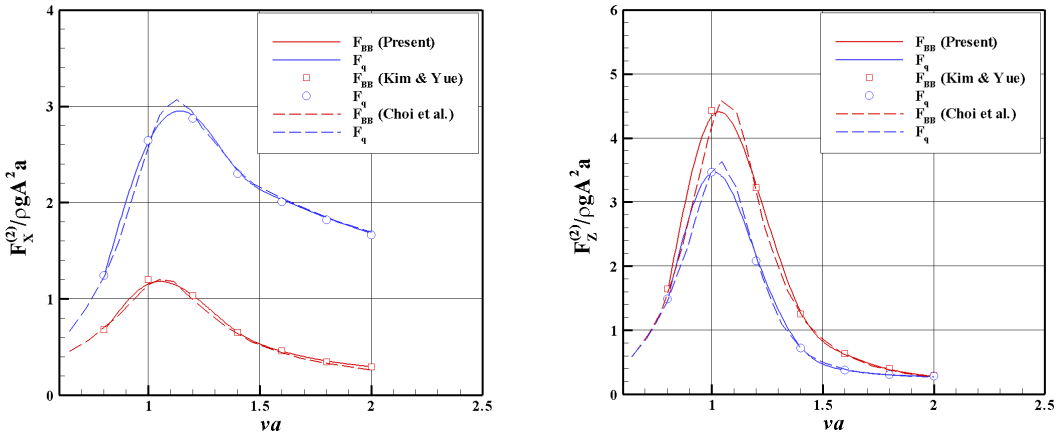

Fig. 5.4 Comparison of surge & heave second-order hydrodynamic forces on a freely-floating hemisphere (F_q & F_{BB})

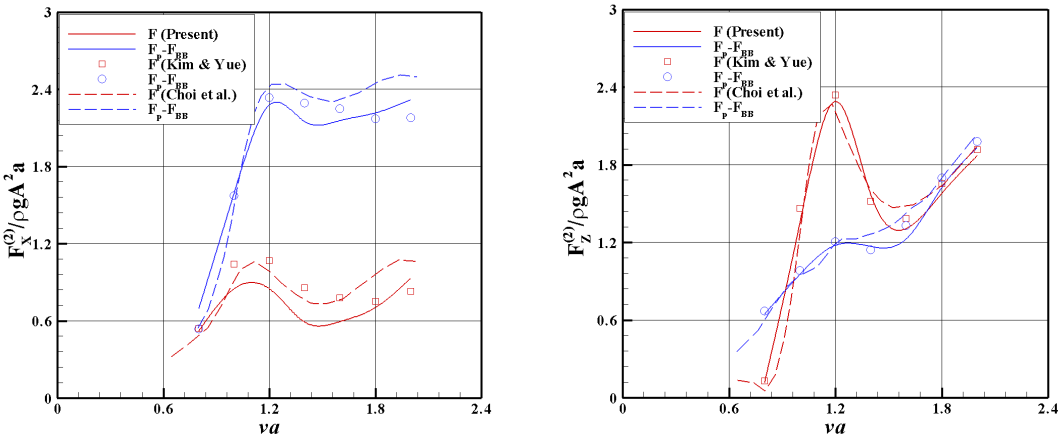

Fig. 5.5 Comparison of surge & heave second-order hydrodynamic forces on a freely-floating hemisphere (*F_P*-*F_{BB}* & *Total force*)

This oscillation in surge direction on free-surface can be confirmed by integration on different range of near-field free-surface region. Figure 5.6 shows that the integration of different ranges (radius of free-surface: 3, 5, 10 *m, See* right figure) changes the second-order velocity potential force considerably over all frequencies.

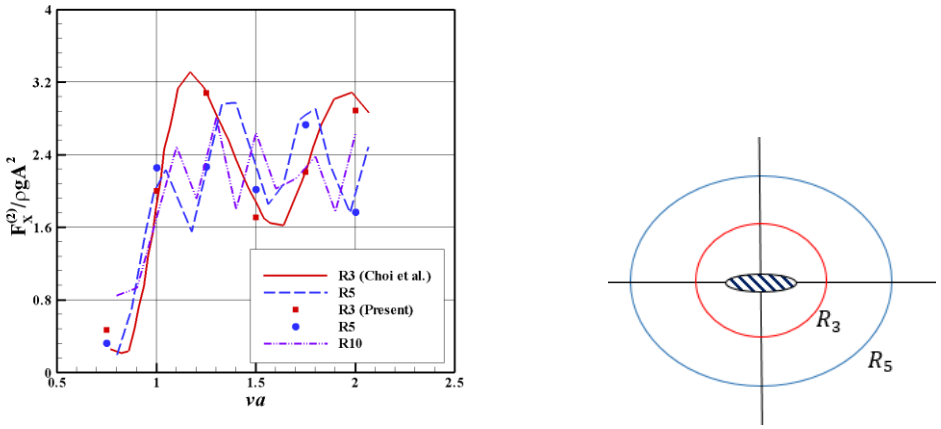

Fig. 5.6 Surge second-order velocity potential force at different range of near-field free-surface range

As mentioned in previous section, the free-surface integration should be evaluated up to quite far region. The comparison study is conducted by changing the radius range in Eqs. (5.55) and (5.57-68). The far-field free-surface integration is evaluated numerically up to finite region and mathematically by asymptotic value of infinite radius range. Figure 5.7 shows that that the real part converges at very far-field region. On the other hands, imaginary part is continuously oscillating depending on radius range. It means the integrand of free-surface integral exists at the very far-field region and also shows that the integration should not be cut at some range.

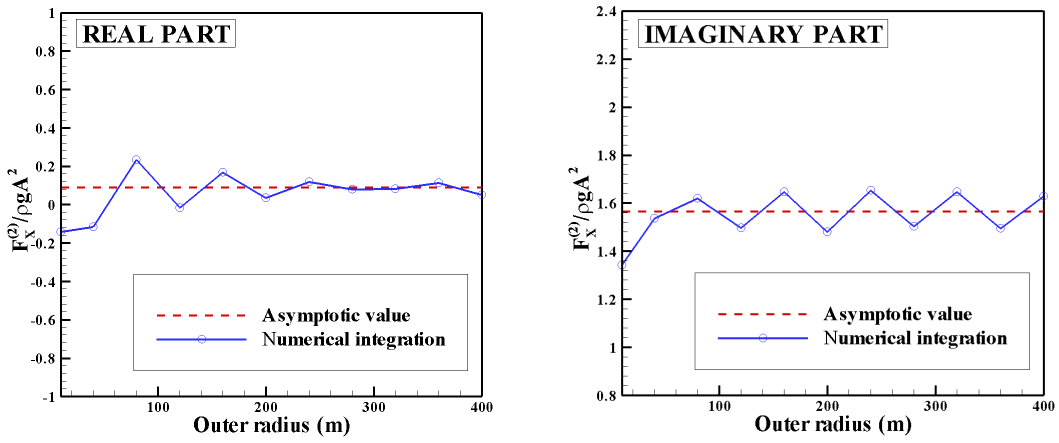

Fig. 5.7 Comparison of far-field free-surface integration at different radius range (*v*a = 1.0)

Using same model and condition, the second-order hydrodynamic force is calculated in bichromatic waves.

Figure 5.8 shows the quadratic product of linear quantities at surge and heave direction. As shown in previous figures, this force has large value near linear resonance region. In the freely-floating hemisphere, there is only one resonance by heave motion. This resonance effect influences stronger to heave direction force directly than surge direction force. Similar tendency is also confirmed in non-linear effect of body on second-order velocity potential force as shown in Figure 5.9.

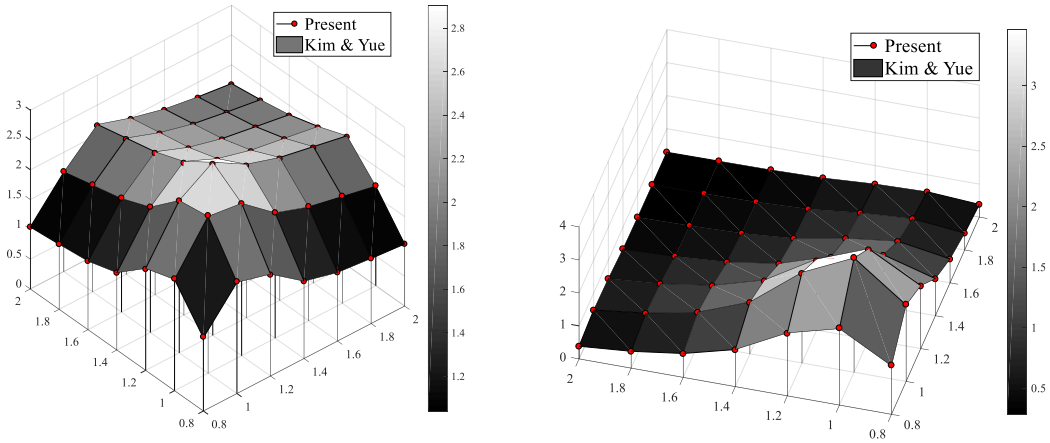

Fig. 5.8 Comparison of surge & heave quadratic product of linear quantities forces (F_q) in bichromatic waves

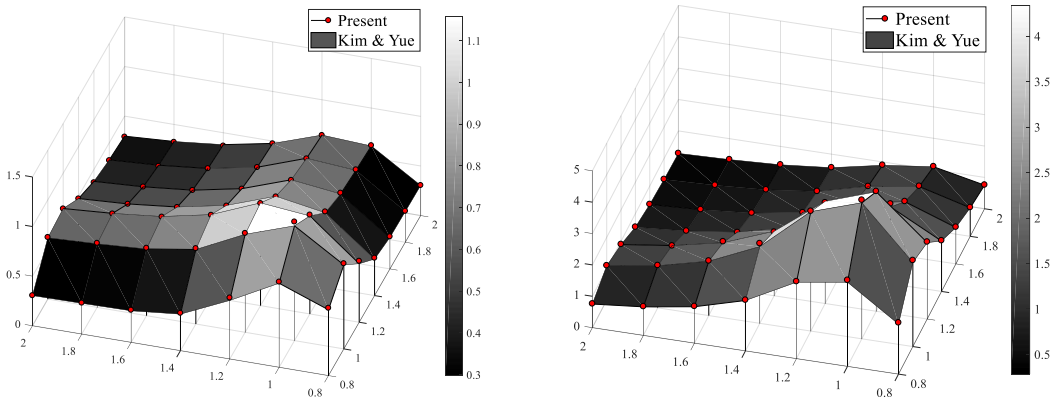

Fig. 5.9 Comparison of surge & heave body non-linear effect on second-order velocity potential force (F_{BB}) in bichromatic waves

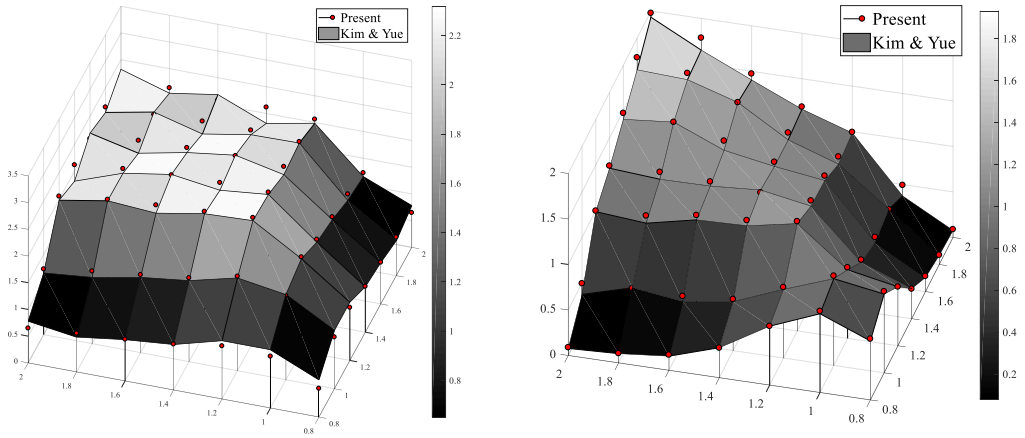

Fig. 5.10 Comparison of surge & heave free-surface non-linear effect on second-order velocity potential force ($F_{p\text{-}BB}$) in bichromatic waves

Figure 5.10 is free-surface non-linear effect on second-order velocity potential force at each direction. It shows that it has large value at high-frequency region in both direction forces, thus the contribution of second-order velocity potential becomes large in this frequency. In figures, we could confirm that diagonal values in QTF matrix are generally larger than non-diagonal terms. The combination of same frequency usually has larger value than that of combination of large different frequency. This phenomenon is also shown mathematically on bottom-fixed vertical cylinder (Newman, 1990). It is also known that this tendency is much larger at difference-frequency forces thus evaluation of QTF without free-surface integral has been suggested by using several approximations depending on the combination of frequencies (Hauteclocque *et al.*, 2012).

CHAPTER 6

Conclusions and future works

6.1 Conclusions

Using generalized mode expansion method and higher-order boundary element method (HOBEM) in the potential flow assumption, linear & second-order hydrodynamic forces and responses of rigid/elastic body are considered. The normal vector variation and body boundary condition are re-defined by using continuum mechanics to consider elastic effect of body surface. Several generalized force including inertial, gravity restoring forces are also derived to obtain hydrodynamic response. Using relatively simple shape's body and structural model, several linear & second-order hydrodynamic variables are checked in numerous conditions. In chapter 4 and 5, obtained numerical results are discussed in monochromatic /bichromatic waves, respectively.

They are summarized as follows:

In chapter 4, direct time-domain simulation is conducted based on Rankine panel method. Several hydrodynamic forces and responses are obtained by using generalized formulation with/without forward speed step by step.

In the zero forward speed problem of a rigid body, several second-order forces including second-order velocity potential are calculated. The linear and second-order velocity potential forces without forward speed are well estimated in diffraction/radiation problem. In the freely-floating condition, however, the second-order velocity potential force does not show good agreement with other results. It might be come from inaccuracy by second derivative of velocity potential and truncated free-surface region.

In the forward speed problem of a rigid body, several Wigley models which have relatively simple shape are studied on the linear and second-order force from linear quantities. In the slender models, the linear results show good accuracy with other results except little overestimated value

near resonance. On the other hands, blunt model shows generally underestimated vertical motions due to simplified m_j-term and accordingly the added resistance is also quite underestimated. The mean drift force is checked as a validation study for all models, the sensitivity on second-derivative of velocity potential could be confirmed. Non-linear force with forward speed should be investigated more by using various methods as a future work.

In the zero forward speed problem of an elastic body, the hydroealstic responses of bottom-mounted flexible cylinder and floating barges are calculated in a validation process. The linear and quadratic force results show a good agreement with that of bottom mounted cylinder. But second-order velocity potential force also shows some difference especially near resonance region. The reason might be same with rigid body motion case. The barge model's response of several points is calculated and compared with other results. In both models, overall response results show a good agreement and it is rather sensitive near resonance region. The mean drift force is also checked by using generalized formulation and the reduction of surge mean drift force is confirmed due to decrease of relative vertical wave elevations as well known.

In the forward speed problem of an elastic body, several quantities are checked by changing forward speed, flexural rigidity and so forth. In the linear motion, the divergence term which only exists in elastic body has no substantial effect. In the second-order, the effect of forward speed and flexural rigidity is checked. The importance of second-order velocity potential force is confirmed well. However, it shows some limitation of calculation for second-order velocity potential force in Rankine panel method on the free body motion in waves.

In chapter 5, bichromatic wave condition is considered without forward speed. Frequency-domain analysis is conducted in steady state assumption by using wave Green function. To calculate generalized second-order velocity potential force, indirect method is adopted instead of solving second-order boundary-value problem. The force formulation is re-defined by generalized formulation as conducted in chapter 4. Several numerical results are compared with other semi-analytic solutions on a fixed/freely floating hemisphere. The results show a good agreement each other without particular difficulty.

On the freely-floating hemisphere, several non-linear effects are discussed. Quadratic product of linear quantities and body non-linear components in second-order velocity potential force are strongly influenced by linear motion. On the other hands, free-surface non-linearity has large value in high-frequency.

In bichromatic waves, body and free-surface non-linearity in combination of several frequencies are also well confirmed on a rigid body. The strong coupling at double frequency force could be also confirmed as same with vertical cylinder model.

Although only rigid body mode is considered as a validation, it could be extended to calculate wave excitation force for elastic motion if the modal vector is simply changed to elastic mode.

6.2 Future works

6.2.1 Improvement of frequency-domain analysis

In this study, the second-order hydrodynamic force on an elastic body is only considered by using indirect method. As well known, however, several local quantities could be calculated after obtaining second-order velocity potential. It could be obtained by solving following boundary integral equation directly as conducted many researchers (*e.g.* Chau and Taylor, 1992; Lee, 1995).

$$C(P)\phi_S^{(2)}(P)+\iint_{S_{B_0}}\phi_S^{(2)}(Q)\frac{\partial G(P,Q)}{\partial n_Q}dS(Q)=\iint_{S_{B_0}}G(P,Q)Q_B dS(Q)+\iint_{S_{F_0}}G(P,Q)Q_F dS(Q) \tag{6.1}$$

Next, more efficient evaluation of free-surface integral could be used. The near-field on free-surface is additionally divided into two parts. The nearest region which includes water line is only integrated by using numerical integral. Since the intermediate region in near-field has circular shape, it could be evaluated semi-analytically. The velocity potential has generally following form.

$$\begin{aligned}\phi \approx -4\sum_{m=1}^{\infty}\sum_{n=0}^{\infty}&\frac{\cos k_m(Z+H)}{\cos k_m h}K_n(k_m r)\left[\tilde{B}_{mn}^c\cos n\theta+\tilde{B}_{mn}^s\sin n\theta\right]\\&+\sum_{n=0}^{\infty}\frac{\cosh k(Z+H)}{\cosh(kH)}H_n(kr)\left[B_n^c\cos n\theta+B_n^s\sin n\theta\right]\end{aligned} \tag{6.2}$$

The azimuthal direction is composed of only trigonometric functions which could be conducted analytically and only radial direction integration is evaluated numerically. This semi-analytic integration could reduce the evaluation of linear velocity potential on the large region of free-surface. Thus it could improve both computational efficiency and numerical accuracy.

6.2.2 Improvement of numerical model

In this study, the head wave condition is only considered thus vertical bending moment is calculated in the elastic motion. In several heading angle, both horizontal and torsional bending modes on the second-order should be considered.

In the structural part, there exist many design issues. For instance, the structural damping is one of important parameter in real sea state on the ship design. Because the springing has very small radiation damping, structural damping influence to the responses considerably. Using more exact modal shape and structural damping, the effect of hydroelastic response on a ship could be confirmed.

In the forward speed problem, we adopted NK assumption thus the steady flow effect is ignored. As shown in chapter 4, however, the steady flow effect is also very important in both linear and non-linear problems. DB flow assumption could be applied on forward speed problem.

We only calculated second-order velocity potential force with forward speed in limited unsteady motion case in monochromatic waves due to uncertainty of present Rankine panel method. However, the obtained result must be validated and complete solution should be calculated by using more trustable way.

6.2.3 Indirect method for second-order velocity potential force with forward speed

As a future work, we would like to introduce the calculation method of second-order velocity potential force with forward speed. As discussed in chapter 4, truncated free-surface integral region might be a reason of error in calculation of second-order force with freely-floating condition. Indirect method used in chapter 5 could be also extended with forward speed provided linear velocity potential is given thus more trustable calculation could be conducted on second-order force with forward speed. Although the calculation is not conducted in this dissertation, the procedure of indirect method with forward speed is briefly explained as a final stage.

Molin (1979) extended the Haskind relation to the second-order problem in the zero forward speed and showed that second-order scattering velocity potential force could be calculated by using linear quantities. This method could be also extended to the forward speed case. First, the second-order velocity potential force with forward speed is written in this form.

$$\vec{F}_{p_i}^{(2)\pm} = -\rho \iint_{S_{B_0}} \left(i\omega^{\pm} \phi^{(2)\pm} + \vec{V} \cdot \nabla \phi^{(2)\pm} \right) \vec{n} dS \tag{6.3}$$

If we conduct the same approach used in Ogilvie and Tuck (1969), it could be rewritten by

$$\vec{F}_{p_i}^{(2)\pm} = -\rho \iint_{S_{B_0}} \left(i\omega^{\pm}\phi^{(2)\pm} + \vec{V}\cdot\nabla\phi^{(2)\pm} \right)\vec{n}dS = -\rho \iint_{S_{B_0}} \left(i\omega^{\pm}n_i - Um_i \right)\phi^{(2)\pm}\vec{n}dS \tag{6.4}$$

$$= -\rho \iint_{S_{B_0}} i\omega^{\pm} \frac{\partial \psi_i^{r\pm}}{\partial n}\phi^{(2)\pm}dS$$

where m_i is m_j-terms on linear body boundary condition with forward speed

Here, superscript ***r*** means reverse flow which has *reverse* forward speed and $\pm$ sign means sum – and difference – frequency components, respectively. This second-order reverse flow velocity potential which is used as an assistant velocity potential satisfies following boundary conditions.

$$\left(i\omega^{\pm} + U\frac{\partial}{\partial X} \right)^2 \psi_i^{r\pm} + g\frac{\partial \psi_i^{r\pm}}{\partial Z} = 0 \qquad \text{on } Z = 0 \tag{6.5}$$

$$\frac{\partial \psi_i^{r\pm}}{\partial n} = \left(n_i - \frac{U}{i\omega}m_{ij} \right) \qquad \text{on } S_{B_0} \tag{6.6}$$

Next, Haskind-Newman approach is applied on second-order boundary condition. It starts from following integral equations.

$$\iint_{S_{B_0}} \left(\phi_s^{(2)\pm}\frac{\partial \psi_i^{r\pm}}{\partial n} - \psi_i^{r\pm}\frac{\partial \phi_s^{(2)\pm}}{\partial n} \right)dS + \iint_{S_{F_0}} \left(\phi_s^{(2)\pm}\frac{\partial \psi_i^{r\pm}}{\partial n} - \psi_i^{r\pm}\frac{\partial \phi_s^{(2)\pm}}{\partial n} \right)dS = 0 \tag{6.7}$$

Provided that bottom and radiation conditions are satisfied, we can substitute second-order boundary condition with forward speed into above integral equations. Hence, Eq. (6.7) could be rewritten by following equations for sum-frequency variable at each boundary condition.

On the body boundary

$$\iint_{S_{B_0}} \left(\phi_s^{(2)+}\frac{\partial \psi_i^{r+}}{\partial n} - \psi_i^{r+}\frac{\partial \phi_s^{(2)+}}{\partial n} \right)dS = \iint_{S_{B_0}} \left(\phi_s^{(2)+}\frac{\partial \psi_i^{r+}}{\partial n} + \psi_i^{r+}\left(\frac{\partial \phi_I^{(2)+}}{\partial n} + Q_B^{+} \right) \right)dS \tag{6.8}$$

On the free-surface boundary

$$\iint_{S_{F_0}}\left(\phi_s^{(2)+}\frac{\partial\psi_i^{r+}}{\partial n}-\psi_i^{r+}\frac{\partial\phi_s^{(2)+}}{\partial n}\right)dS=\iint_{S_{F_0}}\left(\phi_s^{(2)+}\frac{\partial\psi_i^{r+}}{\partial Z}-\psi_i^{r+}\frac{\partial\phi_s^{(2)+}}{\partial Z}\right)dS$$
$$=\frac{1}{g}\iint_{S_{F_0}}\left(-\phi_s^{(2)+}\left(i\omega^+ +U\frac{\partial}{\partial X}\right)^2\psi_i^{r+}-\psi_i^{r+}\left\{\left(i\omega^+ -U\frac{\partial}{\partial X}\right)^2\phi_s^{(2)+}+Q_F^+\right\}\right)dS \tag{6.9}$$
$$=\frac{U^2}{g}\iint_{S_{F_0}}\left(-\phi_s^{(2)+}\left(2i\omega^+\frac{\partial\psi_i^{r+}}{U\partial X}+\frac{\partial^2\psi_i^{r+}}{\partial X^2}\right)+\psi_i^{r+}\left(-2i\omega^+\frac{\partial\phi_s^{(2)+}}{U\partial X}+\frac{\partial^2\phi_s^{(2)+}}{\partial X^2}\right)\right)dS-\frac{1}{g}\iint_{S_{F_0}}\psi_i^{r+}Q_F^+dS$$
$$=\frac{U^2}{g}\iint_{S_{F_0}}\frac{\partial}{\partial X}\left(-\frac{2i\omega^+\phi_s^{(2)+}\psi_i^{r+}}{U}-\phi_s^{(2)+}\frac{\partial\psi_i^{r+}}{\partial X}+\psi_i^{r+}\frac{\partial\phi_s^{(2)+}}{\partial X}\right)dXdY-\frac{1}{g}\iint_{S_{F_0}}\psi_i^{r+}Q_F^+dS$$
$$=\frac{U^2}{g}\int_{WL}\left(-\frac{2i\omega^+\phi_s^{(2)+}\psi_i^{r+}}{U}-\phi_s^{(2)+}\frac{\partial\psi_i^{r+}}{\partial X}+\psi_i^{r+}\frac{\partial\phi_s^{(2)+}}{\partial X}\right)dY-\frac{1}{g}\iint_{S_{F_0}}\psi_i^{r+}Q_F^+dS$$

If we can apply the slender ship assumption as used in linear problem, the line integral could be ignored. Thus,

$$\approx-\frac{1}{g}\iint_{S_{F_0}}\psi_i^{r+}Q_F^+dS \tag{6.10}$$

After substituting Eqs. (6.8-10) into Eq. (6.7), the integral equation for the second-order boundary condition becomes following form.

$$\iint_{S_{B_0}}\phi_s^{(2)+}\frac{\partial\psi_i^{r+}}{\partial n}dS=-\iint_{S_{B_0}}\psi_i^{r+}\left(\frac{\partial\phi_I^{(2)+}}{\partial n}+Q_B^+\right)dS-\frac{1}{g}\iint_{S_{F_0}}\psi_i^{r+}Q_F^+dS \tag{6.11}$$

The right hand sides in Eq. (6.11) could be substituted into force formulation Eq. (6.4). Thus, the second-order velocity potential force in bichromatic waves could be expressed in this form.

$$\vec{F}_{p_{ijl}}^{(2)+}=i\omega^+\iint_{S_{B_0}}\phi_s^{(2)+}\frac{\partial\psi_i^{r+}}{\partial n}dS=-i\omega^+\iint_{S_{B_0}}\psi_i^{r+}\left(\frac{\partial\phi_{I_{jl}}^{(2)+}}{\partial n}+Q_{B_{jl}}^+\right)dS-\frac{i\omega^+}{g}\iint_{S_{F_0}}\psi_i^{r+}Q_{F_{jl}}^+dS \tag{6.12}$$

$$q_{B_{jl}}^+=\frac{1}{2}\left\{\dot{\vec{\gamma}}_{jl}^{(2)}-\vec{\tau}_j^{(1)}\cdot\nabla\nabla\phi_l^{(1)}-\frac{1}{2}\sum_m^3\sum_n^3\tau_{m_j}^{(1)}\tau_{n_l}^{(1)}\frac{\partial}{\partial x_m}\frac{\partial}{\partial x_n}\vec{V}\right\}\cdot\vec{n}$$

where
$$+\frac{1}{2}\left\{\dot{\vec{\tau}}_j^{(1)}-\nabla\phi_j^{(1)}-\vec{\tau}_j^{(1)}\cdot\nabla\vec{V}\right\}\cdot\left\{\left(\nabla\cdot\vec{\tau}_l^{(1)}\right)-\left[\nabla\vec{\tau}_l^{(1)}\right]^T\right\}\cdot\vec{n}$$
$$-\frac{\vec{V}}{2}\cdot\left\{\left(\nabla\cdot\vec{\gamma}_{jl}^{(2)}\right)-\left[\nabla\vec{\gamma}_{jl}^{(2)}\right]^T+\left(\frac{\partial\vec{\tau}_j^{(1)}}{\partial y}\times\frac{\partial\vec{\tau}_l^{(1)}}{\partial z},\frac{\partial\vec{\tau}_j^{(1)}}{\partial z}\times\frac{\partial\vec{\tau}_l^{(1)}}{\partial x},\frac{\partial\vec{\tau}_j^{(1)}}{\partial x}\times\frac{\partial\vec{\tau}_l^{(1)}}{\partial y}\right)\right\}\cdot\vec{n}$$

$$q_{F_{jl}}^{+} = -\nabla\phi_j^{(1)} \cdot \nabla\left(i\omega_l - U\frac{\partial}{\partial X}\right)\phi_l^{(1)} + \frac{1}{2g}\left(i\omega_j - U\frac{\partial}{\partial X}\right)\phi_j^{(1)}\frac{\partial}{\partial Z}\left\{\left(i\omega_l - U\frac{\partial}{\partial X}\right)^2\phi_l^{(1)} + g\frac{\partial^2\phi_l^{(1)}}{\partial Z^2}\right\}$$

and $Q_{B_{jl}}^{+} = \dfrac{q_{B_{jl}}^{+} + q_{B_{lj}}^{+}}{2}$, $Q_{F_{jl}}^{+} = \dfrac{q_{F_{jl}}^{+} + q_{F_{lj}}^{+}}{2}$

As same with zero forward speed problem, the second-order force could be obtained by evaluating the body and free surface integral composed of several linear quantities. In the body surface integral, there are more high-order derivatives of velocity potentials. Although the second derivatives could be removed by using Stokes theorem, there remains a third derivative of steady velocity potential. Thus it might be one of the most difficult problems in the consideration of steady flow effect in second-order velocity potential force. If we ignore the effect of steady flow on the body surface (NK assumption), the non-homogeneous of body surface become much simpler. It is as follows:

$$\begin{aligned} q_{B_{jl}}^{+} = {} & \frac{1}{2}\left\{\dot{\vec{\gamma}}_{jl}^{(2)} - \vec{\tau}_j^{(1)} \cdot \nabla\nabla\phi_l^{(1)}\right\} \cdot \vec{n} + \frac{1}{2}\left\{\dot{\vec{\tau}}_j^{(1)} - \nabla\phi_j^{(1)}\right\} \cdot \left\{\left(\nabla \cdot \vec{\tau}_l^{(1)}\right) - \left[\nabla\vec{\tau}_l^{(1)}\right]^T\right\} \cdot \vec{n} \\ & + \frac{Ui}{2} \cdot \left\{\left(\nabla \cdot \vec{\gamma}_{jl}^{(2)}\right) - \left[\nabla\vec{\gamma}_{jl}^{(2)}\right]^T + \left(\frac{\partial\vec{\tau}_j^{(1)}}{\partial y} \times \frac{\partial\vec{\tau}_l^{(1)}}{\partial z}, \frac{\partial\vec{\tau}_j^{(1)}}{\partial z} \times \frac{\partial\vec{\tau}_l^{(1)}}{\partial x}, \frac{\partial\vec{\tau}_j^{(1)}}{\partial x} \times \frac{\partial\vec{\tau}_l^{(1)}}{\partial y}\right)\right\} \cdot \vec{n} \end{aligned} \tag{6.13}$$

Here, the second derivative of unsteady & double body velocity potentials could be removed by using Stokes theorem as same with zero forward speed problem.

$$\begin{aligned} \iint_{S_{B_0}} \vec{n} \cdot \left[\psi_i^{r+}\vec{\tau}_j^{(1)} \cdot \nabla\nabla\phi_l^{(1)}\right] dS = {} & -\iint_{S_{B_0}} \psi_i^{r+}\left(\nabla \cdot \vec{\tau}_j^{(1)}\right)\left(\nabla\phi_l^{(1)} \cdot \vec{n}\right) dS + \iint_{S_{B_0}} \left\{\psi_i^{r+}\left(\nabla\phi_l^{(1)} \cdot \nabla\vec{\tau}_j^{(1)}\right) \cdot \vec{n}\right\} dS \\ & - \iint_{S_{B_0}} \left\{\nabla\psi_i^{r+} \times \left(\nabla\phi_l^{(1)} \times \vec{\tau}_j^{(1)}\right)\right\} \cdot \vec{n} dS + \oint_{WL} \psi_i^{r+}\left(\nabla\phi_l^{(1)} \times \vec{\tau}_j^{(1)}\right) \cdot \vec{T} dl \end{aligned} \tag{6.14}$$

Thus, the non-homogeneous component could be calculated without higher-order derivative in NK assumption. It is written by

$$\iint_{S_{B_0}} q^{+}_{B_{jl}} \psi_i^{r+} dS = \frac{1}{2}\left\{\dot{\vec{\gamma}}^{(2)}_{jl} - \vec{\tau}^{(1)}_j \cdot \nabla\nabla\phi^{(1)}_l\right\}\cdot\vec{n} + \frac{1}{2}\left\{\dot{\vec{\tau}}^{(1)}_j - \nabla\phi^{(1)}_j\right\}\cdot\left\{\left(\nabla\cdot\vec{\tau}^{(1)}_l\right) - \left[\nabla\vec{\tau}^{(1)}_l\right]^T\right\}\cdot\vec{n}$$
$$+\frac{Ui}{2}\cdot\left\{\left(\nabla\cdot\vec{\gamma}^{(2)}_{jl}\right) - \left[\nabla\vec{\gamma}^{(2)}_{jl}\right]^T + \left(\frac{\partial\vec{\tau}^{(1)}_j}{\partial y}\times\frac{\partial\vec{\tau}^{(1)}_l}{\partial z}, \frac{\partial\vec{\tau}^{(1)}_j}{\partial z}\times\frac{\partial\vec{\tau}^{(1)}_l}{\partial x}, \frac{\partial\vec{\tau}^{(1)}_j}{\partial x}\times\frac{\partial\vec{\tau}^{(1)}_l}{\partial y}\right)\right\}\cdot\vec{n}$$
$$+\frac{1}{2}\iint_{S_{B_0}} \psi_i^{r+}\left(\nabla\cdot\vec{\tau}^{(1)}_j\right)\left(\nabla\phi^{(1)}_l\cdot\vec{n}\right)dS - \frac{1}{2}\iint_{S_{B_0}}\left\{\psi_i^{r+}\left(\nabla\phi^{(1)}_l\cdot\nabla\vec{\tau}^{(1)}_j\right)\cdot\vec{n}\right\}dS$$
$$+\frac{1}{2}\iint_{S_{B_0}}\left\{\nabla\psi_i^{r+}\times\left(\nabla\phi^{(1)}_l\times\vec{\tau}^{(1)}_j\right)\right\}\cdot\vec{n}dS - \frac{1}{2}\oint_{WL}\psi_i^{r+}\left(\nabla\phi^{(1)}_l\times\vec{\tau}^{(1)}_j\right)\cdot\vec{T}dl \tag{6.15}$$

Next, the free-surface integral also becomes much more difficult to be solved than zero forward speed problem. Nevertheless, rather similar approach could be applied on the free-surface integration in case it does not have steady velocity potential. As conducted in zero forward speed problem, the integration could also be divided into near- & far- field regions. In the near-field region, the integration might be conducted by using numerical integration. However, there are also several second derivatives and a third derivative of velocity potential. To conduct the numerical integration it is better to remove these higher-order derivatives as far as possible. The non-homogeneous terms on free-surface in NK assumption could be written by

$$q^{+}_{F_{jl}} = -\frac{\partial\phi^{(1)}_l}{\partial X}\left(i\omega_j\frac{\partial\phi^{(1)}_j}{\partial X} - U\frac{\partial^2\phi^{(1)}_j}{\partial X^2}\right) - \frac{\partial\phi^{(1)}_l}{\partial Y}\left(i\omega_j\frac{\partial\phi^{(1)}_j}{\partial Y} - U\frac{\partial^2\phi^{(1)}_j}{\partial X\partial Y}\right) - \frac{\partial\phi^{(1)}_l}{\partial Z}\left(i\omega_j\frac{\partial\phi^{(1)}_j}{\partial Z} - U\frac{\partial^2\phi^{(1)}_j}{\partial X\partial Z}\right)$$
$$+\frac{1}{2g}\left(i\omega_j\phi^{(1)}_j - U\frac{\partial\phi^{(1)}_j}{\partial X}\right)\left\{\left(-\omega_l^2\frac{\partial\phi^{(1)}_l}{\partial Z} - 2Ui\omega_l\frac{\partial^2\phi^{(1)}_l}{\partial X\partial Z} + U^2\frac{\partial^3\phi^{(1)}_l}{\partial X^2\partial Z}\right) + g\frac{\partial^2\phi^{(1)}_l}{\partial Z^2}\right\} \tag{6.16}$$

Using the 2-D Green theorem on the free-surface, the inner-field of free-surface integration is expressed in this form.

$$\begin{aligned}
\iint_{S_{F_{in}}} q^{+}_{F_{jl}} \psi_i^{r+} dS = {} & \frac{i\omega_j}{2}\left[\oint_{WL+R_s} \left(\phi_j^{(1)} \frac{\partial \phi_l^{(1)}}{\partial Y} \psi_i^{r+} \right) dX - \left(\phi_j^{(1)} \frac{\partial \phi_l^{(1)}}{\partial X} \psi_i^{r+} \right) dY \right] + U\left[\oint_{WL+R_s} \frac{\omega_j \omega_l}{g} \phi_j^{(1)} \frac{\partial \phi_l^{(1)}}{\partial Z} \psi_i^{r+} dY \right] \\
& + U^2 \left[\oint_{WL+R_s} \frac{i\omega_j}{2g} \phi_j^{(1)} \frac{\partial \phi_l^{(1)}}{\partial X \partial Z} \psi_i^{r+} dY \right] - U^3 \left[\oint_{WL+R_s} \frac{1}{2g} \frac{\partial \phi_j^{(1)}}{\partial X} \frac{\partial^2 \phi_l^{(1)}}{\partial X \partial Z} \psi_i^{r+} dY \right] \\
& - i\omega_j \left[\iint_{S_{F_{in}}} \frac{\partial \phi_j^{(1)}}{\partial Z} \frac{\partial \phi_l^{(1)}}{\partial Z} \psi_i^{r+} + \frac{\omega_l^2}{2g} \phi_j^{(1)} \frac{\partial \phi_l^{(1)}}{\partial Z} \psi_i^{r+} dS \right] \\
& - i\omega_j \left[\iint_{S_{F_{in}}} \frac{1}{2} \left\{ \left(\bar{\nabla} \phi_j^{(1)} \cdot \bar{\nabla} \phi_l^{(1)} \right) \psi_i^{r+} - \phi_j^{(1)} \left(\bar{\nabla} \phi_l^{(1)} \cdot \bar{\nabla} \psi_i^{r+} \right) \right\} dS \right] \\
& - U \left[\iint_{S_{F_{in}}} -\nabla \phi_l^{(1)} \cdot \nabla \left(\frac{\partial \phi_j^{(1)}}{\partial X} \right) \psi_i^{r+} + \left(\frac{\omega_j \omega_l}{g} - \frac{\omega_l^2}{2g} \right) \frac{\partial \phi_j^{(1)}}{\partial X} \frac{\partial \phi_l^{(1)}}{\partial Z} \psi_i^{r+} dS \right] \\
& - U \left[\iint_{S_{F_{in}}} \frac{\omega_j \omega_l}{g} \phi_j^{(1)} \frac{\partial \phi_l^{(1)}}{\partial Z} \frac{\partial \psi_i^{r+}}{\partial X} + \frac{1}{2} \frac{\partial \phi_j^{(1)}}{\partial X} \frac{\partial^2 \phi_l^{(1)}}{\partial Z^2} \psi_i^{r+} dS \right] \\
& - U^2 \left[\iint_{S_{F_{in}}} \frac{i\omega_j}{2g} \frac{\partial^2 \phi_l^{(1)}}{\partial X \partial Z} \frac{\partial}{\partial X} \left(\phi_j^{(1)} \psi_i^{r+} \right) - \frac{i\omega_l}{g} \frac{\partial^2 \phi_l^{(1)}}{\partial X \partial Z} \frac{\partial \phi_j^{(1)}}{\partial X} \psi_i^{r+} dS \right] \\
& + U^3 \left[\frac{1}{2g} \iint_{S_{F_{in}}} \frac{\partial^2 \phi_l^{(1)}}{\partial X \partial Z} \frac{\partial}{\partial X} \left(\frac{\partial \phi_j^{(1)}}{\partial X} \psi_i^{r+} \right) dS \right]
\end{aligned} \tag{6.17}$$

In the combination of same frequency components, following relation could be additionally applied.

$$U \iint_{S_{F_{in}}} \left\{ \nabla \phi_l^{(1)} \cdot \nabla \left(\frac{\partial \phi_j^{(1)}}{\partial X} \right) \psi_i^{r+} \right\} dS = -\frac{U}{2} \iint_{S_{F_{in}}} \left\{ \left(\nabla \phi_j^{(1)} \cdot \nabla \phi_l^{(1)} \right) \frac{\partial \psi_i^{r+}}{\partial X} \right\} dS + \frac{U}{2} \oint_{WL+R_s} \left\{ \left(\nabla \phi_j^{(1)} \cdot \nabla \phi_l^{(1)} \right) \psi_i^{r+} \right\} dY \tag{6.18}$$

From the result of Green theorem for the third derivative, several second derivative variables are made additionally. The equation shows that the effect of forward speed is coupled with several derivatives of velocity potentials and it means the numerical accuracy could decrease as forward speed increases.

In the far-field free-surface region which has infinite integral interval, the velocity potential should be expressed by mathematical formulation. In the forward speed problem, the velocity potential at far-field region can be also approximated by using *Kochin* function in this form.

$$\phi_j \sim -\frac{i}{2\pi}\left\{\int_{-\pi+\alpha_0}^{-\frac{\pi}{2}+\vartheta} - \int_{-\frac{\pi}{2}}^{-\frac{\pi}{2}+\vartheta}\right\} H_j(k_1,\theta)\frac{k_1 e^{k_1\left[z+i\left(x\cos\theta+y\sin\theta\right)\right]}}{\sqrt{1+4\Omega\cos\theta}}d\theta$$
$$-\frac{i}{2\pi}\left\{\int_{-\pi+\alpha_0}^{-\frac{\pi}{2}+\Theta}\right\} H_j(k_2,\theta)\frac{k_2 e^{k_2\left[z+i\left(x\cos\theta+y\sin\theta\right)\right]}}{\sqrt{1+4\Omega\cos\theta}}d\theta \tag{6.19}$$

where each variables is defined as follows:

$$\text{where, } H_j(k_m,\theta) = \iint_{S_{B_0}}\left(\frac{\partial\phi_j}{\partial n} - \phi_j\frac{\partial}{\partial n}\right)e^{k_m\left[z'-i\left(x'\cos\theta+y'\sin\theta\right)\right]}dS \text{ (\textit{Kochin} function)}$$

$$\text{and } \alpha_0 = \begin{cases}\cos^{-1}\dfrac{1}{4\Omega}\left(4\Omega>1\right)\\ 0 \qquad\quad (4\Omega<1)\end{cases},\ \begin{cases}\Theta=\cos^{-1}\left(x/\sqrt{x^2+y^2}\right)\\ \vartheta=\tan^{-1}\left(y/x\right)\end{cases},\ \Omega = U\omega_e/g$$

In the low forward speed ($\Omega<0.25$), the k_1 wave component is relatively very small at the far field region and the integration in Eq. (6.19) could be conducted by straightforward way such as stationary phase approximation. It is expressed in this form.

$$\phi_j \sim \Gamma_j(k_2,\theta_s)e^{ik_2\varpi_0(\theta_s)} \tag{6.20}$$

where $\Gamma_j(k_2,\theta_s) = -\dfrac{i}{2\pi}\dfrac{H_j(k_2,\theta_s)k_2}{\sqrt{1+4\Omega\cos\theta_s}}$, θ_s: stationary phase angle, $\varpi_0(\theta) = X\cos\theta + Y\sin\theta$

Using this asymptotic formulation, the far-field free-surface integration could be implemented by numerical or semi-analytic way. However, as the forward speed increases ($\Omega\geq 0.25$) the stationary phase approximation could not be used at cusp point on free-surface and the contribution of k_1 wave components also increase together. In the right of that the inner-field region also has several derivatives of velocity potential coupled with forward speed, it is expected that the high forward speed problems need more efficient and exact numerical scheme for the evaluation of free-surface integration.

References

[1] Bai, W., Teng, B. (2013). Simulation of second-order wave interaction with fixed and floating structures in time domain. *Ocean Engineering*, *74*, 168-177.

[2] Bishop, R. E. D., Bishop, R. E. and Price, W. G. (1979). *Hydroelasticity of ships*. Cambridge University Press.

[3] Bowers, E. C. (1980). Long period disturbances due to wave groups. *Coastal Engineering Proceedings*, *1*(17).

[4] Büchmann, B., Skourup, J. and Cheung, K. F. (1998). Run-up on a structure due to second-order waves and a current in a numerical wave tank. *Applied Ocean Research*, *20*(5), 297-308.

[5] Chau, F. P., Taylor, R. E. (1992). Second-order wave diffraction by a vertical cylinder. *J. Fluid Mech.*, *240*, 571-599.

[6] Chen, X., Wu, Y., Cui, W. and Tang, X. (2003). Nonlinear hydroelastic analysis of a moored floating body. *Ocean Engineering*, *30*(8), 965-1003.

[7] Chen, X. B., Malenica, Š. (1996). Uniformly valid solution of the wave-current-body interaction problem. *Proceedings of the 11th International Workshop on Water Waves and Floating Bodies, Hamburg, Germany*.

[8] Choi, Y. R., Hong, S. Y. and Choi, H. S. (2001). An analysis of second-order wave forces on floating bodies by using a higher-order boundary element method. *Ocean Engineering*, *28*(1), 117-138.

[9] Choi, Y. R. (2004). Analysis of wave drift forces acting on a hydroelastic structure. *Proceedings of the Annual Spring Meeting SNAK*, Chungmu, 162-167 (in Korean).

[10] Choi, Y. R., Yeo, H. T. (2009). A Hydroelastic Analysis of a Floating Fish Cage in Waves. *Journal of Ocean Engineering and Technology*, *23*(6), 7-11 (in Korean).

[11] Choi, Y. M. (2013). *Second order hydroelastic responses of a vertical circular cylinder in monochromatic waves*, MSc Thesis, Pusan National University, Korea.

[12] Cointe, R., Geyer, P. and King, B., Molin, B., Tramoni, M. (1990). Nonlinear and linear motions of a rectangular barge in a perfect fluid, *Proceedings of the 18th Symposium on Naval Hydrodynamics*, Michigan, USA.

[13] Duan, W. Y., Chen, J. K., Zhao, B. B. (2015a). Second-order Taylor Expansion Boundary Element Method for the second-order wave diffraction problem. *Engineering Analysis with Boundary Elements*, 58, 140-150.

References

[14] Duan, W. Y., Chen, J. K., Zhao, B. B. (2015b). Second-order Taylor expansion boundary element method for the second-order wave radiation problem. *Applied Ocean Research*, 52, 12-26.

[15] Ferrant, P. (1998). Fully nonlinear interactions of long-crested wave packets with a three dimensional body. *Proceeding of 22nd ONR symposium on naval hydrodynamics*, 403-415.

[16] Fonseca, N., Guedes Soares, C. (1998). Time-domain analysis of large-amplitude vertical ship motions and wave loads. *Journal of Ship Research*, *42*(2), 139-152.

[17] Gerritsma, J., Beukelman, W. (1972). Analysis of the resistance increase in waves of a fast cargo ship. *International shipbuilding progress*, *19*(217), 285-293.

[18] Hauteclocque, G., Rezende, F., Waals, O., and Chen, X. B. (2012). Review of Approximations to Evaluate Second-Order Low-Frequency Load. *31st International Conference on Ocean, Offshore and Arctic Engineering*, 363-371.

[19] He, G., Kashiwagi, M. (2014). A time-domain higher-order boundary element method for 3D forward-speed radiation and diffraction problems. *Journal of Marine Science and Technology*, 19(2), 228-244.

[20] Hong, S. Y., Kim, B. W. (2014). Experimental investigations of higher-order springing and whipping-WILS project. *International Journal of Naval Architecture and Ocean Engineering*, 6(4), 1160-1181.

[21] Hong, S. Y., Nam, B. W. (2011). Analysis of 2nd-order wave force on floating bodies using fem in time domain. *International Journal of Offshore and Polar Engineering*, *21*(01).

[22] Huang, L. L., Riggs, H. R. (2000). The hydrostatic stiffness of flexible floating structures for linear hydroelasticity. *Marine Structures*, 13(2), 91-106.

[23] Hulme, A. (1982). The wave forces acting on a floating hemisphere undergoing forced periodic oscillations. *J. Fluid Mech.*, 121, 443-63.

[24] Isaacson, M., Cheung, K. F. (1991). Second order wave diffraction around two-dimensional bodies by time-domain method. *Applied Ocean Research*, 13, 175-86.

[25] Isaacson, M., Cheung, K. F. (1992). Time-domain second-order wave diffraction in three dimensions. *Journal of Waterway, Port, Coastal, and Ocean Engineering*, 118(5), 496-516.

[26] Isaacson, M., Ng, J. Y. T. (1993). Second-order wave radiation of three-dimensional bodies by time-domain method. *Int. J. Offshore of Polar Eng*., 13(4), 264-272.

[27] Isasscon, M., Ng, J. Y. T. (1995). Time-domain second-order wave interaction with three-dimensional floating bodies. *Int. J. Offshore of Polar Eng*., 5(3).

References

[28] Iijima, K., Yao, T., Moan, T. (2008). Structural response of a ship in severe seas considering global hydroelastic vibrations. *Marine Structures*, 21, 420-445.

[29] ISSC (2015). *Dynamic response*, Proceedings of the 19th International Ship and Offshore Structures Congress.

[30] ISSC (2018). *Dynamic response*, Proceedings of the 20th International Ship and Offshore Structures Congress.

[31] Jensen, J. J., Pedersen, P. T. (1978). Wave Induced Bending Moments in Ships-a Quadratic Theory. *Royal Inst Naval Architects Supplementary Papers*, 121.

[32] Jensen, J. J. (2001). *Load and global response of ships*, Elsevier.

[33] Joncquez, S. A. G. (2009). *Second-order forces and moments on ships in waves*, Ph.D Thesis, Technical University of Denmark.

[34] John, F. (1950). On the motion of floating bodies II. Simple harmonic motions. *Communications on pure and applied mathematics*, *3*(1), 45-101.

[35] Journee, J. M. J. (1992). *Experiments and calculations on 4 Wigley hull forms in head sea*. Technical Report 0909, Delft University of Technology, Mekelweg 2, 2628 Delft.

[36] Kashiwagi, M. (1998). A new solution method for hydroelastic problems of a very large floating structure in waves. *Proc 17th Int Conf Offshore Mech and Arctic Eng, ASME*.

[37] Kashiwagi, M., Momoda, T. and Inada, M. (1998). A time-domain nonlinear simulation method for wave-induced motions of a floating body. *Journal of the Society of Naval Architects of Japan*, *1998*(184), 139-148.

[38] Kashiwagi, M. (1995). Prediction of surge and its effect on added resistance by means of the enhanced unified theory. *In west-japan society of naval architects, 89*, 77-89.

[39] Kahiwagi, M. (2000). Research on hydroelastic responses of VLFS: Recent progress and future work. *International Journal of Offshore and Polar Engineering*, 10(2).

[40] Kashiwagi, M. (2013). Hydrodynamic study on added resistance using unsteady wave analysis. *Journal of Ship Research*, 57(4), 220-240.

[41] Kashiwagi, M., Kuga, S. and Chimoto, S. (2015). Time- and frequency-domain calculation methos for ship hydroelasticity with forward speed. *Proceeding of 7th International Conference on Hydroelasticity in Marine Technology*.

[42] Kim D. (1996). *Interaction of a large three-dimensional body with waves and currents by THOBEM*, Ph.D Thesis, Texas A&M University, USA.

[43] Kim, M. H., Yue, D. K. P. (1989). The complete second-order diffraction solution for an axisymmetric body Part 1. Monochromatic incident waves. *J. Fluid Mech.*, 200, 235-264.

References

[44] Kim, M. H., Yue, D. K. P. (1990). The complete second-order diffraction solution for an axisymmetric body Part 2. Bichromatic incident waves and body motions. *J. Fluid Mech*., 211, 557-93.

[45] Kim, M. H. (1991). Second-order sum-frequency wave loads on large-volume structures. *Applied Ocean Research*, *13*(6), 287-296.

[46] Kim, J. H., Kim, Y. (2014). Numerical analysis on springing and whipping using fully-coupled FSI models, *Ocean Engineering*, 91(15), 28-50.

[47] Kim, K. H., Bang, J. S., Kim, J. H. and Kim, Y., Kim, S. J., Kim, Y. (2013). Fully coupled BEM-FEM analysis for ship hydroelasticity in waves. *Marine Structure*, 33, 71-99.

[48] Kim, Y., Kim, K. H. and Kim, Y. (2009). Springing analysis of a seagoing vessel using fully coupled BEM–FEM in the time domain. *Ocean Engineering*, 36(11), 785-796.

[49] Kinoshita, T., Bao, W. and Zhu, R. (1997). Higher-order boundary element method for the interaction of a floating body with both waves and slow current. *Journal of Marine Science and Technology*, *2*(4), 268-279.

[50] Koo, W. C., Kim, M. H. (2004). Freely floating-body simulation by a 2D fully nonlinear numerical wave tank. *Ocean Engineering*, 31, 2011-2046.

[51] Koo, W. C., Kim, M. H. (2006). Numerical simulation of nonlinear wave and force generated by a wedge-shape wave maker. *Ocean Engineering*, 33, 983–1006.

[52] Kudou, K. (1977). The drifting force acting on a three-dimensional body in waves. *J. Soc. Naval Arch. of Japan*, 141.

[53] Lee (1995). *WAMIT theory manual*, Massachusetts Institute of Technology, USA.

[54] Lee, J. H., Kim, B. S. and Kim, Y. (2017). Study on steady flow effects in numerical computation of added resistance of ship in waves. *10th International Workshop on Ship and Marine Hydrodynamics*, Taiwan.

[55] Malenica, Š., Molin, B. (1995). Third-harmonic wave diffraction by a vertical cylinder. *J. Fluid Mech.*, 302, 203-229.

[56] Malenica, Š., Taylor, R. E. and Huang, J. B. (1999). Second-order water wave diffraction by an array of vertical cylinders. *J. Fluid Mech*., 390, 349-373.

[57] Malenica, Š., Molin, B. and Senjanociv, I. (2003). Hydroelastic response of a barge to impulsive and non-impulsive wave loads. *Proceeding of 3rd International Conference on Hydroelasticity in Marine Tech.*, Oxford, UK.

References

[58] Malenica, Š., Molin, B., Tuitman, J. T., Bigot, F. and Senjanović, I. (2009). Some aspects of hydrostatic restoring for elastic bodies. *24th International Workshop on Water Waves and Floating Bodies*. Russia.

[59] Malenica, Š., Hauteclocque, G. and Ten, I., Choi, Y. M. (2018). Second order hydroelastic model of floating units. *Proceeding of 8th International Conference on Hydroelasticity in marine technology*, Seoul, Korea.

[60] Maruo, H. (1960), *Wave resistance of a ship in regular head seas*, Bulletin of the faculty of engineering, Yokohama National University.

[61] Miyake, R., Matsumoto, T., Zhu, T., Abe, N., (2008). Experimental studies on the hydroelastic response due to springing using a flexible mega-container ship model. *Procceding of 8th International Conference on Hydrodynamics*, Nantes.

[62] Molin, B. (1979). Second-order diffraction loads upon three-dimensional bodies. *Applied Ocean Research*, 1,197-202.

[63] Nakos, D. E. (1990). *Ship wave patterns and motions by a three dimensional Rankine panel method*. Ph.D Thesis, Massachusetts Institute of Technology, USA.

[64] Newman, J. N. (1977). *Marine hydrodynamics*, MIT press, Cambridge, USA.

[65] Newman, J. N. (1990). Second-harmonic wave diffraction at large depths, *Journal of Fluid Mechanics*, 213, 59-70.

[66] Newman, J. N. (1991). *WAMIT V3.1 second-order module – theoretical background*, MIT, Cambridge, USA.

[67] Newman, J. N. (1994). Wave effects on deformable bodies. *Applied Ocean Research*, 16(1), 47-59.

[68] Ogilvie, T. F. and Tuck, E. O. (1969). *A rational strip theory of ship motions: Part I*, Report No.013, Michigan Univ. Ann Arbor, Dept. of Naval Architecture and Marine Engineering.

[69] Ogilvie, T. F. (1983). Second-Order hydrodynamic effects on ocean platforms. *International workshop on Ship and Platform Motions*, University of California, Berkeley.

[70] Okushu, M. (1980). Added resistance in waves in the light of the unsteady wave pattern analysis. *Proceedings of 13th Symposium on Naval hydrodynamics*, Tokyo, Japan, 413-425.

[71] Park, D. M., Kim, J. H. and Kim, Y. (2016). Numerical analysis of mean drift force on flexible barge in head sea. *The 12th International Conference on Hydrodynamics*, Netherlands.

[72] Park, D. M., Kim, J. H. and Kim, Y. (2019). Numerical study of added resistance of flexible ship. *Journal of Fluids and Structures*, 85, 199-219.

References

[73] Pinkster, J. A. (1980). *Low frequency second order wave exciting forces on floating structures*. Ph.D. Thesis, TU Delft, Netherlands.

[74] Remy, F., Molin, B. and Ledoux, A. (2006). Experimental and numericalstudy of the wave response of a flexible barge. *Proceeding of 4th International Conference on Hydroelasticity in Marine Technology*, Wuxi, China.

[75] Senjanovic, I., Malenica, S., Tomasevic, S. (2007). Investigation of ship hydroelasticity. *Ocean Engineering*, 35(5), 523-535.

[76] Shao, Y. L. (2010). *Numerical potential-flow studies on weakly-nonlinear wave-body interactions with/without small forward speeds*. Ph.D Thesis, NTNU, Norway.

[77] Shao, Y. L., Faltinsen, O. M. (2010). Use of body-fixed coordinate system in analysis of weakly nonlinear wave–body problems. *Applied Ocean Research*, 32(1), 20-33.

[78] Shao, Y. L., Faltinsen, O. M. (2012). Linear seakeeping and added resistance analysis by means of body-fixed coordinate system. *Journal of Marine Science and Technology*, 17(4), 493-510.

[79] Shao, Y. L., Faltinsen, O. M. (2014). A numerical study of the second-order wave excitation of ship springing by a higher-order boundary element method. *International Journal of Naval Architecture and Ocean Engineering*, 6(4), 1000-1013.

[80] Skourup, J., Cheung, K. F., Bingham, H. B. and Büchmann, B. (2000). Loads on a 3D body due to second-order waves and a current. *Ocean Engineering*, *27*(7), 707-727.

[81] Storhaug, G. (2007). *Experimental investigation of wave induced vibrations and their effect on the fatigue loading of ships*, Ph.D Thesis, Dept. Marine Technology, NTNU.

[82] Tanizawa, K. (1995). A nonlinear simulation method of 3-d body motions in waves (1st report). *Journal of the Society of Naval Architects of Japan*, 178, 179-191.

[83] Teng, B., Bai, W., Dong, G. (2002). Simulation of second-order radiation of 3D bodies in time domain by a B-spline method. *Proceeding of Int Offshore Polar Eng Conf.*, 12, 487-493.

[84] Utsunomiya T, Watanabe, E., Nakamura, N. (2001). Analysis of drift force on VLFS by near field approach. *Proceeding of 11th ISOPE*, 1, 217-222.

[85] Vidic-Perunovics, J., Jensen, J. J. (2005). Non-linear springing excitation due to a bidirectional wave field. *Marine Structures*, 18, 332-358.

[86] Watanabe, E., Utsunomiya, T. and Wang, C. M. (2004). Hydroelastic analysis of pontoon-type VLFS: a literature survey. *Engineering Structures*, *26*(2), 245-256.

[87] Williams, A. N., Li, W. (2000). Water wave interaction with an array of bottom-mounted surface-piercing porous cylinders. *Ocean Engineering*, *27*(8), 841-866.

References

[88] Wu, G. X., Taylor, R. E. (1994). Finite element analysis of two-dimensional non-linear transient water waves. *Applied Ocean Research*, *16*(6), 363-372.

[89] Wu, G. X., Taylor, R. E. (2003). The coupled finite element and boundary element analysis of nonlinear interactions between waves and bodies. *Ocean Engineering*, *30*(3), 387-400.

[90] Wu, M. K., Hermundstad, O. A. (2005). Efficient calculation of wave-induced ship responses considering structural dynamic effects. *Applied Ocean Research*, 27, 81-96.

[91] Wu, M. K., Moan, T. (1996). Linear and nonlinear hydroelastic analysis of high-speed vessel, *Journal of Ship Research*, 40(2), 149-163.

[92] Wu, Y. S., Maeda, H. and Kinoshita, T. (1997). The second order hydrodynamic actions on a flexible body. *Journal of Institute of Industrial Science*, University of Tokyo, *49*(4), 8-19.

[93] Xia, J. and Wang, Z. (1997). Time-domain hydroelasticity theory of ships responding to waves. *Journal of Ship Research*, 41, 286-300.

[94] Zhang, J. (2018). *Numerical study on nonlinear wave-body interaction in time domain based on ALE-HOBEM*, Ph.D Thesis, Osaka University, Japan.

[95] Zhao, R., Faltinsen, O. M. (1989). A discussion of the mj-terms in the wave-current-body interaction problem. *3rd Int. Workshop on Water Waves and Floating Bodies*, USA.

[96] Zhou B., Ning, B., Teng. B. and Bai, W. (2013). Numerical investigation of wave radiation by a vertical cylinder using a fully nonlinear HOBEM, *Ocean Engineering*, 70, 1-13.

Appendix A: Vector identity of normal vector variation on a rigid body

The first-order term of normal vector variation in the generalized mode can be written as follows:

$$O(\varepsilon)=\left(\nabla\cdot\vec{\tau}^{(1)}\right)\vec{n}-\left[\nabla\vec{\tau}^{(1)}\right]^{T}\cdot\vec{n} \tag{A.1}$$

On a rigid body, the displacement and its derivative can be expressed in this form.

$$\tau_1^{(1)}=\xi_1^{(1)}+\xi_5^{(1)}z-\xi_6^{(1)}y,\ \nabla\tau_1^{(1)}=\left(\frac{\partial\tau_1^{(1)}}{\partial x},\frac{\partial\tau_1^{(1)}}{\partial y},\frac{\partial\tau_1^{(1)}}{\partial z}\right)=\left(0,-\xi_6^{(1)},\xi_5^{(1)}\right) \tag{A.2.1}$$

$$\tau_2^{(1)}=\xi_2^{(1)}+\xi_6^{(1)}x-\xi_4^{(1)}z,\ \nabla\tau_2^{(1)}=\left(\frac{\partial\tau_2^{(1)}}{\partial x},\frac{\partial\tau_2^{(1)}}{\partial y},\frac{\partial\tau_2^{(1)}}{\partial z}\right)=\left(\xi_6^{(1)},0,-\xi_4^{(1)}\right) \tag{A.2.2}$$

$$\tau_3^{(1)}=\xi_3^{(1)}+\xi_4^{(1)}y-\xi_5^{(1)}x,\ \nabla\tau_3^{(1)}=\left(\frac{\partial\tau_3^{(1)}}{\partial x},\frac{\partial\tau_3^{(1)}}{\partial y},\frac{\partial\tau_3^{(1)}}{\partial z}\right)=\left(-\xi_5^{(1)},\xi_4^{(1)},0\right) \tag{A.2.3}$$

Since the divergence of displacement on a rigid body is zero, *i.e.* $\nabla\cdot\vec{\tau}^{(1)}=0$, the first-order normal vector variation Eq. (A.1) becomes the following

$$O(\varepsilon)=\left(\nabla\cdot\vec{\tau}^{(1)}\right)\vec{n}-\left[\nabla\vec{\tau}^{(1)}\right]^{T}\cdot\vec{n}=\begin{bmatrix}0 & -\xi_6^{(1)} & \xi_5^{(1)}\\ \xi_6^{(1)} & 0 & -\xi_4^{(1)}\\ -\xi_5^{(1)} & \xi_4^{(1)} & 0\end{bmatrix}\cdot\vec{n}=\vec{\alpha}_R^{(1)}\times\vec{n} \tag{A.3}$$

where $\vec{\alpha}_R^{(1)}=(\xi_4^{(1)},\xi_5^{(1)},\xi_6^{(1)})$ is the rotational motion vector.

Next, the second-order component of normal vector variation can be written as follows:

$$O(\varepsilon^2)=\left\{\begin{array}{l}\nabla\cdot\left(\vec{\tau}^{(2)}+\vec{\gamma}^{(2)}\right)\vec{n}-\left[\nabla\vec{\tau}^{(2)}+\nabla\vec{\gamma}^{(2)}\right]^{T}\cdot\vec{n}\\ +\left(\dfrac{\partial\vec{\tau}^{(1)}}{\partial y}\times\dfrac{\partial\vec{\tau}^{(1)}}{\partial z},\dfrac{\partial\vec{\tau}^{(1)}}{\partial z}\times\dfrac{\partial\vec{\tau}^{(1)}}{\partial x},\dfrac{\partial\vec{\tau}^{(1)}}{\partial x}\times\dfrac{\partial\vec{\tau}^{(1)}}{\partial y}\right)\cdot\vec{n}\end{array}\right\} \tag{A.4}$$

In this expression, the quadratic product of linear displacement ($\vec{\gamma}^{(2)}$) can be written in terms of the second-order term in the expansion of Euler-angle matrix **H** as follows:

Appendix A

$$\vec{\gamma}^{(2)} = \mathbf{H}\vec{x} = \begin{bmatrix} -\frac{1}{2}\left(\xi_5^{(1)2} + \xi_6^{(1)2}\right) & 0 & 0 \\ \xi_4^{(1)}\xi_5^{(1)} & -\frac{1}{2}\left(\xi_4^{(1)2} + \xi_6^{(1)2}\right) & 0 \\ \xi_4^{(1)}\xi_6^{(1)} & \xi_5^{(1)}\xi_6^{(1)} & -\frac{1}{2}\left(\xi_4^{(1)2} + \xi_5^{(1)2}\right) \end{bmatrix} \vec{x}$$
$$= \begin{bmatrix} -\frac{1}{2}\left(\xi_5^{(1)^2} + \xi_6^{(1)^2}\right)x \\ \xi_4^{(1)}\xi_5^{(1)}x - \frac{1}{2}\left(\xi_4^{(1)^2} + \xi_6^{(1)^2}\right)y \\ \xi_4^{(1)}\xi_6^{(1)}x + \xi_5^{(1)}\xi_6^{(1)}y - \frac{1}{2}\left(\xi_4^{(1)^2} + \xi_5^{(1)^2}\right)z \end{bmatrix} \tag{A.5}$$

The cross product term in second line of Eq. (A.4) can be calculated using Eq. (A.2) and expressed as follows:

$$\left(\frac{\partial\vec{\tau}^{(1)}}{\partial y}\times\frac{\partial\vec{\tau}^{(1)}}{\partial z}, \frac{\partial\vec{\tau}^{(1)}}{\partial z}\times\frac{\partial\vec{\tau}^{(1)}}{\partial x}, \frac{\partial\vec{\tau}^{(1)}}{\partial x}\times\frac{\partial\vec{\tau}^{(1)}}{\partial y}\right) = \begin{bmatrix} \left(\xi_4^{(1)}\right)^2 & \xi_4^{(1)}\xi_5^{(1)} & \xi_4^{(1)}\xi_6^{(1)} \\ \xi_4^{(1)}\xi_5^{(1)} & \left(\xi_5^{(1)}\right)^2 & \xi_5^{(1)}\xi_6^{(1)} \\ \xi_4^{(1)}\xi_6^{(1)} & \xi_5^{(1)}\xi_6^{(1)} & \left(\xi_6^{(1)}\right)^2 \end{bmatrix} \tag{A.6}$$
$$= \mathbf{H} + \mathbf{H}^T + \left\{\left(\xi_4^{(1)}\right)^2 + \left(\xi_5^{(1)}\right)^2 + \left(\xi_6^{(1)}\right)^2\right\}\mathbf{E}$$

where $\mathbf{E}$ denotes the unit matrix having only the unit diagonal element $\left[\delta_{ij}\right]$.

After substituting upper two equations into Eq. (A.4), each term can be written by

$$\nabla\cdot\left(\vec{\tau}^{(2)} + \vec{\gamma}^{(2)}\right)\vec{n} = \nabla\cdot\left(\mathbf{H}\vec{x}\right)\vec{n} = -\left\{\left(\xi_4^{(1)}\right)^2 + \left(\xi_5^{(1)}\right)^2 + \left(\xi_6^{(1)}\right)^2\right\}\vec{n} \tag{A.7.1}$$

$$-\left[\nabla\vec{\tau}^{(2)}\right]^T\cdot\vec{n} = \vec{\alpha}_R^{(2)}\times\vec{n} \tag{A.7.2}$$

$$-\left[\nabla\vec{\gamma}^{(2)}\right]^T\cdot\vec{n} = -\left[\nabla\mathbf{H}\vec{x}\right]^T\cdot\vec{n} = -\mathbf{H}^T\cdot\vec{n} \tag{A.7.3}$$

$$\left(\frac{\partial\vec{\tau}^{(1)}}{\partial y}\times\frac{\partial\vec{\tau}^{(1)}}{\partial z}, \frac{\partial\vec{\tau}^{(1)}}{\partial z}\times\frac{\partial\vec{\tau}^{(1)}}{\partial x}, \frac{\partial\vec{\tau}^{(1)}}{\partial x}\times\frac{\partial\vec{\tau}^{(1)}}{\partial y}\right)\cdot\vec{n} = \mathbf{H}\cdot\vec{n} + \mathbf{H}^T\cdot\vec{n} + \left\{\left(\xi_4^{(1)}\right)^2 + \left(\xi_5^{(1)}\right)^2 + \left(\xi_6^{(1)}\right)^2\right\}\vec{n} \tag{A.7.4}$$

After collecting all terms, we can find that second-order component of normal vector variation on a rigid body also agrees with classical formulation, as shown below:

$$
\begin{aligned}
O(\varepsilon^2) &= \nabla\cdot\left(\mathbf{H}\vec{x}\right)\vec{n} + \vec{\alpha}_R^{(2)}\times\vec{n} - \mathbf{H}^T\cdot\vec{n} + \mathbf{H}\cdot\vec{n} + \mathbf{H}^T\cdot\vec{n} + \left\{\left(\xi_4^{(1)}\right)^2 + \left(\xi_5^{(1)}\right)^2 + \left(\xi_6^{(1)}\right)^2\right\}\vec{n} \\
&= \vec{\alpha}_R^{(2)}\times\vec{n} + \mathbf{H}\cdot\vec{n}
\end{aligned}
\tag{A.8}
$$

Appendix B: Vector identity of the inertial force on a rigid body

The transformed tensor for the rotational mode shape is defined to consider the rotational motion in the following form:

$$\mathbf{h}_r^{(0)} = \begin{pmatrix} i\times\mathbf{T}^{(0)}\vec{x} \\ j\times\mathbf{T}^{(0)}\vec{x} \\ k\times\mathbf{T}^{(0)}\vec{x} \end{pmatrix} = \begin{pmatrix} 0 & -z & y \\ z & 0 & -x \\ -y & x & 0 \end{pmatrix}, \quad \mathbf{h}_r^{(1)} = \begin{pmatrix} i\times\mathbf{T}^{(1)}\vec{x} \\ j\times\mathbf{T}^{(1)}\vec{x} \\ k\times\mathbf{T}^{(1)}\vec{x} \end{pmatrix} = \begin{pmatrix} i\times\left(\vec{\alpha}_R^{(1)}\times\vec{x}\right) \\ j\times\left(\vec{\alpha}_R^{(1)}\times\vec{x}\right) \\ k\times\left(\vec{\alpha}_R^{(1)}\times\vec{x}\right) \end{pmatrix} \tag{B.1}$$

On a rigid body, the deformation gradient tensor (**T**) could be written as follows:

$$\mathbf{T} = \begin{bmatrix} \frac{\partial X_1}{\partial x_1} & \frac{\partial X_1}{\partial x_2} & \frac{\partial X_1}{\partial x_3} \\ \frac{\partial X_2}{\partial x_1} & \frac{\partial X_2}{\partial x_2} & \frac{\partial X_2}{\partial x_3} \\ \frac{\partial X_3}{\partial x_1} & \frac{\partial X_3}{\partial x_2} & \frac{\partial X_3}{\partial x_3} \end{bmatrix} \approx \begin{bmatrix} 1 & 0 & 0 \\ 0 & 1 & 0 \\ 0 & 0 & 1 \end{bmatrix} + \begin{bmatrix} 0 & -\xi_6^{(1)} & \xi_5^{(1)} \\ \xi_6^{(1)} & 0 & -\xi_4^{(1)} \\ -\xi_5^{(1)} & \xi_4^{(1)} & 0 \end{bmatrix} = \mathbf{T}^{(0)} + \mathbf{T}^{(1)} \tag{B.2}$$

Using the transformed rotational motion tensor, the generalized linear inertial force on a rigid body could be expressed as follows:

$$\begin{aligned} \vec{F}_R^{(1)} &= \iiint_{V_b} \rho_s \left(\mathbf{h}_r^{(0)}\cdot\ddot{\vec{\tau}}^{(1)}\right)dV = \iiint_{V_b} \rho_s \left\{ \begin{pmatrix} 0 & -z & y \\ z & 0 & -x \\ -y & x & 0 \end{pmatrix} \begin{pmatrix} \ddot{\tau}_1^{(1)} \\ \ddot{\tau}_2^{(1)} \\ \ddot{\tau}_3^{(1)} \end{pmatrix} \right\} dV \\ &= \iiint_{V_b} \rho_s \begin{pmatrix} -z\ddot{\tau}_2^{(1)} + y\ddot{\tau}_3^{(1)} \\ z\ddot{\tau}_1^{(1)} - x\ddot{\tau}_3^{(1)} \\ -y\ddot{\tau}_1^{(1)} + x\ddot{\tau}_2^{(1)} \end{pmatrix} dV = \iiint_{V_b} \rho_s \left\{ \vec{x}\times\left(\ddot{\vec{\alpha}}_T^{(1)} + \ddot{\vec{\alpha}}_R^{(1)}\times\vec{x}\right) \right\} dV \end{aligned} \tag{B.3}$$

Thus the linear inertial force for the rotational motion takes the following form:

$$\vec{F}_R^{(1)} = \iiint_{V_b} \rho_s \left(\mathbf{h}_r^{(0)}\cdot\ddot{\vec{\tau}}^{(1)}\right)dV = \iiint_{V_b} \rho_s \vec{x}\times\left(\ddot{\vec{\alpha}}_T^{(1)} + \ddot{\vec{\alpha}}_R^{(1)}\times\vec{x}\right)dV = \mathbf{I}\ddot{\vec{\alpha}}_R^{(1)} + m\left\{\vec{x}_g\times\ddot{\vec{\alpha}}_T^{(1)}\right\} \tag{B.4}$$

Next, the generalized second-order inertial force is written as follows:

$$\vec{F}_R^{(2)} = \iiint_{V_b} \rho_s \left\{ \mathbf{h}_r^{(0)}\cdot\left(\dddot{\vec{\gamma}}^{(2)} + \dddot{\vec{\tau}}^{(2)}\right) + \mathbf{h}_r^{(1)}\cdot\ddot{\vec{\tau}}^{(1)} \right\} dV \tag{B.5}$$

Appendix B

In the second-order inertial force, each component could also be rewritten by substituting the rotation mode tensor into Eq. (B.5) on a rigid body assumption. The last two terms are as follows:

$$\iiint_{V_b} \rho_s \left\{ \mathbf{h}_r^{(0)} \cdot \ddot{\vec{\tau}}^{(2)} \right\} dV = \mathbf{I} \ddot{\vec{\alpha}}_R^{(2)} + m \left\{ \vec{x}_g \times \ddot{\vec{\alpha}}_T^{(2)} \right\} \tag{B.6}$$

$$\iiint_{V_b} \rho_s \left\{ \mathbf{h}_r^{(1)} \cdot \ddot{\vec{\tau}}^{(1)} \right\} dV = \iiint_{V_b} \rho_s \left\{ \left(\vec{\alpha}_R^{(1)} \times \vec{x} \right) \times \ddot{\vec{\alpha}}_T^{(1)} + \left(\vec{\alpha}_R^{(1)} \times \vec{x} \right) \times \left(\ddot{\vec{\alpha}}_R^{(1)} \times \vec{x} \right) \right\} dV \tag{B.7}$$

The quadratic product term could be expressed in the following form:

$$\iiint_{V_b} \rho_s \left\{ \mathbf{h}_r^{(0)} \cdot \ddot{\vec{\gamma}}^{(2)} \right\} dV = \iiint_{V_b} \rho_s \left\{ \mathbf{h}_r^{(0)} \cdot \ddot{\mathbf{H}} \vec{x} \right\} dV \tag{B.8}$$

$$= \iiint_{V_b} \rho_s \left\{ \begin{pmatrix} 0 & -z & y \\ z & 0 & -x \\ y & x & 0 \end{pmatrix} \begin{bmatrix} -\left(\ddot{\xi}_5^{(1)} \xi_5^{(1)} + \dot{\xi}_5^{(1)} \dot{\xi}_5^{(1)} + \dot{\xi}_6^{(1)} \dot{\xi}_6^{(1)} + \xi_6^{(1)} \ddot{\xi}_6^{(1)} \right) x \\ \left\{ \left(\ddot{\xi}_4^{(1)} \xi_5^{(1)} + 2\dot{\xi}_4^{(1)} \dot{\xi}_5^{(1)} + \xi_4^{(1)} \ddot{\xi}_5^{(1)} \right) x - \left(\ddot{\xi}_4^{(1)} \xi_4^{(1)} + \dot{\xi}_4^{(1)} \dot{\xi}_4^{(1)} + \dot{\xi}_6^{(1)} \dot{\xi}_6^{(1)} + \xi_6^{(1)} \ddot{\xi}_6^{(1)} \right) y \right\} \\ \left\{ \left(\ddot{\xi}_4^{(1)} \xi_6^{(1)} + 2\dot{\xi}_4^{(1)} \dot{\xi}_6^{(1)} + \xi_4^{(1)} \ddot{\xi}_6^{(1)} \right) x + \left(\ddot{\xi}_5^{(1)} \xi_6^{(1)} + 2\dot{\xi}_5^{(1)} \dot{\xi}_6^{(1)} + \xi_5^{(1)} \ddot{\xi}_6^{(1)} \right) y \right. \\ \left. -\left(\ddot{\xi}_4^{(1)} \xi_4^{(1)} + \dot{\xi}_4^{(1)} \dot{\xi}_4^{(1)} + \dot{\xi}_5^{(1)} \dot{\xi}_5^{(1)} + \xi_5^{(1)} \ddot{\xi}_5^{(1)} \right) z \right\} \end{bmatrix} \right\} dV$$

$$= \iiint_{V_b} \rho_s \left\{ \vec{x} \times \ddot{\mathbf{H}} \vec{x} \right\} dV$$

Here, the second term in (B.7) plus (B.8) could be written with so-called quadratic inertial force in [69] as follows:

$$\iiint_{V_b} \rho_s \left\{ \vec{x} \times \ddot{\mathbf{H}} \vec{x} \right\} + \left\{ \left(\vec{\alpha}_R^{(1)} \times \vec{x} \right) \times \left(\ddot{\vec{\alpha}}_R^{(1)} \times \vec{x} \right) \right\} dV = \mathbf{I} \begin{Bmatrix} \dot{\xi}_5^{(1)} \dot{\xi}_6^{(1)} + \xi_6^{(1)} \ddot{\xi}_5^{(1)} \\ -\dot{\xi}_4^{(1)} \dot{\xi}_6^{(1)} - \xi_6^{(1)} \ddot{\xi}_4^{(1)} \\ \dot{\xi}_4^{(1)} \dot{\xi}_5^{(1)} + \xi_5^{(1)} \ddot{\xi}_4^{(1)} \end{Bmatrix} + \vec{\alpha}_R^{(1)} \times \mathbf{I} \ddot{\vec{\alpha}}_R^{(1)} + \dot{\vec{\alpha}}_R^{(1)} \times \mathbf{I} \dot{\vec{\alpha}}_R^{(1)} \tag{B.9}$$

After collecting all terms, we can confirm that the second-order inertial force takes the same expression as the classical expression on a rigid body, as shown below:

$$\vec{F}_R^{(2)} = \iiint_{V_b} \rho_s \left\{ \mathbf{h}_r^{(0)} \cdot \left(\ddot{\vec{\gamma}}^{(2)} + \ddot{\vec{\tau}}^{(2)} \right) + \mathbf{h}_r^{(1)} \cdot \ddot{\vec{\tau}}^{(1)} \right\} dV$$

$$= \mathbf{I} \ddot{\vec{\alpha}}_R^{(2)} + m \left\{ \vec{x}_g \times \ddot{\vec{\alpha}}_T^{(2)} \right\} + \mathbf{I} \begin{Bmatrix} \dot{\xi}_5^{(1)} \dot{\xi}_6^{(1)} + \xi_6^{(1)} \ddot{\xi}_5^{(1)} \\ -\dot{\xi}_4^{(1)} \dot{\xi}_6^{(1)} - \xi_6^{(1)} \ddot{\xi}_4^{(1)} \\ \dot{\xi}_4^{(1)} \dot{\xi}_5^{(1)} + \xi_5^{(1)} \ddot{\xi}_4^{(1)} \end{Bmatrix} + \vec{\alpha}_R^{(1)} \times \mathbf{I} \ddot{\vec{\alpha}}_R^{(1)} + \dot{\vec{\alpha}}_R^{(1)} \times \mathbf{I} \dot{\vec{\alpha}}_R^{(1)} + m \left\{ \left(\vec{\alpha}_R^{(1)} \times \vec{x}_g \right) \times \ddot{\vec{\alpha}}_T^{(1)} \right\} \tag{B.10}$$

Acknowledgement

To conduct the research and write this dissertation, I have received various help from many people. I would like to express my gratitude to them here.

First of all, I would like express deep gratitude to Prof. Masashi Kahiwagi for giving me the opportunity to study in Japan as a supervisor of this dissertation. I can learn many things from his advising, encouragement, social manner, experience and I will remember it.

I also deeply appreciate Prof. Munehiko Minoura. He is always considerate and helped whatever happened in the laboratory. As a committee member, Prof. Kazuhiro Ijima gave me precious comments and I would appreciate it a lot.

I am thankful to receiving help for administration from Ms. Tamae Miyabe. I also thank to Dr. Kyung-Kyu Yang, Chen Chen, Jie Zhang, Takahito Iida, Ardhana Waskito and would like to say my thankfulness for all our laboratory members. For 3 years in the laboratory, they are always kind and have made good atmosphere for the study.

Although this work is conducted in Osaka University, I would like to express my deep gratitude for Prof. Yoon-Rak Choi. If I don't know him, it is impossible to continue studying this topic.

At last, I would like to say my sincere gratitude and love for my father, mother and brother.

The financial support by JASSO and Osaka University for private supported foreign student has been given during this work. I would like to express gratitude for it.

August, 2019

Kyeonguk Heo